Electronic Theses and Dissertations   Theses, Dissertations, and Major Papers

2009

Ferritic nitrocarburizing process development for minimization of distortion

Chunyan Nan
University of Windsor

Follow this and additional works at: https://scholar.uwindsor.ca/etd

Ferritic Nitrocarburizing Process Development

for Minimization of Distortion

by

Chunyan Nan

A Thesis

Submitted to the Faculty of Graduate Studies

through Materials Engineering

in Partial Fulfillment of the Requirements for

the Degree of Master of Applied Science at the

University of Windsor

Windsor, Ontario, Canada

2009

Canada

DECLARATION OF CO-AUTHORSHIP/PREVIOUS PUBLICATIONS

I hereby declare that this thesis incorporates material that is the result of a joint research undertaken in collaboration with Dr. Xichen Sun from the Powertrain Materials Engineering Department of Chrysler LLC under the supervision of professors Derek O. Northwood and Randy J. Bowers. The research collaboration is covered in Chapters 4, 5, and 6 of the thesis. In all cases, the key ideas, primary contributions, experimental designs, data analysis and interpretation, were performed by the author, and the contributions of the co-authors was in the capacity of supervision of the research in the form of technical advice and suggestions.

I am aware of the University of Windsor Senate Policy on Authorship and I certify that I have properly acknowledged the contributions of other researchers to my thesis, and have obtained permission from each of the co-authors to include the above materials in my thesis.

I certify that, with the above qualification, this thesis, and the research to which it refers, is the product of my own work.

This thesis includes five original papers that have been previously published/submitted for publication in peer reviewed journals, as follows:

1. C. Nan, D.O. Northwood, R.J. Bowers, X. Sun and P. Bauerle, Residual Stresses and Dimensional Changes in Ferritic Nitrocarburized Navy C-rings and Prototype Stamped Parts Made from SAE 1010 Steel, Proceedings of the SAE World Congress & Exhibition, April 2009, Detroit, MI, U.S.A., Paper No. 2009-01-0425, SAE International, Warrendale, PA, U.S.A. Also accepted for publication in the SAE International Journal of Materials & Manufacturing.

2. C. Nan, D.O. Northwood, R.J. Bowers and X. Sun, Distortion in Ferritic Nitrocarburized SAE 1010 Plain Carbon Steel, Proceedings of the 2009 SEM Annual Conference and Exposition on Experimental and Applied Mechanics, 1-3 June 2009, Albuquerque, New Mexico, U.S.A.

3. C. Nan, D.O. Northwood, R.J. Bowers, X. Sun and P. Bauerle, The use of Navy C-ring specimens to study distortion in ferritic nitrocarburized 1010 steel,

Proceedings of the Surface Effects and Contact Mechanics IX, Computational Methods and Experiments, WIT Transactions on Engineering Sciences, WIT Press 2009, Vol. 62, pp. 13-25.

4. C. Nan, D.O. Northwood, R.J. Bowers and X. Sun, Study on the Dimensional Changes and Residual Stresses in Carbonitrided and Ferritic Nitrocarburized SAE 1010 Plain Carbon Steel. Accepted for publication in the Proceedings of the Thermec' 2009 International Conference, 25-29 August 2009, Technical University-Berlin, Germany.

5. C. Nan, D.O. Northwood, R.J. Bowers and X. Sun, Nitrocarburizing of a SAE 1010 Steel Automotive Component. Submitted on 25 April 2009 for publication in Materials Forum.

I certify that I have obtained permission from the copyright owners to include the above published materials in my thesis. I certify that the above material describes work completed during my registration as a graduate student at the University of Windsor.

I declare that, to the best my knowledge, my thesis does not infringe upon anyone's copyright nor violate any proprietary rights and that any ideas, techniques, quotations, or any other material from the work of other people included in my thesis, published or otherwise, are fully acknowledged in accordance with the standard referencing practices. Furthermore, to the extent that I have included copyrighted material that surpasses the bounds of fair dealing within the meaning of the Canada Copyright Act, I certify that I have obtained permission from the copyright owners to include such materials in my thesis.

I declare that this is a true copy of my thesis, including any final revisions, as approved by my thesis committee and the Graduate Studies office, and that this thesis has not been submitted for a higher degree to any other University or Institution.

ABSTRACT

Nitrocarburizing is a thermochemical diffusion process that has been proposed as an alternative to carbonitriding to improve the surface characteristics of automotive components without producing unacceptable part distortion. In this study, gas, ion and vacuum ferritic nitrocarburizing using various heat treatment schedules were investigated and compared with a current carbonitriding procedure. Dimensional distortion and residual stresses in Navy C-Rings and torque converter pistons resulting from each treatment process were evaluated. The microstructure and microhardness, as well as the phase composition of the specimens, were also characterized.

The results of this study indicated that the nitrocarburizing process utilizing suitable heat treatment procedures gave rise to smaller size and shape variations in specimens than carbonitriding. However, given the tensile surface residual stresses induced by nitrocarburizing, additional wear testing needs to be carried out to confirm the possibility of replacing the current carbonitriding process with an appropriate ferritic nitrocarburizing procedure.

To My Dear Family

ACKNOWLEDGEMENTS

First and foremost, I would like to express my heartfelt appreciation to my advisors Dr. Derek O. Northwood and Dr. Randy J. Bowers for their instructive supervision, encouragement, and steadfast support during my graduate studies. It has been a great pleasure working with them, and my academic experience here has been both challenging and rewarding.

I also wish to extend my thanks to my committee members: Dr. J. Johrendt, Dr. V. Stoilov, and Dr. D. Ting for their invaluable suggestions and time. The laboratory assistance of Mr. J. Robinson is also much appreciated.

Special thanks are extended to Dr. Xichen Sun for providing technical suggestions and coordinating the tests performed at the Chrysler Technology Center and the commercial heat treaters throughout this project. The financial support of the Powertrain Materials Engineering Department of Chrysler LLC and the University of Windsor are graciously acknowledged.

TABLE OF CONTENTS

LIST OF TABLES

LIST OF FIGURES

Chapter 2

Chapter 4

Chapter 5

Chapter 6

LIST OF ABBREVIATIONS

CMM   coordinate measuring machine

EDM   electrical discharge machining

OD   outside diameter

ID   inside diameter

$\mathbf{M_s}$ martensite start temperature

SEM   scanning electron microscopy

XRD   x-ray diffraction

FCC   face-centered cubic

BCC   body-centered cubic

$\mathbf{Ac_1}$ eutectoid temperature

I. INTRODUCTION

The term "Surface Engineering" is defined in the ASM Handbook as "treatment of the surface and near surface regions of a material to allow the surface to perform functions that are distinct from those functions demanded from the bulk of the material" [1]. Surface engineering has been divided into six sectors by the Surface Engineering Division of the Institute of Materials, Minerals and Mining: high value; energy/aerospace; transport; packaging; white goods; biomedical [2]. As pointed out by Rickerby [3], many of our modes of transport are improved by surface engineering. For example, coatings are applied to reduce rolling and frictional losses within mechanical assemblies in order to both extend component lifetimes and minimize total lifecycle energy consumption of automobiles. Surface engineering has also been utilized to help overcome corrosion problems that once plagued the automotive industry [3].

Surface engineering can be performed through the following methods: (1) changing the surface metallurgy, such as flame hardening and laser melting; (2) changing the surface chemistry, for example, ferritic nitrocarburizing and carbonitriding; (3) adding a surface layer or coating, for instance, organic coatings and electroplating. These methods ensure that the desired characteristics of surface-engineered components can be obtained, such as improved corrosion and wear resistance, enhanced fatigue and toughness, and improved mechanical properties [4]. Among these methods of surface engineering, both the carbonitriding and nitrocarburizing processes have been extensively adopted by the automotive industry to impart a hard and wear resistant case to steel components while maintaining the tough interior to resist the impact that occurs during operation [5].

Carbonitriding is generally regarded as a modified carburizing process, in which ammonia (NH_3) is added into the carburizing atmosphere to release nitrogen with the ability to diffuse into the austenite of steel simultaneously with carbon [6-9]. During carbonitriding, the austenite composition is changed and the hard and wear resistant surface is obtained by quenching to form martensite [10]. A variety of automotive

1

components are carbonitrided in the current production cycles, such as the pistons and retainer rings for the torque converters of transmissions [8].

Chrysler LLC uses a carbonitriding process to improve the hardness and wear resistance of torque converter pistons [11]. The torque converter piston is primarily used to engage the converter case to lock the impeller and the turbine during the manipulation of the torque converter, ensuring complete power transfer and reducing fuel consumption [12]. The control principle of the torque converter piston defines the importance of accurate inside diameter, total flatness, and flatness taper of the lockup surface for the normal operation of the torque converter [11]. Although the desired hardness and wear resistant surface properties were achieved using the carbonitriding process, there were issues associated with the quenching step to form martensite, especially the size and shape distortion in the final component. The phenomenon of surface oxidation and nonuniform surface hardness also accompanied the process. In order to meet the dimensional specifications, the surface defects resulting from carbonitriding and quenching were corrected using finish grinding, a technique in which excess material is removed from the surface of the steel [13]. However, this additional manufacturing step contributes to longer production times and higher part costs, and also raises the risk of grind burns.

Gaseous ferritic nitrocarburizing has been investigated as a potential replacement for carbonitriding for minimizing dimensional distortion in the torque converter pistons [14-16]. Ferritic nitrocarburizing is a modified form of nitriding, which involves the diffusion of both nitrogen and carbon into the surface of ferrous materials at temperatures completely within the ferrite phase field [8, 10, 17, 18]. The low-temperature nitrocarburizing process contributes to the absence of a phase transformation from ferrite to austenite or the need for further quenching to form martensite; consequently, distortion resulting from either the released induced stresses, the thermal shock of quenching, or the incomplete transformation to martensite can be significantly reduced [17, 19]. The surface oxidation and nonuniform surface hardness associated with quenching can also be reduced. As a result, additional processing operations, such as finish grinding to

2

improve surface characteristics, can be eliminated, which will contribute to a shorter production cycle and lower part costs.

In the present study, gas, ion and vacuum nitrocarburizing using different heat treatment schedules were investigated as well as carbonitriding using current production practice for SAE 1010 plain carbon steel. Two types of specimens were used for the study, namely Navy C-rings and torque converter pistons. Navy C-rings are specially designed specimens used to examine distortion in heat-treated components [20]. Navy C-rings with thicknesses between 2.8 mm and 19.05 mm were used to examine the effects of specimen thickness and heat treatment process on distortion. The distortions in the C-ring specimens are compared to those found in torque converter pistons that were subjected to the same heat treatment process.

The intent of this work focused mainly on the comparison of the effects of various ferritic nitrocarburizing and carbonitriding processes on dimensional distortion (size and shape) and surface residual stresses. The distortion was correlated with the microstructural changes and surface residual stresses resulting from the heat treatment. Optical microscopy (OM) and scanning electron microscopy (SEM) were used to evaluate the interrelationships between the microstructure and properties within the specimens and the nitrocarburizing or carbonitriding processes applied. X-ray diffraction (XRD) techniques were used to characterize the residual stresses in the surface of the nitrocarburized and carbonitrided specimens, and to analyze the surface phase composition and texture for the different nitrocarburizing processes. Vickers hardness testing was performed on cross sections of the nitrocarburized specimens to evaluate the hardness of the compound layer and the underlying diffusion zone.

Based on the analyses and comparisons of the various ferritic nitrocarburizing and carbonitriding processes mentioned above, an appropriate heat treatment process and treatment schedule will be put forward, which will reduce distortion and manufacturing costs, while maintaining the desired surface characteristics in the finished products.

3

II. LITERATURE REVIEW

The objective of this chapter is to introduce the various diffusion methods of surface hardening, include the carburizing, carbonitriding, nitriding, and nitrocarburizing processes. Special attention is given to a comparison of the carbonitriding and nitrocarburizing procedures, with respect to the dimensional distortion and residual stresses that result from each process.

2.1 Surface Hardening of Steel

Surface hardening is a heat treatment method *used to improve the wear resistance of parts without affecting the more soft, tough interior of the part* [5, 8]. For applications where low or moderate core properties, together with a high degree of surface hardness are desired, the combination of a hard surface and softer interior is useful, e.g., a cam or ring gear. Surface hardening also helps to reduce distortion and eliminate cracking that might be induced by through hardening, especially in large sections of low-carbon and medium-carbon steels [21].

As noted by Davis [8], there are three different methods for surface hardening: thermochemical diffusion methods; applied energy or thermal methods; and surface coating or surface-modification methods. The difference between the first two approaches is that the diffusion methods modify the chemical composition of the surface using hardening species such as carbon and nitrogen, whereas the latter alters the surface metallurgy without modifying the chemical composition [8]. Carburizing, carbonitriding, nitriding and nitrocarburizing processes from the first group of diffusion methods will be briefly reviewed in this section, with an emphasis placed on comparing carbonitriding and nitrocarburizing with various heat treatment procedures.

2.1.1 Carburizing

Of the case hardening treatments, carburizing is by far more extensively used than the carbonitriding, nitriding and nitrocarburizing processes [22]. Carburizing is achieved by adding carbon to the surface of low-carbon steels at elevated temperatures in the homogeneous austenite phase field, followed by quenching and tempering to form a

4

martensitic microstructure [8, 23, 24]. Carburizing can be performed at temperatures between 790 to 1090 °C, but in production practice, it is generally done at temperatures between 850 and 950 °C. Higher temperatures reduce the effective life of furnace equipment; lower temperatures slow the completion of the carburizing procedure [22, 23].

Carburizing produces a hardness gradient below the surface of the material owing to the decreasing carbon content with depth. It also produces compressive residual stresses at the surface due to the volume expansion resulting from the martensitic transformation [9]. The main objective of carburizing is to provide a hard high-carbon martensitic surface with good wear and fatigue resistance, along with compressive surface residual stresses that contribute to longer service life in ferrous engineering components [22, 25]. The microstructure of the carburized case is mainly composed of plate martensite and retained austenite, whereas the core contains lath martensite, or for larger components, bainite or ferrite and pearlite [9].

Carburizing can be performed using gas carburizing, plasma (ion) carburizing, vacuum carburizing, salt bath carburizing, and pack carburizing. Different methods are classified according to their carbon sources, which originate from a gaseous environment (atmospheric gas, plasma and vacuum), a liquid salt bath, or a solid carbonaceous compound [8, 22]. Gas carburizing is the most widely used method of the various carburizing processes while plasma and vacuum carburizing are also useful due to the absence of oxygen in the furnace atmosphere [8]. Traditionally, gas carburizing atmospheres are produced by combustion of natural gas or other hydrocarbon gas in exothermic or endothermic gas generators. The components of the atmosphere may be any of several carrier gases, principally composed of CO, CO_2, CH_4, H_2, H_2O and N_2 [21, 24]. It should be noted that the nitrogen component in the atmosphere is inert, and acts only as a diluent [24]. The carburizing time depends on the desired depth of diffusion.

2.1.2 Carbonitriding

Carbonitriding is being used increasingly as a modified carburizing process in industry for the production of parts of better wear and temper resistance. The key

difference between carbonitriding and carburizing is the addition of ammonia (NH_3) into the carbonitriding atmosphere. Nascent nitrogen forms by the dissociation of ammonia and diffuses into the steel simultaneously with carbon [6, 8, 9]. Similar to carburizing, the austenite composition is changed and high surface hardness is produced by quenching to form martensite[10], though the quenching process is less severe than carburizing [8]. Besides the improved surface hardness, carbonitriding can also increase the effective service life of components. As noted by Gesser *et al.* [26], the average life of tools after carbonitriding can be extended by three or four times compared to uncarbonitrided tools in life tests.

Carbonitriding has more strict requirements for application than carburizing because deeper case depths require prohibitive time cycles and higher temperatures and, moreover, the control of nitrogen addition in the furnace atmosphere is more difficult than that of carbon [8, 23]. Typically, carbonitriding is conducted at lower temperatures ranging between 705 and 900 °C and for a shorter processing time than carburizing. The reduced process time and temperature, together with the fact that the nitrogen restrains the diffusion of carbon, results in a shallower iron-carbon-nitrogen compound layer at the surface of steel than usual carburizing practice. The layer thickness ranges from 0.075 to 0.75mm [10, 27]. The exact case composition depends on the process parameters of temperature, time, atmosphere composition, and the type of steel [6, 8]. The preferred case depth of carbonitrided steels is determined by the core hardness and surface requirements of the component. Case depths up to 0.75 mm may be applied to components such as cams for resisting high compressive loads. Many factors will promote the uniformity of case depth for carbonitriding, including uniform processing temperature, accurate time control, adequate circulation and replenishment of the furnace atmosphere, and reasonable distribution of the furnace charge [6, 8, 23].

The concentrations of carbon, nitrogen, and other alloying elements in the case, as well as its phase composition, will influence the hardenability of steel [28]. Nitrogen enhances the hardenability of steel by lowering the critical cooling rate, and improves the resistance of steel to softening at slightly elevated temperatures [9, 29]. Similar to carbon, nitrogen is an austenite stabilizer, which reduces the transformation of austenite

to ferrite and pearlite and lowers the martensite start temperature M_S. [23]. Excessive nitrogen may cause a large amount of retained austenite and case porosity during longer processing times [6, 27].

While carbonitriding can be performed using a salt bath, in a furnace gas atmosphere, or by plasma processing [8], the emphasis in this section is placed on the gas carbonitriding process. The carbonitriding atmosphere is generally composed of a mixture of carrier gas, enriching gas, and ammonia. The atmosphere can be controlled by producing a carrier gas with constant chemical composition and dew point, and by altering the proportion of the enriching gas and ammonia to maintain the desired composition of nitrogen and carbon in the carbonitrided case [6]. The exact gas composition is usually measured through flowmeters, and the gases may be premixed just before they enter the furnace. A typical carbonitriding atmosphere contains 2-12% ammonia within a standard gas carburizing atmosphere [6, 8]; the ammonia is anhydrous ammonia of 99.9+% purity [23].

Depending on the allowable distortion and metallurgical requirements, as well as the type of furnace equipment used, carbonitrided components can be quenched in water, oil or gas. Water quenching is usually applied to low-carbon steel components when the resulting distortion is acceptable. It is optimum for the parts to be directly transferred from the carbonitriding furnace into the air before quenching to avoid possible contamination of the furnace atmosphere by water vapor. Oil quenching is generally used to obtain full hardness with less distortion. It is generally performed at approximately 40 to 105 °C. It is worthwhile noting that quenching oils with a low capacity for dissolving water are desirable to achieve the maximum effectiveness in quenching. Gas quenching is primarily used for reducing distortion, and usually adapted to small-mass components [6, 8, 23].

Although the desired surface properties are obtained by carbonitriding, other issues associated with this process need to be considered. During carbonitriding and its subsequent quenching process, the phase transformation from face-centered cubic austenite to the more open body-centered structures of ferrite and martensite results in both size and shape distortion in the final components [30]. Dimensional distortion may

cause serious assembly issues such as binding or "freezing" in components with high tolerance specifications [6, 10]. Moreover, surface oxidation takes place during processing, and nonuniform surface hardness results from the delayed heat transfer between the quenching die and the workpiece.

Tempering is often performed after carbonitriding by reheating a quench-hardened ferrous alloy to a temperature below the eutectoid temperature (Ac$_1$) for a fixed length of time, then cooling to room temperature at a suitable rate. [31]. Low-carbon steel components are usually tempered in the range of 135-175 °C to stabilize austenite and minimize dimensional distortion [8]. Tempering is primarily used to transform the unstable and brittle as-quenched martensite into a more stable tempered martensite, which increases ductility, yield strength, and toughness, as well as increases the grain size of the matrix [32, 33].

2.1.3 Nitriding

Derived from nitrocarburizing, nitriding is a ferritic thermochemical diffusion method being used in many industrial applications. Similar to carbonitriding, nitriding changes the surface composition by diffusing atomic nitrogen into the steel surface to obtain a hard and wear resistant surface [34-36]. However, nitriding is usually carried out at comparatively low temperatures, ranging from 495 to 565 °C for all steels. Because at these temperatures, nitrogen is added into ferrite instead of austenite, the body-centered cubic ferrite does not change its crystallographic structure or transform into the face-centered cubic austenite. Moreover, because no rapid cooling or quenching occurs during the complete nitriding procedure, dimensional changes resulting from the phase change from austenite to martensite are significantly reduced [17, 23]. All these factors determine how nitriding of steels can produce less dimensional distortion and deformation than the traditional carburizing processes. Only slight volumetric changes of the steel surface exist as a result of the nitrogen diffusion [34].

Several types of nitriding methods have been developed; it can be performed in a gas flow, in a powder, in saline melts, or in a plasma [8, 36]. The primary component of

the nitriding atmosphere is ammonia, sometimes diluted with additional gases such as nitrogen and hydrogen [9].

Generally, the nitriding process produces a thin compound layer at the surface, with a relatively thick (300-500 μm) and hard (900-1200 HV) diffusion zone underneath [37]. The compound layer is also known as the white layer because it etches white in metallographic preparation. The hard and brittle compound layer contains two intermixed phases, epsilon (ε) and gamma prime (γ'). The region below the compound layer is called the "diffusion zone", and consists of stable nitrides formed by the reaction of nitrogen with nitride-forming elements [17]. The solubility of nitrogen in iron leads to the formation of a solid solution with ferrite at nitrogen contents up to about 6%. When the nitrogen content is about 6%, gamma prime Fe_4N is produced. When the nitrogen content is greater than 8%, the epsilon compound Fe_3N is produced. The carbon content also influences the composition of the compound layer. Higher carbon contents of the steel lead to the formation of more ε-phase, whereas a lower carbon content is responsible for an increase in the γ' phase. The thickness of the compound layer depends on the nitriding time, temperature, and gas composition [17, 34].

2.1.4 Ferritic Nitrocarburizing

Nitrocarburizing is a modified form of nitriding, which involves the addition by diffusion of both nitrogen and carbon to the surface of ferrous or non-ferrous materials at elevated temperature. Nitrocarburizing can be classified into ferritic nitrocarburizing and austenitic nitrocarburizing, depending on the type of phase transitions and material properties obtained. Ferritic nitrocarburizing is primarily used to improve the surface properties of low alloy steels by producing a hard, wear and corrosion resistant surface without changing the core properties. Austenitic nitrocarburizing is usually applied to plain carbon steels to upgrade both the surface and the core properties [38, 39]. The emphasis of this section is on the ferritic nitrocarburizing process.

Ferritic nitrocarburizing takes place completely within the ferrite phase field below the Ac_1 temperature, in the range of 525 and 650 °C [8, 18]. In this procedure, nitrogen resulting from the dissociation of ammonia penetrates into a solid solution of

iron simultaneously with carbon and gets trapped within the interstitial lattice spaces in the steel structure [8, 17, 40]. The nitrogen is considerably more soluble in steel than carbon and therefore mainly diffuses into the material, while the carbon forms iron or alloy carbide particles at, or near, the surface [41].

Typically, nitrocarburizing imparts a nitrogen-rich compound layer at the surface of the material, and an underlying diffusion zone [8, 17]. Similar to nitriding, the compound layer for nitrocarburizing consists predominantly of the same two metallurgical phases of both epsilon and gamma prime nitrides. The single-phase epsilon (ε) iron-carbonitride ($Fe_{2-3}(N,C)$) is a ternary compound of iron, nitrogen and carbon with a hexagonal structure. Both the carbon content of the steel and the presence of nitride-forming elements on the steel surface will affect the balance of the epsilon and gamma prime phases. The composition of the process atmosphere is another factor influencing the phase composition [8, 19]. The compound layer is usually 10 to 40 μm thick, providing good physical and chemical properties against galling, scuffing, wear and corrosion [10, 42]. The diffusion zone, which consists of iron (and alloy) nitrides and dissolved nitrogen, improves fatigue endurance and case hardness [4, 8, 43]. The diffusion depth of nitrogen is directly responsible for the improvement in fatigue properties, particularly in carbon and low-alloy steels [18, 44]. The compound-diffusion layer may contain varying amounts of gamma prime (γ'), ε-phase, cementite and various alloy nitrides and carbides, depending on the nitride-forming elements in the material, temperature, nitrocarburizing time, and the composition of the atmosphere. The total thickness of the compound layer and the diffusion zone can reach 1mm [8, 18, 45].

A comparison of the typical metallographic structures of nitrocarburized and carbonitrided steel is shown in Figure 2.1 [46]. The ferritic nitrocarburizing was performed at a lower temperature of 570 °C, and nitrogen is the predominant element in the epsilon compound layer and diffusion zone. Whereas the carbonitriding was carried out at a higher temperature of 850 °C, and carbon predominates in the formation of the martensitic layer. The thickness difference of the compound layer between the two is also obvious, with only a very thin compound layer being formed on the steel surface after nitrocarburizing.
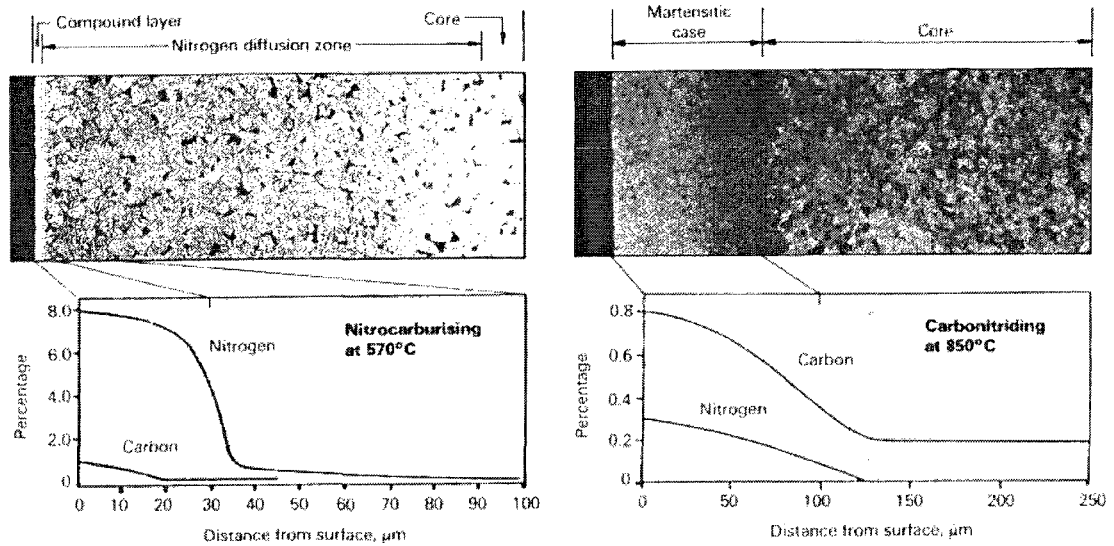
Figure 2.1 Comparison between the nitrocarburizing and carbonitriding [46].

Besides the improvements to the surface characteristics, ferritic nitrocarburizing can also reduce the risk of distortion. Because the procedure is carried out at a low temperature, the steel microstructure remains in the ferritic region and no phase transformation occurs. Moreover, the subsequent quenching process commonly used to form martensite is eliminated. As a result, distortion resulting from either the released induced stresses, the thermal shock of quenching, or the incomplete transformation to martensite can be significantly reduced [17, 19, 47]. Additional processing operations, such as finish grinding to correct distortion, can be eliminated, which helps to lower production times and part costs. Previous studies by the research group at the University of Windsor have demonstrated the advantages of nitrocarburizing over carbonitriding with respect to the dimensional changes in a stamped automotive component fabricated from SAE 1010 plain carbon steel [14, 48].

The nitrocarburizing atmosphere is predominantly composed of ammonia and some carbon- and oxygen-bearing gases [9]. The carbon in the nitrocarburizing atmosphere is an ε-phase stabilizer, which helps to form the compound layer at much lower nitrogen contents. The oxygen or combined oxygen additions in the nitrocarburizing atmosphere are used to decrease the carbon activity in the gas phase

11

[18]. Another important function of oxygen is to create a surface oxide layer on top of the diffusion-formed case to resist corrosion [19].

Several different methods of accomplishing the ferritic nitrocarburizing process have been developed in the last few decades, including liquid procedures, gaseous methods, and ion (plasma) procedures. The gas, vacuum, and ion ferritic nitrocarburizing processes are detailed in the following sections.

2.1.4.1 Gas Ferritic Nitrocarburizing

Gas ferritic nitrocarburizing as an industrial process was patented by Lucas (Industries) Ltd. in 1961, and has received serious industrial attention since the early 1970s [42, 49]. Gas nitrocarburizing is performed just below the austenite range for the iron-nitrogen system, in a temperature range of 450-590 °C [18, 50]. Parts are generally treated at about 570 °C for 1 to 3 hours [8]. A number of gas mixtures are used for commercial production; a typical industrial gas nitrocarburizing atmosphere is comprised of ammonia (NH_3), hydrocarbon gas (*e.g.* methane or propane), and an endothermic gas [19].

Gas nitrocarburizing is a significant improvement over the conventional liquid approach. The cost for gas nitrocarburizing is much lower, and the whole process is nontoxic. The compound layer formed after gas nitrocarburizing is denser and its surface is not eroded. Further, it is easier to control the gas atmosphere and to optimize the structure and composition of the nitride layer, which make the automatic batch production possible [51].

2.1.4.2 Vacuum Ferritic Nitrocarburizing

Heat treating in vacuum commonly refers to a process carried out in a space with a highly reduced gas density, rather than a space entirely devoid of matter. The primary objective of using vacuum for heat treating is to avoid the surface oxidation that occurs during heat treatment in air. It can be accomplished in several ways. One is to replace the air in the treatment furnace with a protective atmosphere that contains almost no oxygen, such as by using nitrogen as the inert atmosphere. Another way is to reduce the amount of air surrounding the workpieces during processing to keep the oxygen content below

12

the oxidation level of the material [52, 53]. The latter approach is applicable to vacuum nitrocarburizing.

Vacuum nitrocarburizing is a subatmospheric nitrocarburizing process that uses a basic atmosphere of 50% ammonia / 50% methane, as well as controlled oxygen additions of up to 2% [31, 54]. Vacuum processing has several predominant advantages: it produces a very pure starting atmosphere; and it eliminates the need for a nitrogen purge. It is also a more environmentally friendly process; no fumes or exhaust gases are released during vacuum nitrocarburizing [42, 55]. The cold vacuum furnaces are also favorable to smaller heat accumulation and faster heating and cooling performance. On the other hand, there are problems associated with vacuum nitrocarburizing, such as the greater adsorption of gases and water vapor on both the cooled furnace walls, as well as the insulation after opening of the furnace [52].

2.1.4.3 Ion Ferritic Nitrocarburizing

Ion (plasma) nitrocarburizing is a modified ion nitriding method that involves glow discharge technology to add elemental nitrogen to the work surface for subsequent diffusion into the material [56]. Ion nitrocarburizing is generally conducted near 570 °C to form a compound layer greater than 5 μm and a surface hardness higher than 350 HV [8, 50]. The composition of the plasma atmosphere is a mixture of hydrogen, nitrogen and a carbon-bearing gas, such as methane (natural gas) or carbon dioxide [8]. Control of the gas flow to obtain the appropriate phases during ion ferritic nitrocarburizing is not simple, due to the difficulties in measuring the gas decomposition, nitrogen potential, and the content of free oxygen. Usually, it is accomplished by controlling the gas ratios of the nitrogen, hydrogen, and hydrocarbon gases in the atmosphere [19].

The compound layer produced by ion nitrocarburizing is usually composed of ε and γ' phases for low carbon-level atmospheres [8, 18]. Previous research has indicated that a monophase structure is favored for improving tribological properties; other phases existing in the compound layer can help to enhance the corrosion resistance [57, 58].

Ion nitrocarburizing is an environmentally friendly process that produces no toxic fumes or waste. There are no significant dirt, noise or heat pollution, or even risks of

13

explosion accompanying it [8, 18]. Ion nitrocarburizing is also an economical heat treatment method that accelerates the penetration of nitrogen and carbon, contributing to reduced processing times and energy consumption [59, 60]. Moreover, the plasma processes offer several additional possibilities for parameter variation, which consequently provide a better control of the layer structure, morphology, and service characteristics [39, 61]. Ion nitrocarburizing has been widely applied to various materials such as carbon steels, alloy steels, tool steels, stainless steels, cast irons, and sintered materials [62, 63]. However, the use of direct plasma processes can lead to sputtering and accordingly decrease the diffusion depth for a given time [64].

2.2 Navy C-Rings and Torque Converter Pistons

For some period of time, Navy C-ring specimens have been an important tool in studying distortion of heat treated materials [20, 65]. The use of Navy C-rings can be traced back to 1921, when they were first used by the US Navy in the inspection of class 5 tool steels [66]. Currently, there are no standard dimensions for Navy C-ring specimens. Specimens are typically fabricated from the desired testing material and machined into a variety of sizes. A simplified Navy C-ring sample used in a quench distortion study and a modified Navy C-ring distortion test specimen are shown in Figure 2.2 [13, 67].

(a)   (b)
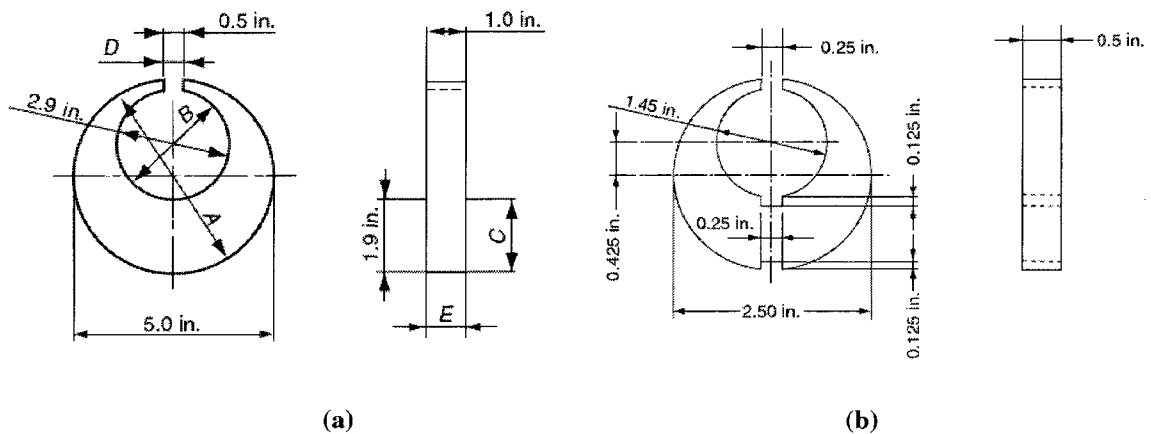
Figure 2.2 Navy C-ring Geometry.
(a) Simplified Navy C-ring specimen; (b) Modified Navy C-ring specimen [13, 67].

A torque converter piston is an important component of an automotive transmission. The desired specifications for a piston used by Chrysler are as follows: outside diameter (OD) of 260 mm, inside diameter (ID) of 62 mm and a weight of 1.8 kg [11]. The geometry of a piston sample and an assembled unit are shown in Figures 2.3 (a) and (b), respectively.

(a)   (b)
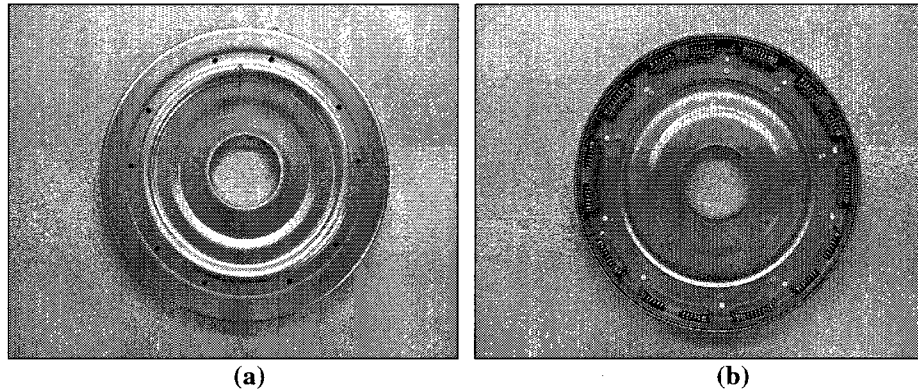
Figure 2.3 Torque converter piston and piston-retainer assembly.

(a) Torque converter piston; (b) Piston assembled with springs and retainer.

2.2.1 Fabrication of Torque Converter Pistons

The torque converter pistons are made from 2.8 mm thick sheets of cold-worked SAE 1010 steel. The current manufacturing process for torque converter pistons consists of three basic steps: surface hardening, press quenching, and tempering, as illustrated schematically in Figure 2.4.
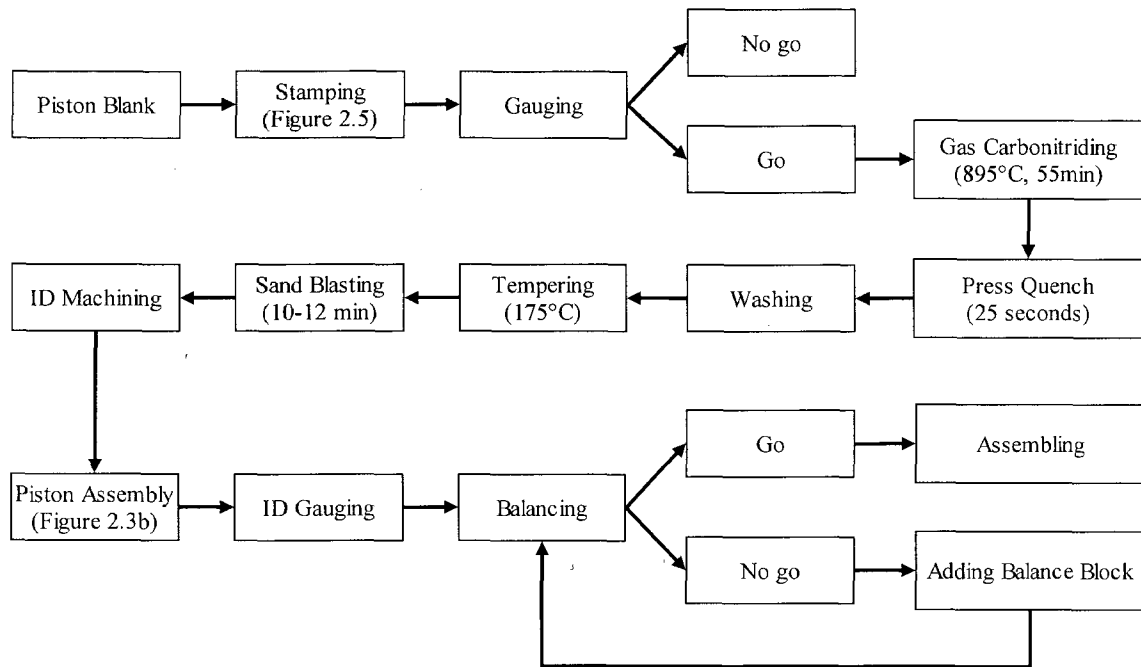
Figure 2.4 Flowchart of torque converter piston fabrication.

Beginning as circular blanks, the pistons go through a progressive five-stage stamping operation to form the desired geometrical dimensions and shapes, Figure 2.5. The qualified pistons will be selected by gauging and delivered to the subsequent case hardening station.

Carbonitriding is applied to the pistons to improve the surface hardness and wear resistance. After a pre-cleaning step to remove surface contaminants, the pistons are fed into a rotary hearth furnace with an atmosphere mixture of natural gas, nitrogen and ammonia. The carbonitriding temperature was set at 895 °C, and the furnace cycle time for a batch of pistons is about 55 minutes. During processing, both nitrogen and carbon are absorbed and diffused into the surface of pistons to enhance the surface hardness. The heat treated components are then removed from the furnace and go through a press quenching process. Press quenching can offer remarkable dimensional control, because the workpiece is restrained in dies while the quenchant flows across the various parts of the surface until the part is fully cooled to a predetermined temperature [68]. The pistons are subjected to press quenching for 25 seconds in Aqua-Quench 140, a water-based

16

quench medium maintained at a concentration of 9-11%. The quench bath temperature is controlled at 50 °C, and forces up to 50 kN are used. A typical profile of a press-quench die is shown in Figure 2.6. The surface hardness of pistons is remarkably improved upon quenching by the formation of a martensitic case.

(a)   (b)

(c)   (d)

(e)   (f)
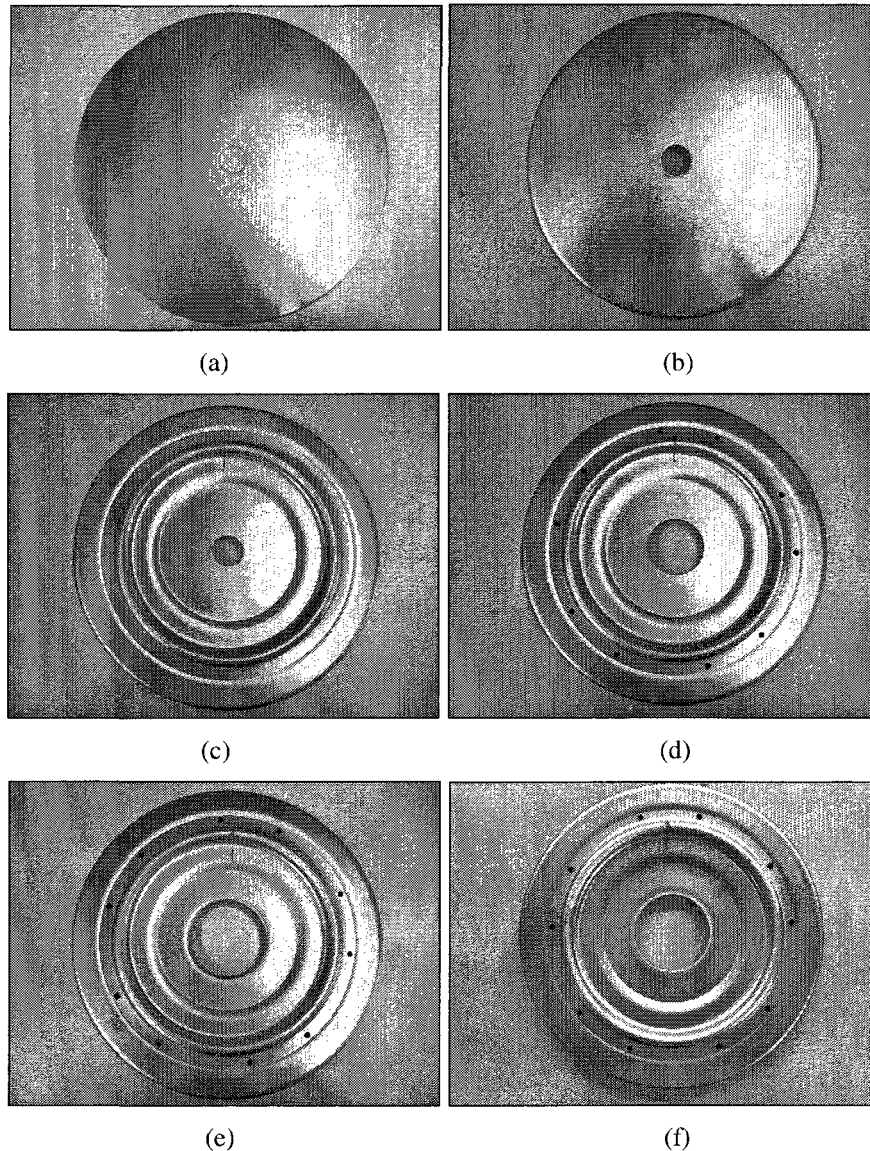
Figure 2.5 Five stage stamping operation of a torque converter piston. (a) Piston blank; (b) piston at stamping stage 1; (c) at stamping stage 2; (d) at stamping stage 3; (e) at stamping stage 4; and (f) at stamping stage 5.
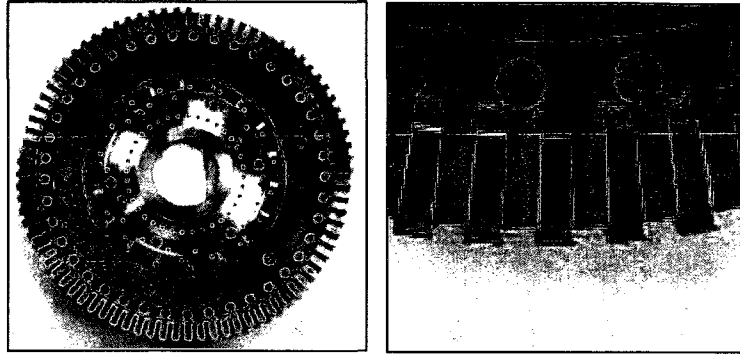
Figure 2.6 A press-quench die. (a) Front view of a press-quench die; (b) magnified view of the die edge. *Courtesy of Toledo Machining Plant, Toledo, Ohio U.S.A.*

The pistons are then drained, washed, and dried prior to tempering. Tempering is conducted to stabilize the austenite and minimize dimensional variations. Pistons are reheated to 175 °C for 1 hour, before being removed from the furnace and transferred to a cooling station, where they are cooled to ambient temperature. The pistons are then subjected to a sand blasting operation for 10-12 minutes to remove the surface oxide scale formed during the heat treatment. After grinding the inside diameter (ID) of piston to meet the dimension specifications, each piston is joined together with a retainer and springs using rivets, the assembled unit was shown in Figure 2.3(b). In the final stages of production, the assembly undergoes two more quality inspections: ID gauging, and mass balancing.

2.2.2 Pistons in Torque Converter

A torque converter is a modified form of fluid coupling, which is used to transfer rotating power from a prime mover, such as an internal combustion engine or electric motor, to a rotating driven load. Similar to basic fluid coupling, the torque converter takes the place of a mechanical clutch, allowing the load to be separated from the power source. The superiority of a torque converter over fluid coupling is that it can multiply the torque when there is a substantial difference between input and output rotational speed, thus providing the equivalent of a reduction gear [69, 70].

In a torque converter, there are at least three rotating elements: the pump impeller, which is mechanically driven by the prime mover; the turbine runner, which drives the

18

load; and the stator, which is interposed between the pump and turbine so that it can alter oil flow returning from the turbine to the pump [70]. These elements are shown in Figure 2.7.
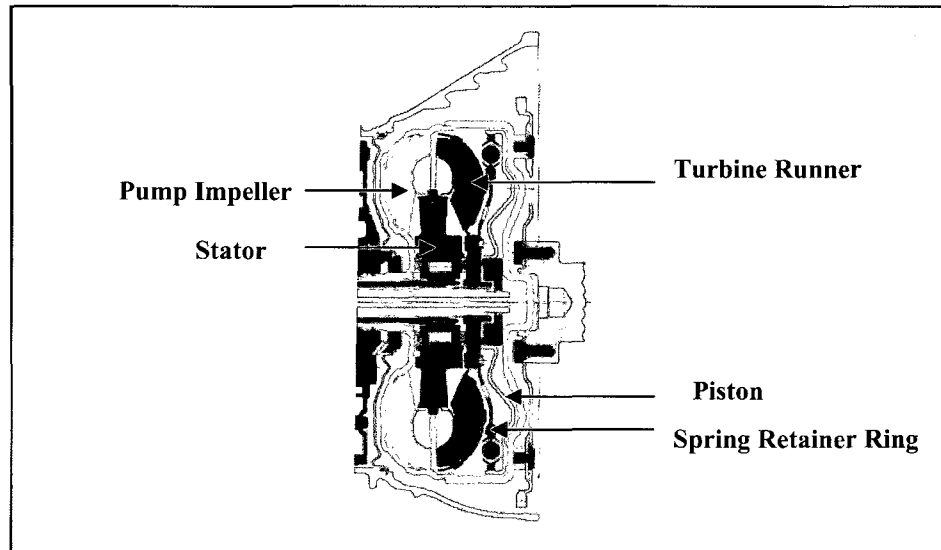
Figure 2.7 Schematic diagram of a torque converter assembly including the stator, impeller, turbine, spring retainer ring, and torque converter piston. *Courtesy of Chrysler LLC, Auburn Hills, Michigan U.S.A.*

When the impeller and turbine are rotating at almost the same speed, no torque multiplication takes place, and the ratio of output torque to input torque equals to one. In practice, however, there is an approximately 4-5% difference in rotational speed between the turbine and impeller, which leads to energy losses. A lockup piston clutch is used to prevent this problem. The lockup piston clutch consists of a piston, damper assembly, and a clutch friction plate. The damper assembly, which contains a damper and several coil springs, is used to transmit driving torque and absorb shock. The lockup piston clutch is located between the front of the turbine and the interior front face of the shell. Under the control of hydraulic valves, engaging and disengaging of the lockup clutch is implemented by the difference in pressure on either side of the lockup clutch. Successful engagement of the lockup piston clutch between the impeller and the turbine assembly can substantially improve fuel economy and reduce operational heat and engine speed [12, 71].

2.3 Distortion

Distortion is an inevitable problem associated with thermal processing techniques, especially for heat treatment procedures, due to high temperatures and severe thermal gradients during heating and quenching. When parts are heat treated, unpredictable or inconsistent change in size or shape is produced by the complex interaction between the heat treating environment and the thermal-mechanical and metallurgical evolution in the heat treated components [72].

2.3.1 Basic Distortion Mechanisms

There are three fundamental reasons accounting for the size and shape variations of workpieces during heat treating [13, 73].

First of all, residual stresses may lead to shape distortion during heating once they exceed the yield strength of the material. Materials containing residual stresses prior to heat treatment will relieve those stresses during heat treatment. The relaxation of these stresses is achieved when the existing residual stresses exceed the yield strength of the material upon heating [68, 74]. A typical diagram illustrating the relationship of the stress and strain for a tension test is shown in Figure 2.8 [75]. During the initial stages of the tension test, elastic deformation of the material takes place. When the increased stress becomes larger than the yield strength of the material, permanent plastic deformation occurs. As the dimensional shape of the components is varied by plastic flow, the stresses present in the material are gradually relieved. In general, the yield strength of a material decreases as the heat treating temperature increases. Moreover, the extent of the resulting plastic deformation depends on the magnitude and distribution of the stress field in the material [13].
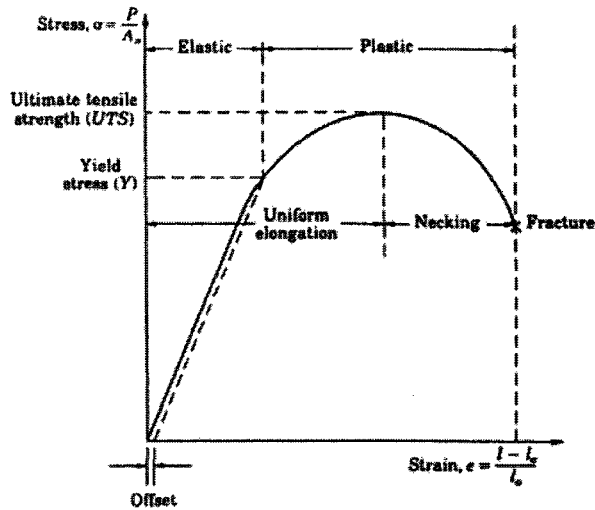
Figure 2.8 Characteristics of a typical stress-strain curve obtained from a tension test [75].

Secondly, thermal stresses resulting from the differential expansion associated with the thermal gradients may produce plastic deformation when the stresses exceed the yield strength of the material. If a part could be processed at the same heating rate throughout the whole section, uniform expansion occurs and the part dimensions will be maintained. However, in actual heat treatment practice, a thermal gradient exists across the cross section of the part. Differential thermal expansion will cause sizable thermal strains, whereby the first part of the component to be heated will expand earlier and occupy a greater volume than the colder surrounding area, consequently leading to thermal stresses within the components. When the thermal stresses exceed the yield strength of the material, plastic deformation occurs [76]. These material movements are associated with the heating rate applied, the coefficient of thermal expansion, and the geometry and properties of the component.

Thirdly, phase transformations during heat treating result in volume changes; these changes are constrained in the residual stress systems until the resulting stresses exceed the yield strength of the material. When a steel part is heat treated, phase transformations occur accompanied by their respective volume changes due to the variation of the microstructure and carbon content in the steel. As an example, consider the phase transformation of a ferrite/cementite microstructure during heating and cooling. On heating, a volume contraction occurs due to the formation of the close-packed atomic

21

structure of the face-centered cubic (fcc) austenite phase. On cooling, there is a subsequent volume expansion. Variations in the linear dimensions of a steel under both slow cooling and fast quenching conditions are shown in Figure 2.9 [67]. On slow cooling, the steel component experiences a size distortion as its crystal structure changes from the more densely packed fcc austenite phase to the less densely packed body-centered cubic (bcc) ferrite phase. When the steel is treated at a faster cooling rate by quenching, instead of forming ferrite, the even less densely packed body-centered tetragonal structure of martensite will be produced. When the stresses resulting from these volume changes exceed the yield strength of the material, dimensional deformation takes place. As shown in the Figure 2.9, the steel contracts until the M_S temperature is reached, at which point there is a volumetric expansion during martensite formation at lower temperatures. The volume and shape variations are related to the heating rate, the geometry of the component, and the phase volume change [13, 67, 77].
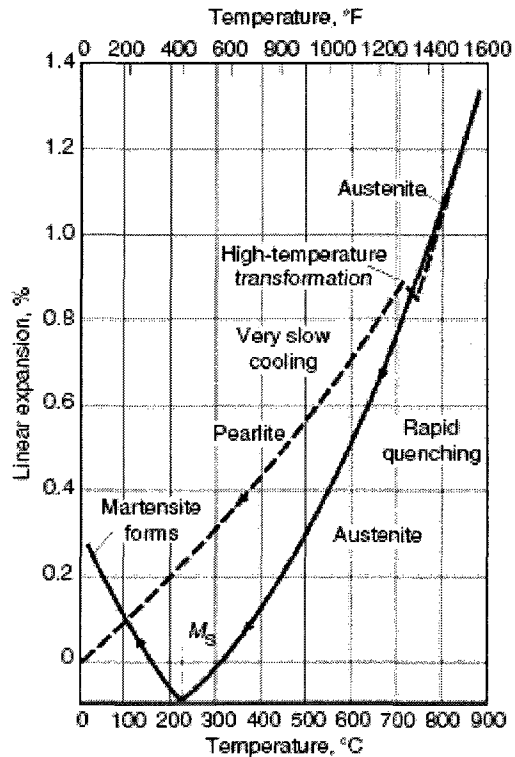
Figure 2.9 The dimension expansion and contraction of steel upon cooling [67].

2.3.2 Size and Shape Distortion

Distortion is generally classified as size distortion and shape distortion according to the sources from which the deformation occurs and the various types of dimensional variation. Size distortion is the result of changes in the volume or linear dimensions of a part, and manifests in the form of elongation, shrinkage, thickening, or thinning [17, 19, 78]. It is induced by the thermal expansion or contraction of a material microstructure during heating and cooling, and is directly related to the variation in crystal structure that accompanies phase transformations during heat treatment [10, 19]. Size distortion is somewhat predictable and can usually be accommodated in the design stage because it is mainly related to the density change between the initial phases and the newly formed phases [10, 79, 80].

Shape distortion refers to changes in the geometrical form or shape of a part, which undergoes changes of curvature or angular relations, twisting, bending, and other nonsymmetrical changes in dimensions without any volume change [13, 17, 78]. Shape distortion results from either residual or applied stresses due to the nonuniform thermal gradients throughout the components, asymmetrical changes in metallurgical structure, and variations in homogeneity of the material [10, 78]. Compared to size distortion, shape distortion is often more difficult to predict due to its more complex nature and causes.

2.3.3 Distortion during Carbonitriding and Nitrocarburizing

Generally, both size and shape distortions are generated during a heat treatment process. For carbonitriding procedure, the occurrence of distortion primarily results from the diffusion of surface hardening elements and the quenching operation. The penetration of carbon and nitrogen atoms into steel modifies the crystal structure of steel surface, resulting in volume expansion and stretching of the core. As a result, tensile stresses develop in the core, which are balanced by compressive stresses present at the surface. Once the internal stresses exceed the yield strength of the material, permanent distortion occurs. The amount of volume growth is related to the thickness of the compound layer formed at the surface of the material [13, 19].

The phase transformation from austenite to martensite upon quenching is another source of distortion [10]. The transformation to martensite is accompanied by a volume expansion given by the following formula [68, 77, 80]:

Percentage volume expansion = [4.64 - 0.53× (wt. % carbon)] ×100%   **Equation 2-1**

When the steel component is quenched to the martensite start temperature M_S, martensite formation occurs. The martensite transformation is accompanied by a volume expansion, because the untempered martensite phase has the largest volume of all the steel phases. Increasing carbon content in the steel further lowers the M_S, and ultimately influences the extent of distortion. On the other hand, the thermal gradients resulting from the nonuniform heat transfer during quenching are responsible for shape distortion. The resultant distortions are associated with the cooling rate, quenching uniformity, the geometry and properties of the steel, as well as the surface condition of the components. It is known that faster cooling rates result in a greater risk of distortion [13, 68]. After the martensite transformation, the steel ultimately experiences thermal contraction upon further cooling to room temperature [21, 77].

Moreover, the presence of residual stresses from a previous manufacturing operation also leads to dimensional changes, when the stresses are relieved by heating and exceeding the yield strength of the material.

During nitrocarburizing, when the hardening species of carbon and nitrogen are absorbed and diffuse into the steel, a certain degree of volume expansion occurs due to the changes of crystal structure, and new structure formations, *e.g.*, $Fe_{2-3}(C,N)$ [19]. Because the nitrocarburizing process is performed at relatively low temperatures, and quenching is not a necessary procedure, distortion due to phase transformations is a minor problem. The size and shape distortion is believed to be associated with the thermochemical treatment process itself [20].

2.3.4 Distortion Correction

The irreversible changes in size or shape of steel components can be corrected by thermal processing approaches, such as cold treating, annealing or tempering.

Mechanical processing such as finish grinding is also used to remove excess material or to redistribute residual stresses.

Grinding is traditionally regarded as a final machining process which uses hard abrasive particles as the cutting medium to remove superfluous matter from the part surface. As a primary manufacturing method, grinding has accounted for about 20-25% of the total cost of machining operations in industrialized countries [81]. Preferred properties can be obtained through grinding by correcting dimensional changes of components, eliminating excessive surface roughness, and removing unwanted surface microstructural characteristics [13, 82]. A schematic of a straight surface grinding operation is shown in Figure 2.10 [81]. A wheel with diameter of d_s rotates with a peripheral velocity of v_s, cutting off a wheel depth of a from the workpiece as it moves at velocity v_w. The depth of cut a depends on the machine down feeds, and is usually in the range of 10-50 μm [81].
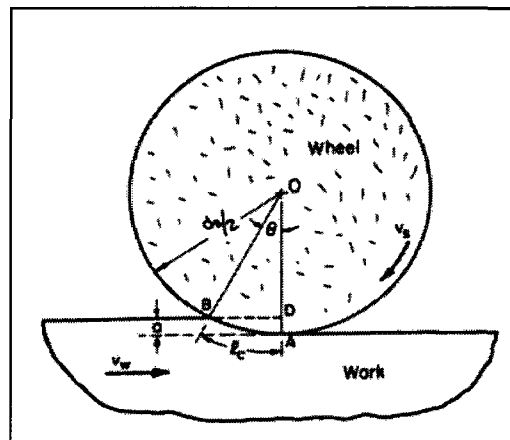
Figure 2.10 Illustration of two-dimensional plunge grinding operation on straight surface [81].

Great care is needed in the grinding operation to ensure accurate dimensional controls, especially for parts with close tolerances that may cause serious assembly problems. An example of gear grinding after case hardening is shown in Figure 2.11. The tooth of the gear has distorted to the right, and excessive material is ground away from the right side of the tooth. The resultant nonuniform case thickness causes uneven

residual stresses. Moreover, the actual mechanical strength of the gear has been weakened. Also, with a considerable amount of material being removed during grinding, there is an increasing risk of grinding burns and cracking [13, 83].
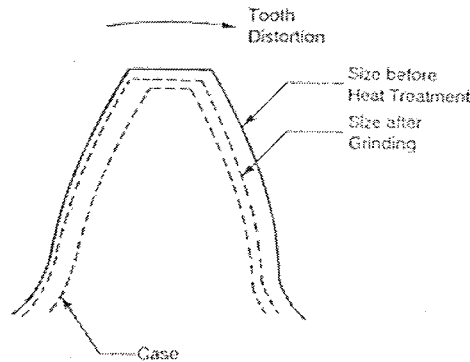
Figure 2.11 Schematic of material ground from a distorted gear tooth after case hardening treatment [13, 83].

As pointed out by Parrish [82], the observed residual stresses distributions resulting from grinding can be classified into three types, Figure 2.12. The stress distribution in Type I are caused by abusive grinding, which is accompanied by surface burning or cracking. A typical residual stress distribution after grinding is shown in Type II, in which heat is generated to produce the tensile peak, but where plastic deformation near the surface has regained the balance a little. When extremely good grinding techniques are adopted, the residual stress profile shown in Type III can be obtained. Type III is an ideal condition in which the whole heat treatment process is under good control so that only mechanical effects such as surface work hardening will be operational. It also helps to improve the fatigue resistance of the component [82, 84].
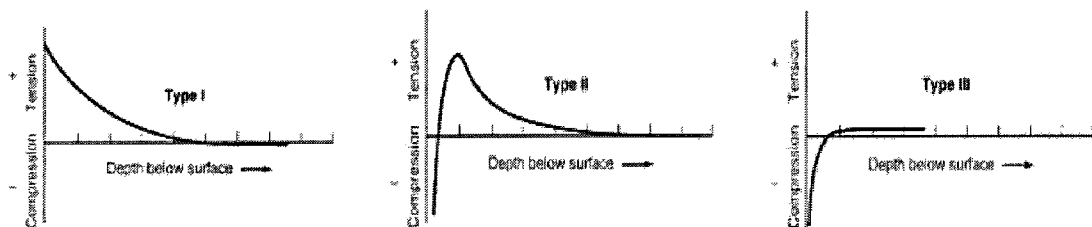
Figure 2.12 Three types of grinding stress distributions [82].

26

2.4 Residual Stresses

Residual stresses are defined as the stresses present in a component with no external force or moment acting upon it [85, 86]. They are an inevitable result of thermomechanical processing of steel, and can significantly affect the effective service life of a component [87]. The residual stresses present in a heat treated component results from the thermal or transformation stresses existing in the material [88].

2.4.1 Origins of Residual Stresses

The origins of residual stresses can be essentially divided into two categories, namely thermal stresses and transformation stresses. Thermal stresses usually develop in components where thermal expansion or contraction occurs due to temperature gradients, especially when nonuniform heating or cooling takes place. If one part of the workpiece is hotter or cooler than the other, it tends to expand more whereas the rest expands less, consequently causing thermal stresses to arise [80, 88]. In a heat treatment process, the heating and cooling procedure results in temperature differences between the surface and the core. If a quenching process is used to obtain a fast cooling rate, then much greater residual stresses will develop as a result of the high temperature gradients present through the cross section of the component [80, 86].

Figure 2.13 shows an example of the temperature difference between the surface and core of an ideal linear-elastic cylinder after quenching [86]. At the beginning of quenching, the surface of the cylinder contracts more rapidly than the core due to the temperature difference. As a result, tensile stresses are produced in the longitudinal and tangential directions, and compressive stresses in the radial direction of the cylinder surface. These stresses are balanced by the compressive stresses in the longitudinal, tangential and radial directions within the core of the cylinder. The largest temperature difference occurs at time t_{max}, where the slopes of temperature-time curves are identical for both the core and the surface. In the graph, σ_l^{sh} represent the longitudinal thermal stresses.
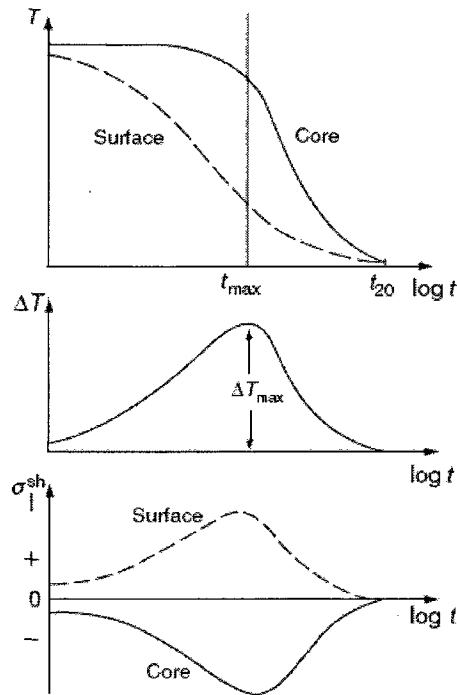
Figure 2.13 Temperature difference during transformation-free quenching of an ideal linear-elastic cylinder [86].

The range of thermal stresses is influenced by a number of factors, including the thermal conductivity of the material, modulus of elasticity, and the coefficient of expansion of the material. The interrelationship between these factors can be indicated in the following formula, which is used to evaluate the thermal stresses developed in a constrained part due to temperature differences upon cooling [77, 88].

$$\sigma_{thermal} = E \cdot \alpha \cdot \Delta T \qquad\qquad \textbf{Equation 2-2}$$

In the above equation, $\sigma_{thermal}$ is the thermal stress; E is the modulus of elasticity; α is the coefficient of thermal expansion of the material; and ΔT is the temperature difference between different material sections. The temperature gradients are affected by the thermal conductivity of the material. For good conductors such as copper and aluminum, high temperature gradients are not likely to accumulate. Conversely, conductors with lower thermal conductivity values, such as steel and titanium, are more susceptible to developing higher temperature gradients accompanied by greater thermal stresses values.

28

The second type of residual stresses, transformation stresses, are developed as a result of the crystal structure changes in components, usually occurring in high temperature heat treatment processes. Any phase transformation that is accompanied by a volume changes will produce or modify the residual stress state in a material [80, 89]. Transformation stresses are influenced by the microstructure and properties of the material (*e.g.* hardenability), transformation characteristics such as volume changes and temperature ranges, and cooling rate [10, 30].

Transformation stresses are commonly developed in steel components after quenching, in which the decomposition of austenite to martensite results in a volume expansion of the microstructure and leads to the formation of residual stresses [80, 88]. In Figure 2.14, pure longitudinal transformation stresses are developed in an ideal linear-elastic cylinder after quenching. As noted, the formation of martensite is responsible for the volume expansion. After reaching the martensite start temperature M_S at time t_1, the martensitic transformation starts, causing compressive transformational stresses to develop at the surface. In order to establish equilibrium, tensile transformational stresses within the core of the cylinder are produced. Both the tensile and compressive stresses start to increase upon further surface cooling, reaching maximum values at time t_2, and decrease thereafter [86, 90].
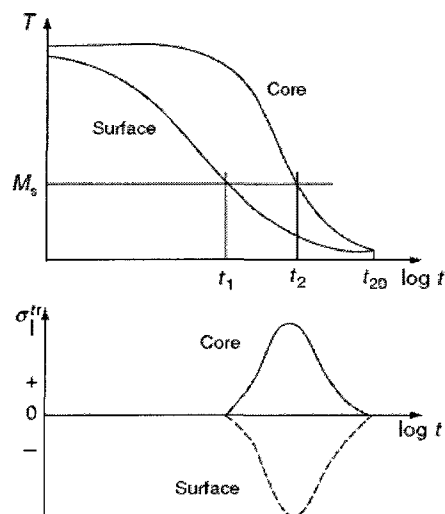
Figure 2.14 Development of longitudinal transformation stresses in an ideal linear-elastic cylinder after quenching [86].

29

2.4.2 Residual Stresses in Surface Hardened Steels

When both the thermal and transformation stresses are present in the material, the residual stress pattern gets more complicated and less predictable. In Figure 2.15, the thermal and transformation stresses act simultaneously on the same cylinder that discussed above. The stresses arise due to the temperature gradient and phase transformation from austenite to martensite upon quenching. The upper graph shows the longitudinal thermal and transformation stresses at surface and core as a function of time. The superposition of the two stresses is shown in the lower graph. The ideal total stress curve reveals that, with the increasing martensitic transformation, a stress reversion takes place in both the surface and the core of the cylinder [86].
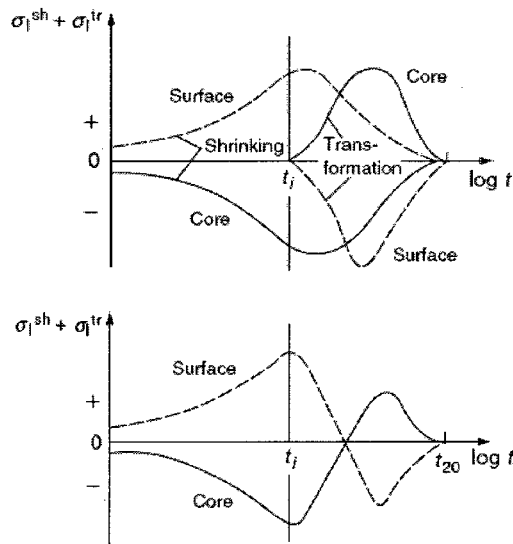
Figure 2.15 Combined thermal and transformation stresses during quenching of an ideal linear-elastic cylinder that transformations from austenite to martensite [86].

Residual stresses are generally present in case hardened components. Compressive residual stresses in the surface layer are beneficial because they enhance the overall surface quality of the material by improving resistance to fatigue, stress corrosion, and hydrogen embrittlement, as well as preventing the occurrence of new cracks and possible propagation of existing cracks. Conversely, tensile surface stresses are detrimental due to the decrease in fatigue strength. The fatigue strength of a

30

component depends on the material properties, the quality of the surface treatment, and its response to the dynamic load such as tension-torsion, and the resulting stresses and their distribution across the section [80, 86].

2.4.2.1 Residual Stresses in Carbonitrided Steels

Carburizing and carbonitriding generally result in compressive residual stress in the surface of steel components, which can be used to enhance the surface properties including fatigue and wear resistance [6, 84]. Quenching of carbonitrided or carburized steel initially causes thermal stresses to develop due to the thermal gradient in the steel; these stresses lead to a volumetric contraction. During quenching, the phase transformation from austenite to martensite or to ferrite and pearlite also occurs, which results in transformation stresses. The thermal stresses combined with the transformation stresses determine the total stress state in the material. As noted by Macherauch and Völhringer [91], the actual residual stress state in steel cannot be obtained by simply superimposing the thermal and transformation stresses. In general, the martensitic transformation upon quenching, which is accompanied by a volume contraction, always contributes to more negative values of the existing stress. The inhomogeneous distribution of carbon and nitrogen based on the thermochemical surface treating also affects the resultant residual stresses fields in the material. Tempering is often performed after the quenching process to relieve residual stresses, especially when unfavorable tensile surface stresses are developed [84, 88].

2.4.2.2 Residual Stresses in Nitrocarburized Steels

The residual stresses resulting from nitriding and nitrocarburizing processes are more complicated due to the special characteristics of the compound layer and the diffusion zone. The residual stresses in the compound layer are less understood due to not only the technical difficulties associated with using XRD techniques on thin layers, but also related to the dissolution in the compound layer of carbide particles from the pearlite grains of the substrate [92]. Because nitrocarburizing is performed at lower temperature, no austenitic transformation occurs and the structure remains in the ferritic field.

Consequently, no specific transformational residual stresses arise. It is generally agreed that tensile stresses are present within the epsilon compound surface layer, whereas compressive stresses are associated with the underlying diffusion zone. The compressive stresses play a more important role in the residual stress state of the steel due to their considerable contribution toward the improvement in fatigue strength [77, 92].

2.4.3 Measurement of Residual Stresses Using X-Ray Diffraction

X-ray diffraction (XRD) has been widely applied to the measurement of residual stress in crystalline materials in industry. It is a nondestructive measurement method with high spatial resolution and speed, as well as excellent accuracy [93]. A crystalline sample is irradiated with x-rays and the distance between crystallographic planes is used as a strain gage to evaluate the residual stresses. The diffracted angle (2θ) is measured experimentally and the x-ray wavelength (λ) is already known. The interplanar spacing (d-spacing) for any set of parallel crystallographic planes is calculated using Bragg's Law [13, 93, 94], Equation 2-3. This relationship is illustrated in Figure 2.16. The value of n is an integer equal to the order of reflection. For stress measurements, the value of n is usually unity.

$$n\lambda = 2d\sin\theta \qquad\qquad \textbf{Equation 2-3}$$
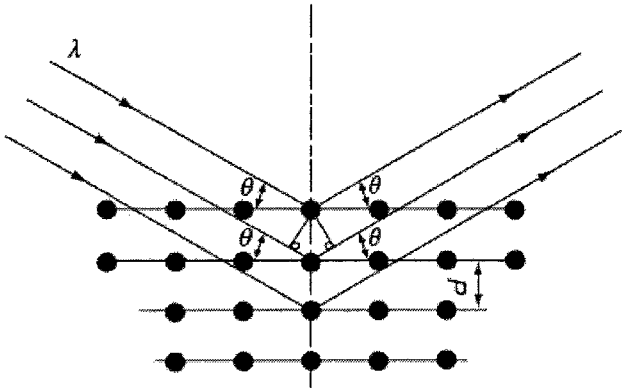
Figure 2.16 Illustration of the Bragg relation [13].

When residual stresses are developed in material, they cause a shift in the x-ray diffraction peak angular position, which can be directly measured by a detector to

determine the residual stress state. The d-spacing increases when the material is in tension and decreases when it is in compression. Because the spacing between the planes is so small, it is affected by both macro and micro stresses both of which are measured using the x-ray method [93, 94]. Based on the d-spacing values measured for the unstressed (d_o) and stressed (d) conditions, the strain (ε) is then calculate using Equation 2-4 [94, 95]:

$$\varepsilon = \frac{d - d_o}{d_o}$$ **Equation 2-4**

Since the x-ray diffraction method was first applied to the evaluation of the residual stresses, several improvements have been made in the methodology. The most common one is the $\sin^2\psi$ method, in which the crystallographic sample is irradiated and changes in the diffraction pattern are related to the interplanar spacing (d) and thus to strain (ε) [13]. A number of d-spacings are measured and stresses are calculated from an equation derived from Hooke's law for isotropic, homogeneous, and fine grained materials. The stress-strain relationship is given in Equation 2-5 [93-95]. The definition of the reference axes and the direction of measurement are presented in Figure 2.17.

$$\varepsilon_{\phi\psi} = \frac{1}{2}S_2(\sigma_\phi - \sigma_{33})\sin^2\psi + \frac{1}{2}S_2\sigma_{33} - S_1(\sigma_{11} + \sigma_{22} + \sigma_{33}) + \frac{1}{2}S_2\tau_\phi \sin 2\psi$$

$$\sigma_\phi = \sigma_{11}\cos^2\phi + \sigma_{12}\sin 2\phi + \sigma_{22}\sin^2\phi \qquad \tau_\phi = \sigma_{13}\cos\phi + \sigma_{23}\sin\phi$$

Equation 2-5

In these equations, ½ S_2 and S_1 are the x-ray elastic parameters of the material replacing the mechanical parameters (1+v)/E and v/E, respectively; σ_ϕ is the stress in the measurement direction; ψ is the angle subtended by the bisector of the incident and diffracted beam and the surface normal; and $\varepsilon_{\phi\psi}$ is the strain for a given $\phi\psi$ orientation [93-95].
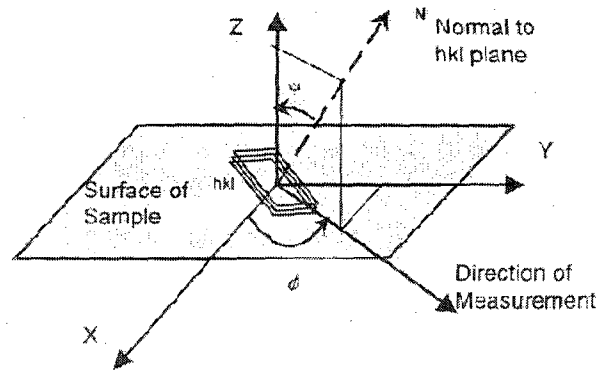
Figure 2.17 Definition of the axis and the direction of measurement [93, 95].

Evaluation of the stress tensor components σ_{ij} is generally straightforward, and is normally carried out by plotting the measured d-spacing versus $\sin^2\psi$, with careful selection of the measurement directions ψ and ϕ. A variety of mathematical models and measurement approaches have been proposed to evaluate the stress-tensor components of interest. The data can be categorized as follows: linear, elliptical with ψ-splitting, and non-linear with oscillatory behavior. In general a minimum of five ψ tilts are required for a reasonable assessment of shape of the d-spacing versus $\sin^2\psi$ curve; however, it is recommended that more than five tilts be used as a general practice [93].

The penetration depth of the x-rays is limited and influenced by both the wavelength of the incident radiation and the mass absorption coefficient of the material. The common depth of x-ray penetration for most metals is in a range of 10 and 20µm [93]. In order to evaluate the residual stress profile distribution from the surface to the substrate of the material, electropolishing techniques are used to etch back from the surface in controlled increments. The removal of material layers associated with the residual stress will cause relaxation due to the establishment of a new equilibrium state; measurement results must be corrected for this effect [59]. Other possible sources of x-ray measurement errors include: error in peak position, stress relief by aging, and sample anisotropy [13, 95].

III. EXPERIMENTAL DETAILS

3.1 Overview

In the present study, a number of gas, ion and vacuum ferritic nitrocarburizing processes were carried out to compare with a current carbonitriding procedure for automotive applications. Navy C-rings with varying thicknesses and torque converter pistons made from SAE 1010 plain carbon steel were used in the testing. For each combination of heat treatment schedule and specimen thickness, the following parameters were evaluated: (1) the microstructure and phase composition of the nitrocarburized and carbonitrided specimens; (2) the microhardness of the case and diffusion zone; (3) the changes in size (OD, ID, gap) and shape (flatness) of the piston and C-ring samples; (4) the residual stress state at the surface of the specimens. The testing methodology is summarized in Figure 3.1.
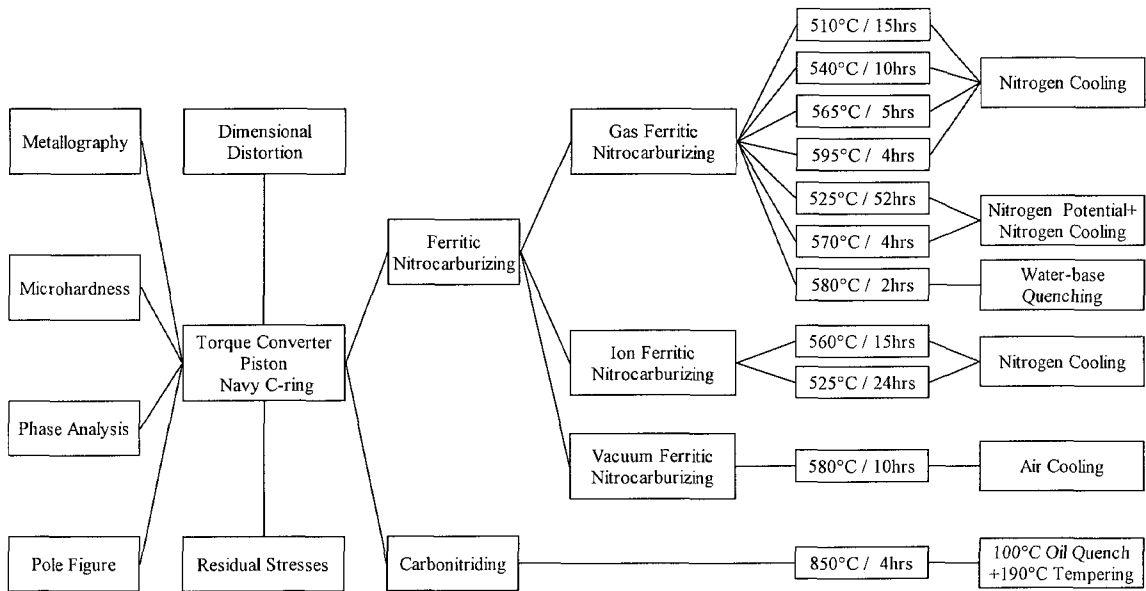
Figure 3.1 Schematic of experimental procedures for piston and Navy C-ring specimens.

Initially, the gas ferritic nitrocarburizing and gas carbonitriding processes were compared, with emphasis on the dimensional distortion and residual stress state. Thereafter, more detailed comparisons between the gas, ion, and vacuum ferritic

nitrocarburizing processes were carried out. All of the results were then analyzed and used to recommend a suitable heat treatment schedule (processing method, temperature, and time) for lowering part distortion and manufacturing costs while improving product quality and manufacturing productivity.

3.2 Test Specimens

3.2.1 Material and Texture

A total of 103 Navy C-ring specimens and 105 torque converter pistons were used in the testing. All parts were fabricated from SAE 1010 plain carbon steel, the chemical composition of which is given in Table 3.1.

Table 3.1 Composition of SAE 1010 plain carbon steel [wt. %].

Material	C	Mn	P	S	Si	Cr	Ni	Mo	Cu	Al	V	Ti	B	Ca
SAE 1010 steel	0.12	0.43	0.008	0.008	0.03	0.03	0.01	0.01	0.02	0.052	0.001	0.002	0.0003	0.0001

A pole figure is defined as *a stereoscopic projection of a polycrystalline aggregate showing the distribution of poles or plane normals of a specific crystalline plane, using specimen axes as reference axes* [54]. In the present study, crystallographic texture measurements were carried on carefully prepared and oriented piston samples after the stamping station. The equipment used for texture investigation is the D8 Discover with HI-STAR area detector, in Figures 3.2 and 3.3.
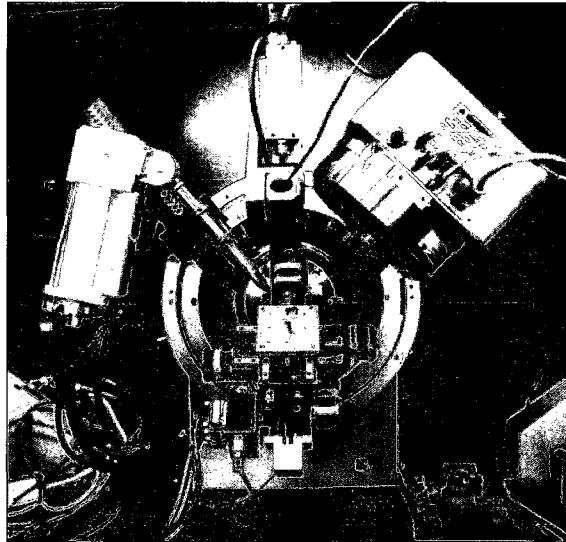
Figure 3.2 D8 Discover x-ray diffraction system at Bruker AXS Inc., Michigan, USA.
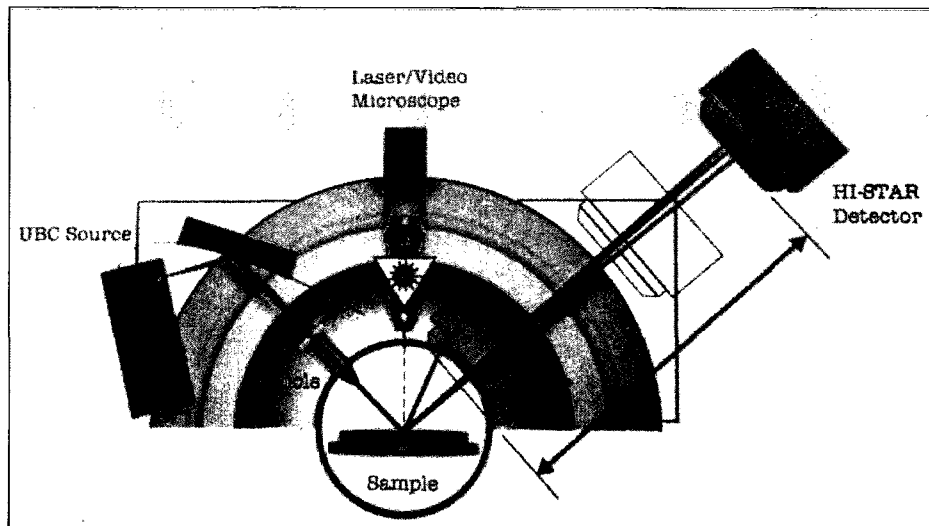
Figure 3.3 Geometry of the D8 Discover with HI-STAR area detector. *Courtesy of Bruker AXS Inc., Michigan, USA.*

The procedure for the texture analyses is as follows: place the sample on stage, zoom in with the laser/video microscope and center the sample. After setting up a start and end angle, measurement time, and resolution, start the data collection with PILOT software. Then a series of XRD patterns was obtained. The (200) reflection was used to estimate the orientation parameters in the rolling (RD) and transverse (TD) directions.

Ultimately, a MULTEX AREA software was used to complete the texture analysis. A detailed procedure for X-ray pole figure measurements was outlined by Kocks et al [96].

3.2.2 Geometry of Navy C-rings

The Navy C-rings were cut from bar stock of hot rolled SAE 1010 steel by EDM (Electrical Discharge Machining). The geometry of the Navy C-rings used in this study is shown in Figure 3.4. The structural dimensions of the C-ring specimens are 50.8 mm OD, 31.75 mm ID, and 6.35 mm gap width, with a specified tolerance range of ±0.127 mm. In order to determine the effects of specimen thickness on distortion and microstructure properties, Navy C-rings with five different thicknesses, ranging from 19.05 to 2.8 mm, were used in the testing. According to their thickness, the Navy C-rings were divided into five groups identified as the 1-NC to 5-NC series.
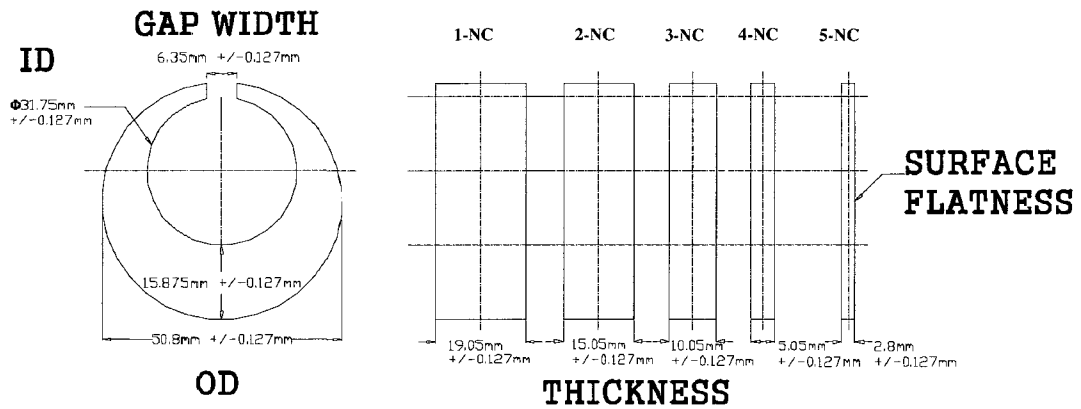
Figure 3.4 Navy C-ring's geometry and distortion measurement positions.

The distortion of the C-ring samples was evaluated by dimensional measurements using a Coordinate Measuring Machine (CMM) both before and after heat treatment. Four specified dimensions for each C-ring sample were measured, namely OD, ID, gap width for size distortion, and surface flatness for shape distortion, Figure 3.4. These results were then used to compare both size (OD, ID, and gap) and shape (flatness) distortion for the different heat treatment processes.

3.2.3 Geometry of Torque Converter Piston

The torque converter piston is an important component of an automotive transmission, with an OD of 260mm, ID of 62 mm, and a weight of 1.8kg [11]. Beginning with sheets of cold-worked SAE 1010 steel, the pistons were formed by a progressive five-stage stamping operation and were then subjected to case hardening processes. The geometry as well as the distortion measurement positions of the piston samples is shown in Figure 3.5.

The changes of OD, ID, total flatness, and flatness taper were used to determine the dimensional distortion. The OD dimensions were measured at -7.5 mm and -21.5 mm longitudinal height positions from the lockup surface. The ID dimensions were evaluated at -11 mm and -15 mm longitudinal height positions from the lockup surface. The total flatness was evaluated along six separate diameters (225, 230, 235, 240, 245, 250 mm) across the lockup surface. The flatness taper was determined by scanning along four directions (±X, ±Y) of the lockup surface.

(a)   (b)
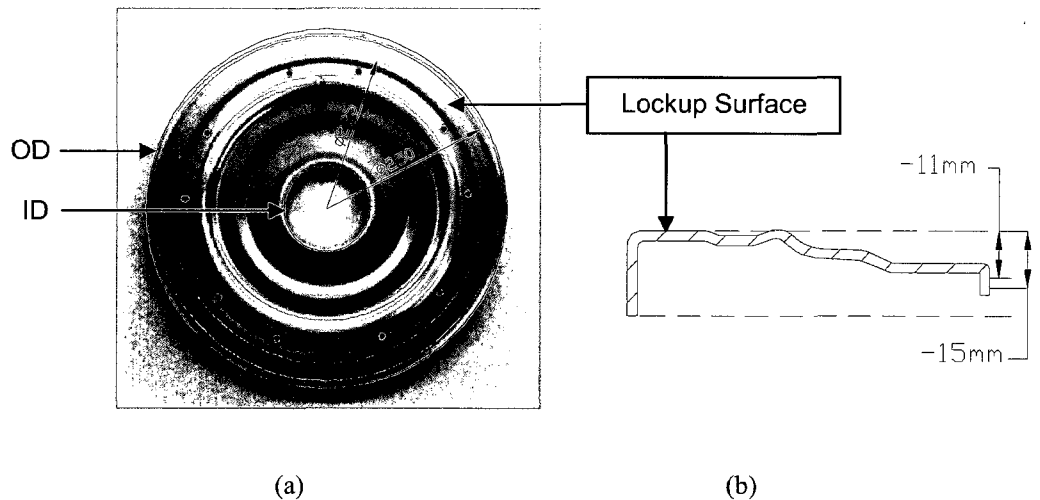
Figure 3.5 Torque converter piston geometry and distortion measurement positions. (a) Front view of piston with lockup surface highlighted in pink; (b) Half cross section of piston showing ID measurement positions at -11 mm and -15 mm from the lockup surface.

3.3 Heat Treatment Details

In order to demonstrate the relative advantages of nitrocarburizing with respect to the microstructure as well as dimensional control of specimens, a comparison was first made between gas ferritic nitrocarburizing with different temperature-time schedules and a current gas carbonitriding process. A detailed comparison was then carried out between the different ion, gas and vacuum ferritic nitrocarburizing processes to seek an appropriate heat treatment schedule for improving surface properties and minimizing dimensional distortion. Based on the different heat treatment schedules used, both the Navy C-ring and piston specimens were divided into 11 separate groups to undergo either ferritic nitrocarburizing or gas carbonitriding and a subsequent cooling process. Table 3.2 lists the heat treatment details that were applied to the pistons and C-ring specimens during heat treatment. To simplify the identification of the heat treatment schedule, each process was identified using the symbols *a* to *k*.

Table 3.2 Heat treatment processing matrix for piston and Navy C-ring specimens.

No.	Heat Treatment Schedule		Symbol	Number of Samples	
	Process 1	Process 2		Piston	C-ring
1	Gas ferritic nitrocarburizing	510 °C / 15 hrs	Nitrogen cooling + air cooling to room temperature	*a*	10	10
2		540 °C / 10 hrs		*b*	10	10
3		565 °C / 5 hrs		*c*	10	10
4		595 °C / 4 hrs		*d*	10	10
5	Ion ferritic nitrocarburizing	560 °C / 15 hrs	Nitrogen cooling + air cooling to room temperature	*e*	10	10
6		525 °C / 24 hrs		*f*	10	10
7	Gas ferritic nitrocarburizing (controlled nitrogen potential)	525 °C / 52 hrs	Nitrogen cooling + air cooling to room temperature	*g*	10	10
8		570 °C / 4 hrs		*h*	10	10
9	Vacuum ferritic nitrocarburizing	580 °C / 10 hrs	Air cooling to room temperature	*i*	10	10
10	Gas ferritic nitrocarburizing	580 °C / 2 hrs	Water-base quenching	*j*	10	10
11	Gas carbonitriding	850 °C / 4 hrs	100 °C Oil quenching + 190 °C tempering	*k*	5	3

The gas ferritic nitrocarburizing (*a-d*) treatments for pistons and C-ring samples were conducted at Woodworth Inc., Detroit, Michigan U.S.A. in the large commercial nitrocarburizing furnace shown in Figure 3.6. The specimens were separately placed in

the small pit-type furnace (proprietary gas composition) and held at different temperatures and time periods. Subsequently, the specimens were furnace-cooled to about 400 °C using nitrogen gas, and then removed from the furnace and air cooled to room temperature.

<div align="center">(a)   (b)</div>
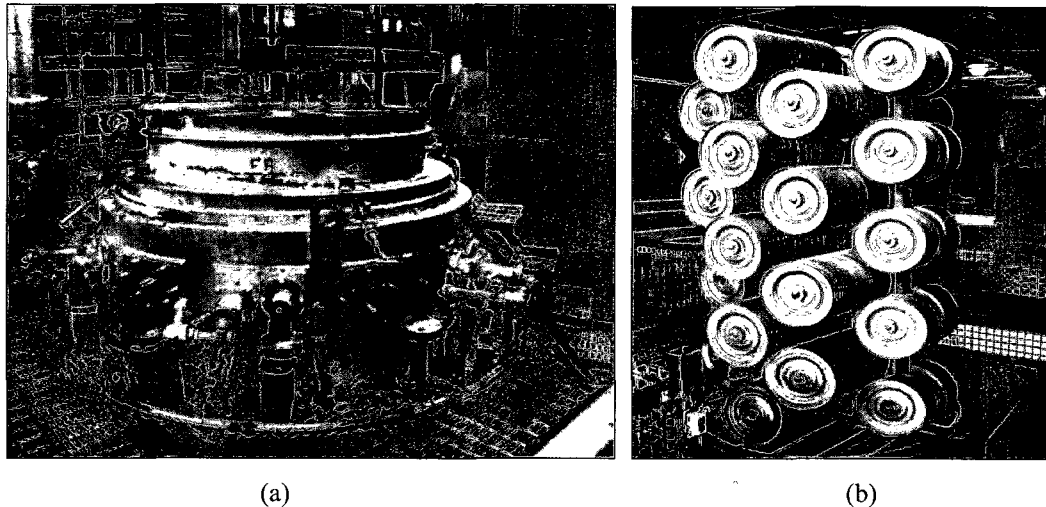
Figure 3.6 Nitriding/nitrocarburizing furnace used in the gas ferritic nitrocarburizing (processes *a-d*) of the Navy C-rings and torque converter pistons at Woodworth Inc., Detroit, Michigan U.S.A. (a) Small pit-type furnaces used for gas ferritic nitrocarburizing and nitriding; (b) Load of pistons after gas ferritic nitrocarburizing.

A gas ferritic nitrocarburizing process module is shown in Figure 3.7. With the decomposition of the nitrocarburizing atmosphere in the furnace, active nitrogen and carbon penetrate into the steel surface to form a compound layer and an underlying diffusion zone [19].
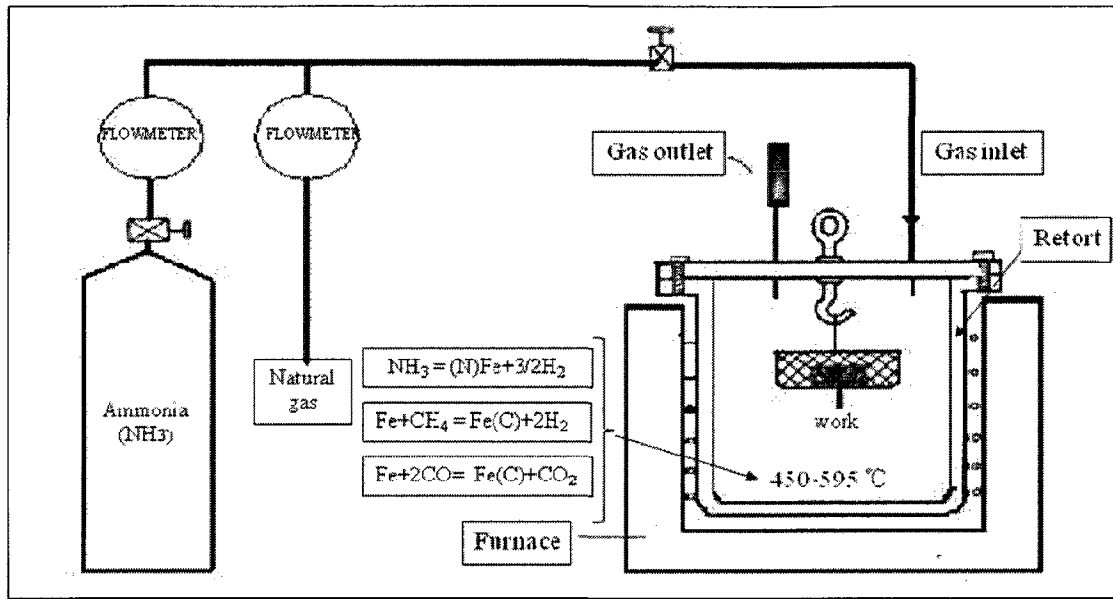
Figure 3.7 Schematic module of gas ferritic nitrocarburizing process.

The ion ferritic nitrocarburizing (e and f) and gas ferritic nitrocarburizing with controlled nitrogen potential processes (g and h) were carried out at Advanced Heat Treat Co., Monroe, Michigan U.S.A. In order to determine the influence of treatment temperature and time, the ion ferritic nitrocarburizing was performed at both 560 °C for 15 hours and 525 °C for 24 hours. The atmosphere of ion ferritic nitrocarburizing consists of a mixture of nitrogen and hydrogen with small additions of carbon-bearing gases. Glow discharge reactions are very complex. The reactions on the surface of the components involve both the ionization and dissociation of the gas molecules to form nascent nitrogen and carbon atoms, as well as the absorption and diffusion of these atoms into the material substrate. A typical ion ferritic nitrocarburizing process carried out at Advanced Heat Treat Co., and the layout of work parts going through the furnace is shown in Figure 3.8. The control of nitrogen potential for the gas ferritic nitrocarburizing is implemented with stage electronic controllers.

42
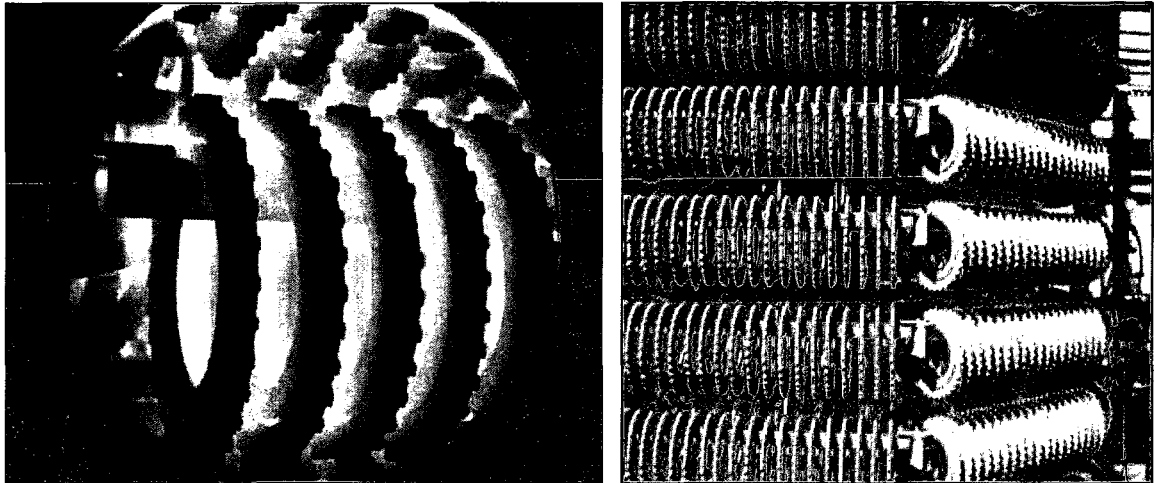
(a)   (b)

Figure 3.8 Ion nitriding/nitrocarburizing of low-density sintered metal products at Advanced Heat Treat Co., Monroe, Michigan U.S.A. (a) Work parts under plasma glow in a furnace; (b) A load of sintered metal products after ion ferritic nitrocarburizing.

For vacuum ferritic nitrocarburizing (i), the piston and C-ring samples were first heated in vacuum to the temperature of 580 °C. Then the samples were exposed to the gas mixtures under a partial pressure, in which the nitrogen diffuses into the ferrous metals simultaneously with carbon. The vacuum chamber enabled precision processing with microprocessor controls for the temperature, gas flow meters, and cycle times. The vacuum furnace used at Woodworth Inc., Detroit, Michigan U.S.A. is shown in Figure 3.9.
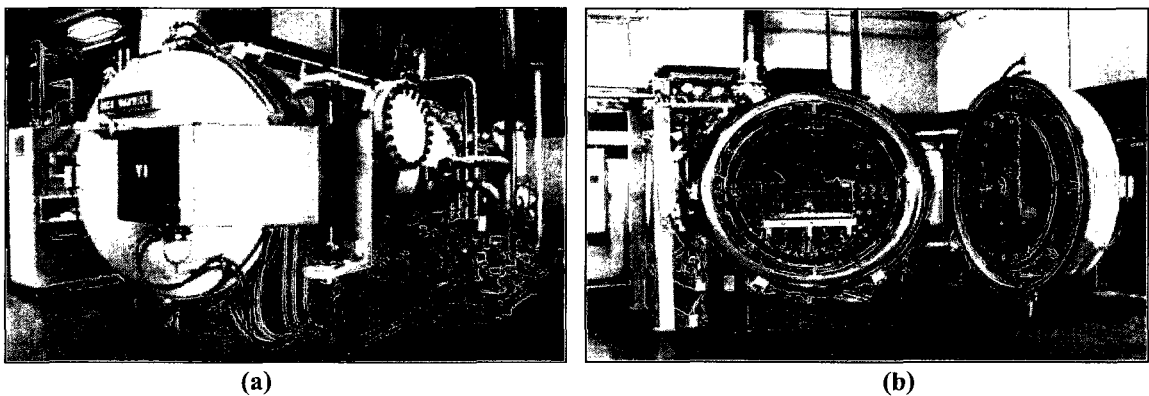
(a)   (b)

Figure 3.9 A vacuum furnace used at Woodworth Inc., Detroit, Michigan U.S.A.
(a) Outside view of the vacuum furnace; (b) Inside view of the vacuum furnace.

Gas ferritic nitrocarburizing and subsequent water-base quenching (j) was performed at Trutec Industries, Inc. in Springfield, Ohio U.S.A. The vertical section view of the batch furnace for gas ferritic nitrocarburizing is shown in Figure 3.10. Both the piston and C-ring samples are delivered into the furnace for gas nitrocarburizing treatment, followed by a water base quenching in the quenching tank. Because the specimens for quenching are delivered directly from the nitrocarburizing furnace, any surface oxidation usually associated with the processing can be significantly reduced.
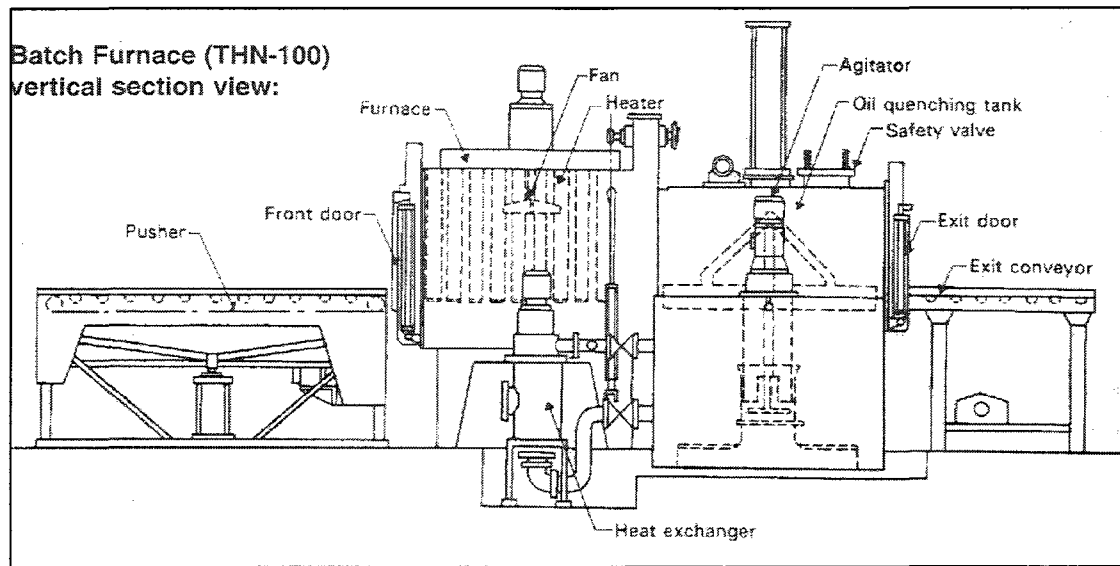
Figure 3.10 Schematic of a gas ferritic nitrocarburizing furnace with integrated water base quenching. *Courtesy of Trutec Industries, Inc., Springfield, Ohio U.S.A.*

A typical gas carbonitriding process (k) followed by oil quenching is shown in Figure 3.11. The treatment was performed at Woodworth Inc., Detroit, Michigan U.S.A. Both ammonia and carburizing gases are introduced into the carbonitriding atmosphere, so that nascent nitrogen dissociated from ammonia diffuses into the steel simultaneously with carbon [6, 8]. The specimens were held at 850 °C for 4 hours in the carbonitriding furnace, and then were directly delivered to the quenching chamber and immerged into 100 °C oil for surface hardening. Upon quenching, a hard martensitic case is formed at the surface of the work parts [10].

44
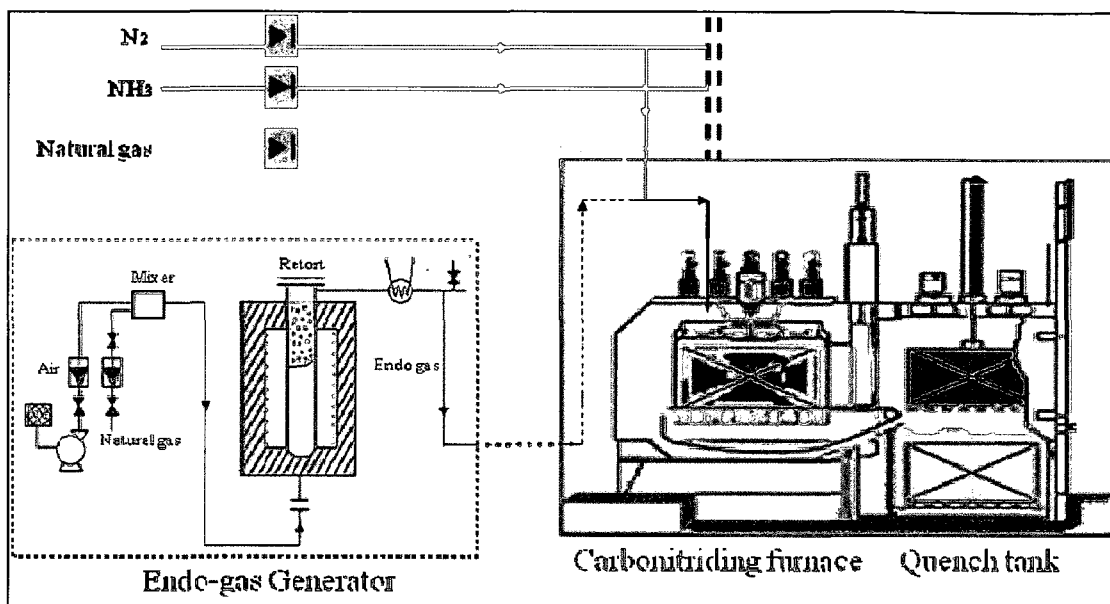
Figure 3.11 Schematic flowchart of carbonitriding and quenching processes. *Courtesy of Woodworth, Inc., Detroit, Michigan U.S.A.*

3.4 Metallographic Procedures

Torque converter pistons and Navy C-ring specimens selected from each heat treatment group were cut, mounted, polished, etched and examined with optical microscopy and scanning electron microscopy (SEM). The interrelationship between the microstructural properties within the specimens and the case hardening processes applied were determined [17].

3.4.1 Optical Microscopy

Small samples were sectioned from the main body of the piston and C-rings using a Buehler Isomet 1000 Precision Saw with a diamond blade. The piston samples were cut from the lockup surface in a direction parallel to the radius of the specimen. The C-ring samples were cut from the "bottom" of each specimen, which is located opposite the C-ring gap. All the samples were mounted using a Buehler Simplimet 3 Mounting Press using Buehler Mineral Filled Diallyl Phthalate powder. Mounted samples then underwent rough grinding on a Buehler Handimet II Roll Grinder through 240, 320, 400, and 600 grit silicon carbide papers, followed by a rough polishing using 9 μm diamond compound on a Buehler Ecomet 3 Variable Speed Grinder-Polisher. Final polishing was performed

45

on a Buehler Metaserv Grind-Polisher using 1.0 µm and 0.05 µm alumina oxide (Al_2O_3) water suspension, respectively. After polishing, the samples were etched using a 2% Nital solution, which consists of 2 ml nitric acid (HNO_3) and 98 ml ethanol. Once the etching was complete, the samples were immediately rinsed with cold water, then with ethanol, and finally dried.

A ZEISS Axiovert 25 light optical microscope was used to analyze the microstructures of the specimens after different heat treatment processes, Figure 3.12 (a). The thickness of the compound layer formed by various heat treatments was also measured at ten locations with different surface morphologies on the digital images of each sample.

(a)   (b)
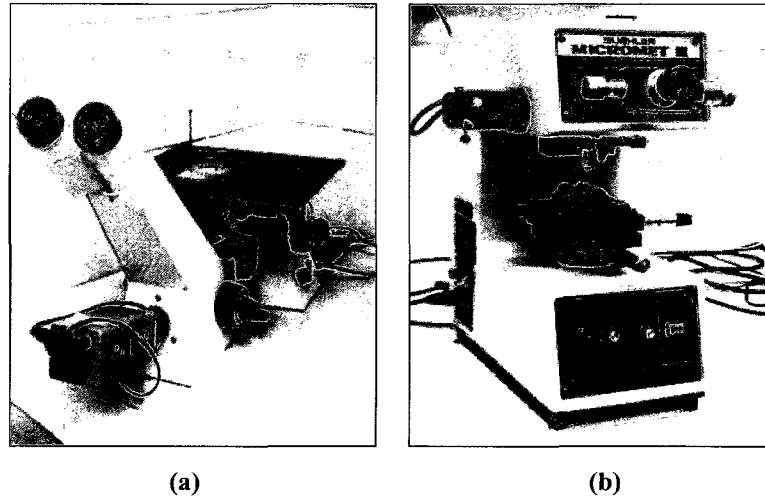
Figure 3.12 Instruments for metallographic analyses.
(a) A light optical microscope; (b) A microindentation hardness tester.

3.4.2 Scanning Electron Microscopy

The scanning electron microscope (SEM) is a powerful instrument available for the observation and analysis of the microstructural characteristics of materials down to a submicrometer (µm) scale [97]. Due to its high resolution, the JEOL 5800 scanning electron microscope was applied to the mounted piston samples to examine the compound layer and diffusion zone after gas and ion ferritic nitrocarburizing processes,

Figure 3.13. A gold conductive coating is required for the mounted piston sample for good imaging [97].
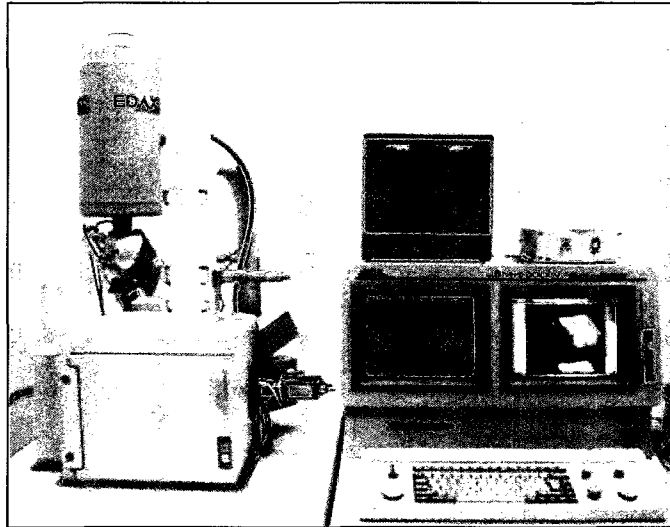
Figure 3.13 A scanning electron microscope for microstructure analyses.

3.5 Microhardness Testing

Hardness testing was performed on the nitrocarburized and carbonitrided piston samples using a Buehler Micromet II microhardness tester, Figure 3.12 (b). Vickers hardness testing was performed on a polished cross section of the nitrocarburized specimens to evaluate the hardness of the compound layer and the underlying diffusion zone. Correspondingly, the hardness profile in SAE 1010 steel under various nitrocarburizing conditions was investigated. The case hardness of the carbonitrided sample was also characterized using the Vickers microhardness scale.

3.6 Phase Analyses

X-ray diffraction (XRD) techniques were used to analyze the phase composition of the compound layer of the C-ring specimens after different nitrocarburizing processes. The thickest C-ring series, 1-NC, were selected for this analysis.

3.7 Dimensional Measurements and Calculation of Distortion

A coordinate measuring machine (CMM) is one of the most versatile metrological instruments that is widely used in manufacturing plants to measure various shapes of workpieces. Given physical representations of a three-dimensional rectilinear Cartesian coordinate system, CMM can measure the actual shape of a component to compare with a desired shape, and then evaluate the metrological information, such as size and orientation. The measurement was performed by probing the surface at discrete measuring points [98].

In the present study, a PRISMO coordinate measuring machine (CMM) was used to measure the dimensions of the pistons and C-ring specimens both before and after the various nitrocarburizing and carbonitriding processes, Figure 3.14. The measurement was performed by means of a physical contact scan of the specimen surface with a mechanical set-up probe. It requires approximately 20 minutes for a piston measurement and 2 minutes for a C-ring sample. The scanning results are then analyzed using Imageware surface scanning software, which is an advanced 3D surface modeling and verification technology using a set of data analysis tools to compute the differences of cloud-cloud, cloud-surface, and curve-curve data [99]. The dimensional value is accurate to 0.1 μm. The average values obtained from the individual tests were then used to evaluate the dimensional changes in terms of percentage dimensional change, as noted in Equation 3.1.

$$\text{Percentage dimensional change} = \frac{\text{Final dimension - Initial dimension}}{\text{Initial dimension}} \times 100\%$$

Equation 3.1

The initial and final dimensions were those values measured by CMM before and after heat treatment, respectively.
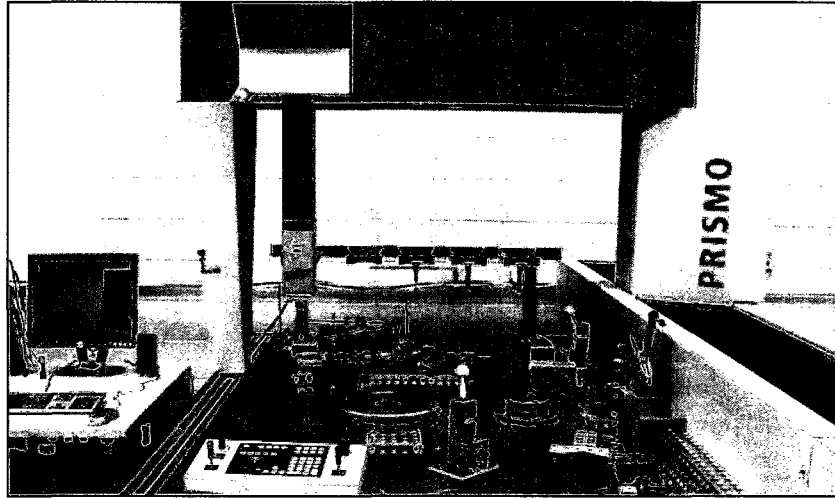
Figure 3.14 A PRISMO Coordinate measuring machine (CMM). *Courtesy of Chrysler LLC, Auburn Hills, Michigan U.S.A.*

3.7.1 CMM Measurements of C-ring Specimens

Four specified dimensions for each C-ring sample both before and after heat treatment were measured using CMM for the evaluation of both size and shape distortion. The size distortion was represented in the form of dimensional changes of the outside diameter (OD), inside diameter (ID), and gap width. The shape distortion was characterized by the changes of surface flatness.

OD, ID, and gap width measurements were used to give an indication of the volumetric or linear changes associated with size distortion [78]. Two C-ring samples with the same thickness were used for each heat treatment condition. Both OD and ID were measured at multiple locations along each C-ring to calculate the average value. The result of gap width is the average value of gap breadth measured at the top and bottom positions of the gap with respect to the C-ring cross section, respectively.

Flatness is used to represent the shape changes of specimens after heat treatment. Flatness is a geometric control of the part surface compared to a reference surface, usually the perfectly flat geometric counterpart of the surface itself, to check the irregularity of the surface [78, 100]. In the present study, the values of flatness refer to the difference between the maximum and minimum values derived from a reference surface. The flatness values of the C-ring samples were determined by scanning

49

approximately 2100 points along the C-ring perimeter. An example of a flatness form plot is shown in Figure 3.15. The C-ring specimen from the 1-NC series was treated by gas ferritic nitrocarburizing at 595 °C for 4 hours. From the following graph, a small amount of variation in flatness is observed. The plane designated as "1-2-3-4" is the reference surface, which coincides with the minimum point of deviation. The small circles noted by points "A" and "B" represent the maximum and minimum points of deviation away from the reference surface.
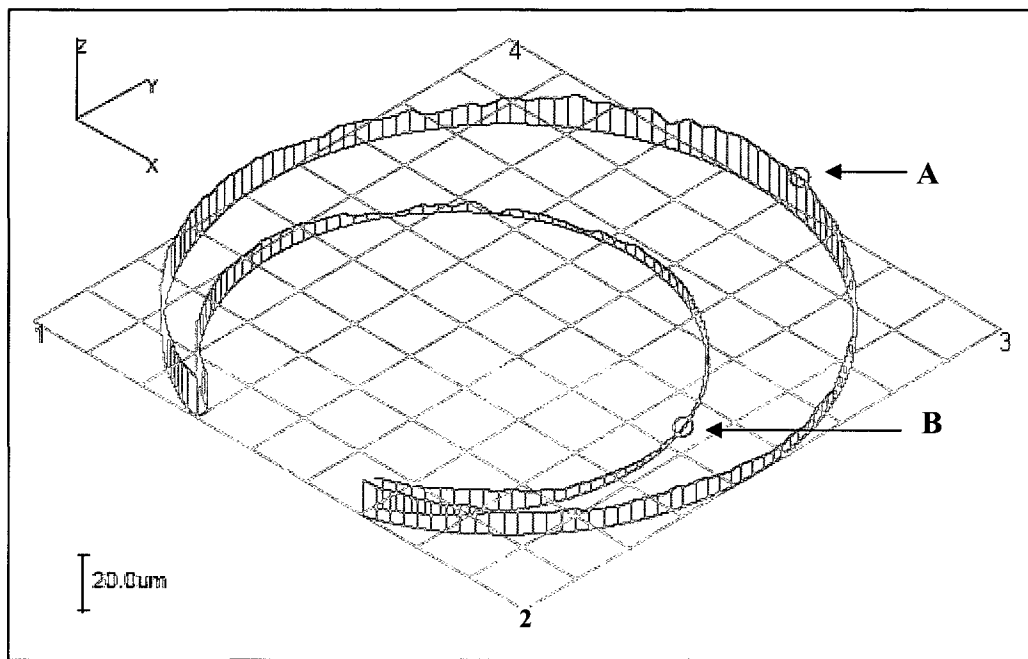
Figure 3.15 Example plot of flatness measurements obtained using CMM; 1-NC C-ring sample after gas ferritic nitrocarburizing (process *d*, 595 °C /4 hrs). Points "A" and "B" are the points of maximum and minimum deviation away from surface "1-2-3-4", respectively.

3.7.2 CMM Measurements of Pistons

The size and shape distortions of the piston samples were characterized by the dimensional changes of OD, ID, total flatness, and flatness taper of the lockup surface. An accurate control of the ID dimension, flatness and the flatness taper of the lockup surface of a piston is vital to ensure the proper operation of a torque converter [11]. Taking the lockup surface as the basic measurement plane, the OD was evaluated at -7.5

mm and -21.5 mm and ID evaluated at -11 mm and -15 mm longitudinal height positions from the lockup surface.

The total flatness of pistons was evaluated at the lockup surface along six separate diameters (225, 230, 235, 240, 245, 250 mm), and approximately 7000 points were scanned around each circle. Combining the results from six separate scans together, the difference between the overall highest and lowest points of deviation from the reference surface is the value of total flatness. The flatness taper of pistons was obtained by scanning about 490 points along the ±X and ±Y directions across the lockup surface. An example of the plot of total flatness and flatness taper of an ion ferritic nitrocarburized piston sample is shown in Figures 3.16 and 3.17. Points "A" and "B" are the maximum and minimum points of deviation away from a reference surface. The reference surface, designated as "1-2-3-4" coincides with the minimum point of deviation.
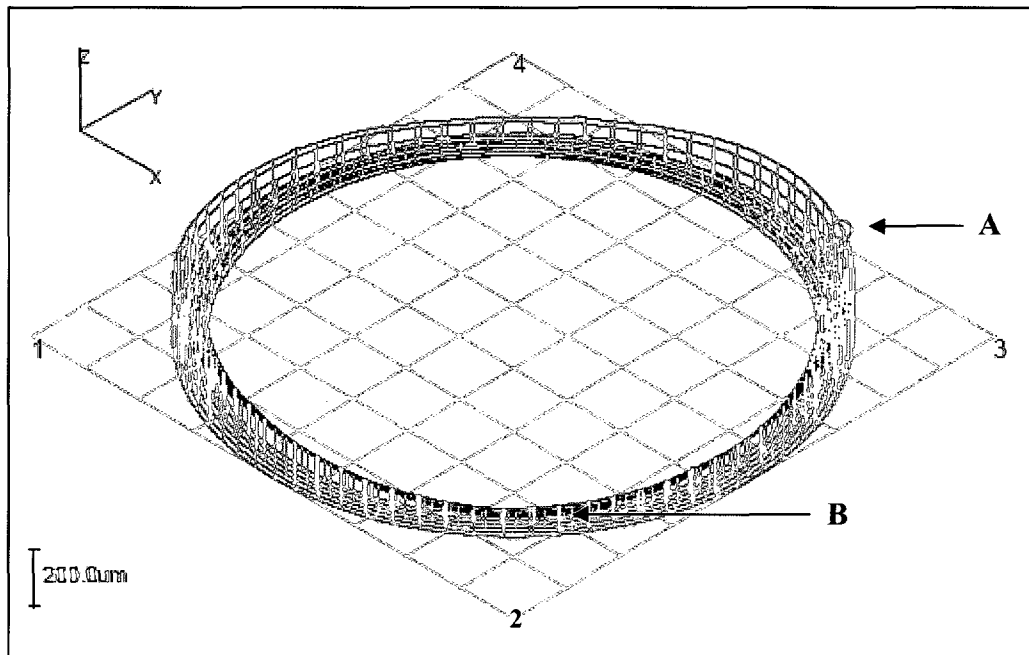
Figure 3.16 Example plot of total flatness measurements obtained using CMM; piston after ion ferritic nitrocarburizing (process *e*, 560 °C /15 hrs). Total flatness represents the maximum and minimum points of deviation along the lockup surface, measured at six separate diameters. Points "A" and "B" are the points of maximum and minimum deviation away from surface "1-2-3-4", respectively.
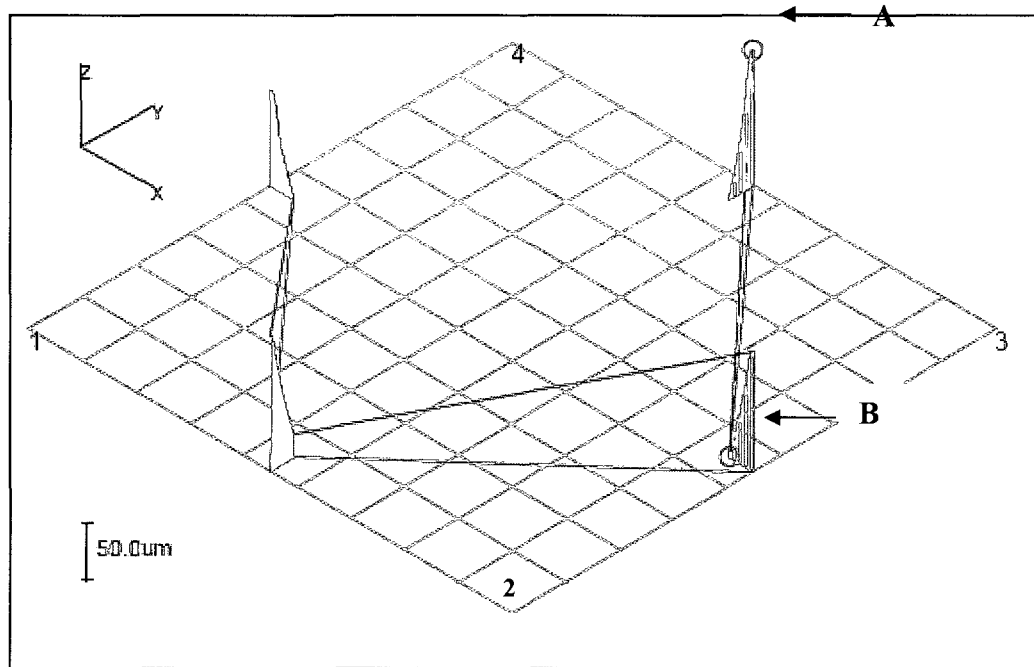
Figure 3.17 Example plot of flatness taper measurements obtained using CMM; piston after ion ferritic nitrocarburizing (process *e*, 560 °C /15 hrs). The flatness taper represents the maximum and minimum points of deviation measured along the ±X and ±Y directions of the lockup surface. Points "A" and "B" are the points of maximum and minimum deviation away from surface "1-2-3-4", respectively.

3.8 Residual Stresses Measurement

X-ray Diffraction (XRD) techniques were used to evaluate the residual stress state on the surface of specimens after nitrocarburizing and carbonitriding, according to ASTM Standard E915 [101]. A total of eleven pistons for the various nitrocarburizing or carbonitriding treatment and four C-ring samples for gas ferritic nitrocarburizing (processes a-d) were examined. The (302) reflection of the ϵ-phase (Fe_3N) and the (211) martensite reflection were used to determine the residual stresses in the nitrocarburized and carbonitrided samples, respectively. The Cr target power was 40 kV and 40 mA, and the wavelength of X-rays was 0.2291 nm. For the nitrocarburized samples, the Bragg angle (2θ) was set at 165.00° and the Ψ angles used were 0°, ±30.00°, ±23.46°, ±11.95° and ±7.58°. For the carbonitrided sample, the Bragg angle was 156.00°. The residual stress values were determined at the following Ψ angles: 0°, ±5.51°, ±12.00°, ±19.41°,

±25.00°. A detailed description of the XRD residual stress analysis method is given in references [65, 87, 93].

The measurement positions of the surface residual stresses are shown in Figure 3.18. The measurements were taken at the lockup surface of the piston sample and the thickest OD section of the C-ring specimen.
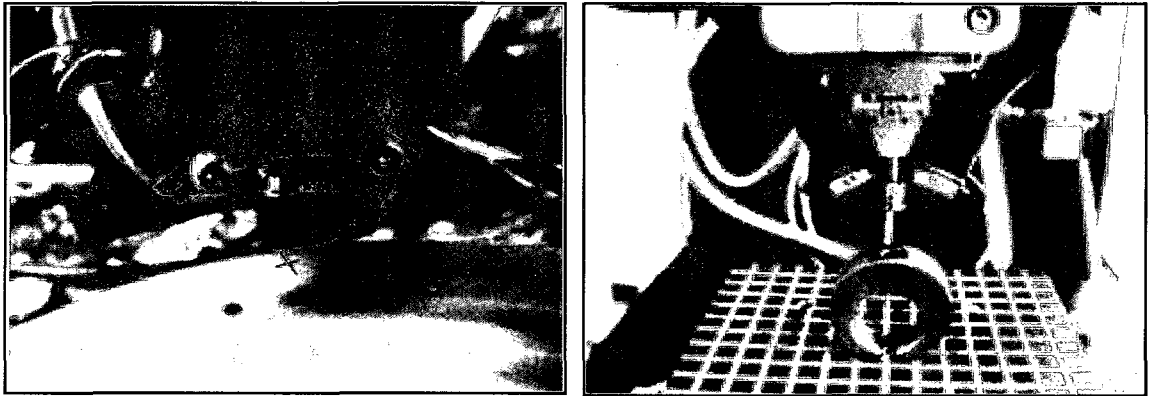
Figure 3.18 Location of surface residual stress measurement. (a) Measured at the lockup surface of a piston sample; (b) Measured at the thickest OD section of a C-ring sample.

IV. EFFECTS OF HEAT TREATMENT ON THE MICROSTRUCTURES OF SAE 1010 STEEL

This section focuses on the microstructures of both piston and C-ring samples after the nitrocarburizing and carbonitriding processes. The microstructure of the piston samples for the various nitrocarburizing and carbonitriding processes are compared to those found in the C-ring series with varying thickness. The surface phase compositions, as well as the microhardness of the case and the diffusion zone were characterized for the different nitrocarburizing processes. Texture analysis was done on piston samples by means of x-ray diffraction, to reveal the distribution of poles for specific crystalline planes after stamping.

4.1 Texture from Pole Figure

The results of the X-ray pole figure analysis is shown in Figure 4.1. The orientation intensities are represented as contour lines and shading levels instead of discrete points in the projection. It shows the rolling direction of <111> and rolling plane of (112) of pistons after stamping, which is in agreement with the findings of Hu [102]. It should be noted that it is impossible to determine the entire space of the pole figure due to the geometry of the pole figure measurement. Generally, the maximum polar angles range between 75 to 80° [103].
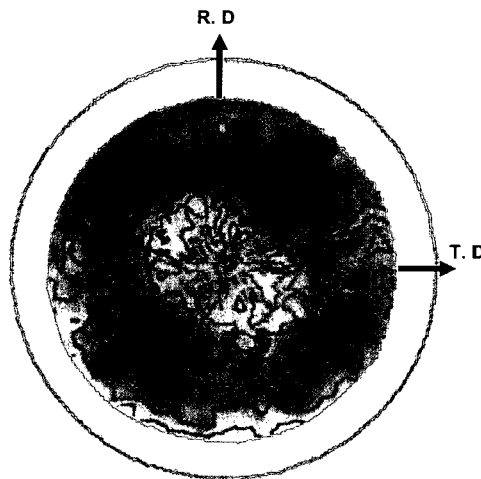
Figure 4.1 Pole figure of stamped SAE 1010 plain carbon steel for torque converter piston.

4.2 Optical Metallography

As detailed in the previous chapter, the piston and C-ring specimens were cut and mounted in a thermoplastic molding resin. The surface of the mounted samples was ground using silicon carbide papers, 9 µm diamond, and finally by 0.1 µm and 0.05µm alumina polishing. The polished surface was periodically checked under the optical microscope to determine if the scratches introduced by the polishing media were being removed. Then the samples were etched with 2% Nital to bring out the phase structure.

4.2.1 Microstructure of Carbonitrided Specimens

The microstructures of the carbonitrided pistons are shown in Figure 4.2. A martensitic case is formed at the steel surface upon quenching, which consists of tempered martensite and retained austenite. The case depth is noted in Figure 4.2 (a), with an average depth of 0.32 mm. The core of the piston sample is comprised of ferrite, needle-like bainite, and pearlite displayed as dark islands, Figure 4.2 (b).

| (a) | (b) |
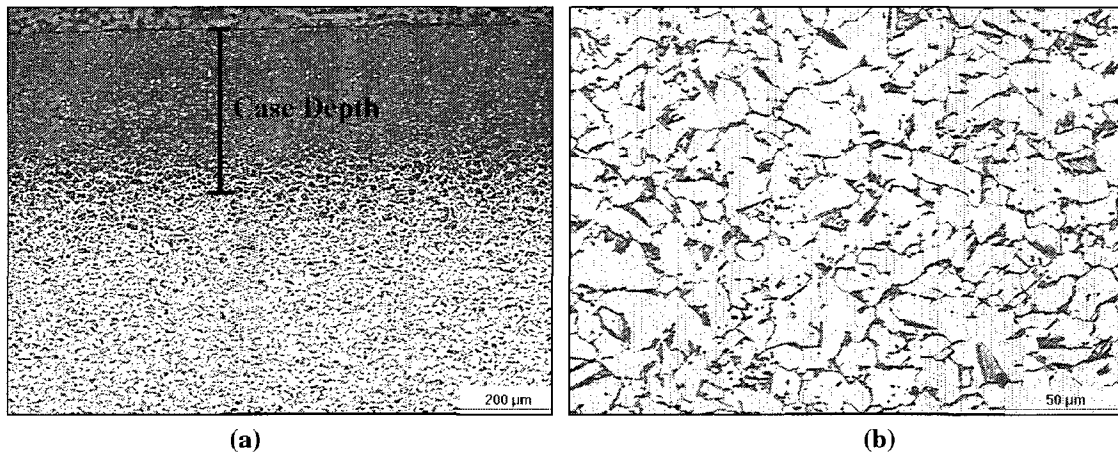
Figure 4.2 Optical micrographs of piston sample, gas carbonitriding at 850°C for 4 hrs, with a subsequent 100 °C oil quenching and 190 °C tempering (process *k*). (a) Microstructure at the martensitic case; (b) Microstructure at the core.

4.2.2 Microstructure of Nitrocarburized Specimens

Both torque converter pistons and Navy C-rings were examined by optical microscopy to analyze the microstructural differences that resulted from the same nitrocarburizing

treatment. Five different thicknesses of Navy C-rings were examined to compare the effects of specimen thickness on the microstructure changes.

4.2.2.1 Compound Layer and Diffusion Zone of Pistons

The cross-section microstructures of the nitrocarburized piston samples are shown in Figures 4.2-4.11; they show a typical nitrocarburized structure with a compound layer at the surface and an underlying diffusion zone [8]. The formation of molecular nitrogen resulted in a certain amount of porosity in the compound layer [42, 44]. For the gas ferritic nitrocarburized pistons (processes a-d), a well-formed compound layer is produced at the steel surface, accompanied by needle-like γ' phases primarily located near the interface of the case and the diffusion zone, Figures 4.3-4.6.
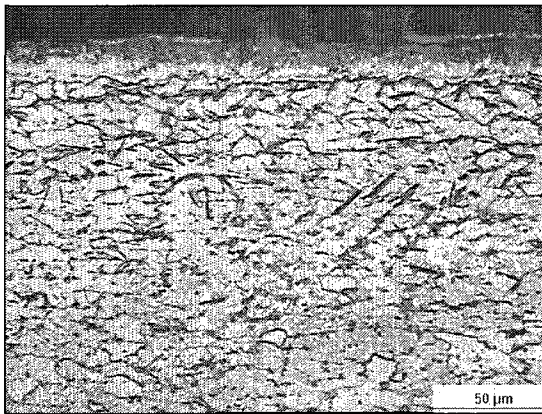
Figure 4.3 Microstructure of the gas ferritic nitrocarburized piston (process a, 510 °C / 15 hrs)
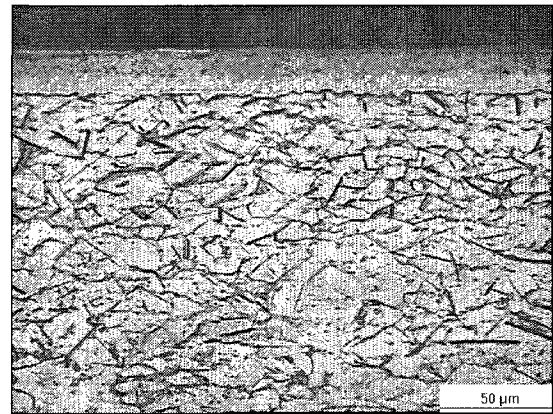
Figure 4.4 Microstructure of the gas ferritic nitrocarburized piston (process b, 540 °C / 10 hrs)
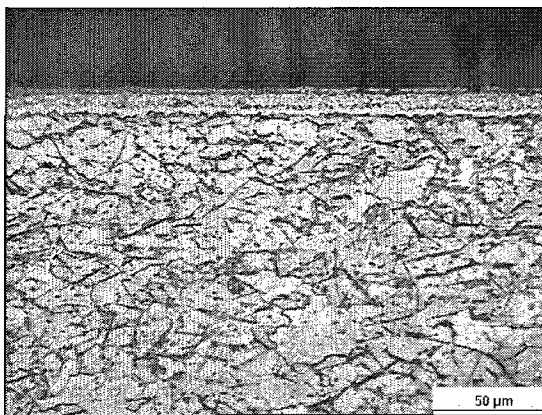
Figure 4.5 Microstructure of the gas ferritic nitrocarburized piston (process c, 565 °C / 5 hrs)
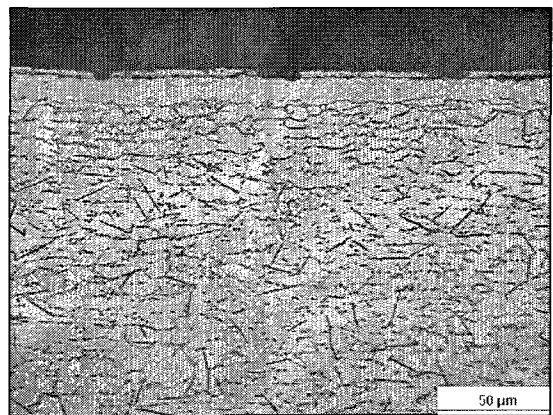
Figure 4.6 Microstructure of the gas ferritic nitrocarburized piston (process d, 595 °C / 4 hrs)

The ion ferritic nitrocarburizing processes (e and f) produced a very thin compound layer at the surface of the specimen with little penetration of needle-like γ' phase into the diffusion zone, Figures 4.7 and 4.8. Though the same gas ferritic nitrocarburizing method was used with controlled nitrogen potential (g and h), the resultant thicknesses of the compound layer were quite distinct from each other. A very thin compound layer was formed at 525 °C for 52 hrs, where as a very thick layer was produced at 570 °C for 4 hrs, as shown in Figures 4.9 and 4.10. Generally, the thickness of the compound layer is dependent on the nitrocarburizing time and temperature, the chemical composition of the steel, and the concentration gradient of a given hardening species. The way in which the part was preliminarily treated can also affect the compound layer thickness [8, 9]. The surface layer thickness differences present in these samples is associated with the different temperature and time combinations applied. The higher temperature used in process h had a significant influence on the formation of a thicker compound layer.
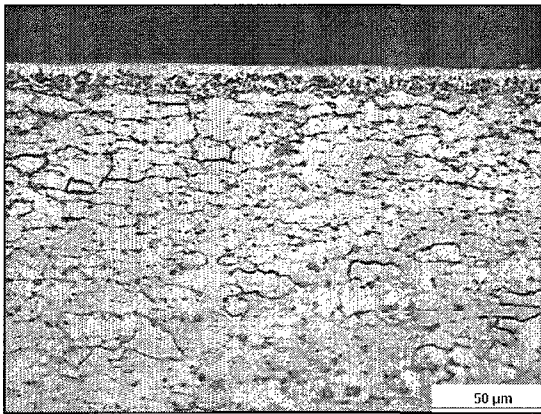
Figure 4.7 Microstructure of the ion ferritic nitrocarburized piston (process e, 560 °C / 15 hrs)
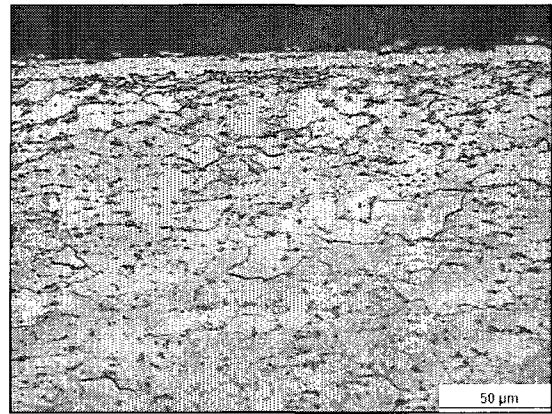
Figure 4.8 Microstructure of the ion ferritic nitrocarburized piston (process f, 525 °C / 24 hrs)
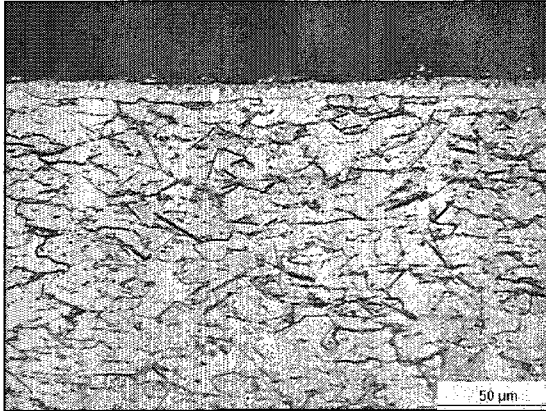
Figure 4.9 Microstructure of the gas ferritic nitrocarburized piston (process g, 525 °C / 52 hrs)
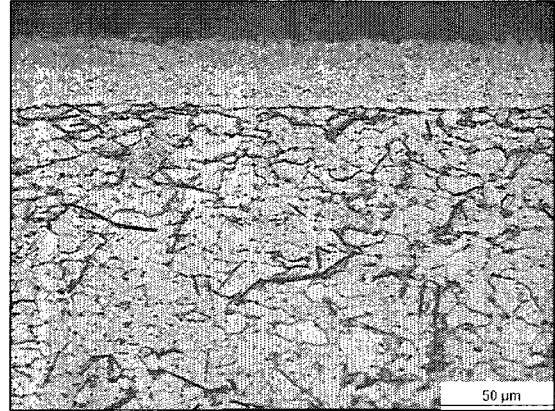
Figure 4.10 Microstructure of the gas ferritic nitrocarburized piston (process h, 570 °C / 4 hrs)

The vacuum ferritic nitrocarburizing process (i), Figure 4.11, shows a well-formed compound layer, with a diffusion zone containing needle-like γ' phases underneath. In Figure 4.12, the gas ferritic nitrocarburizing with its subsequent water base quenching (j) led to a well-formed compound layer at the surface, whereas the penetration of gamma prime phases into the diffusion zone was not evident.
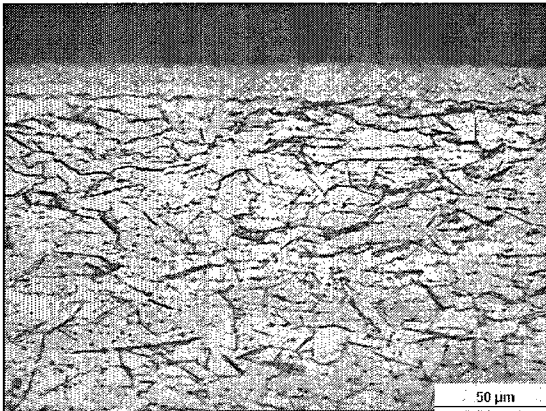
Figure 4.11 Microstructure of the vacuum ferritic nitrocarburized piston (process i, 580 °C / 10 hrs)
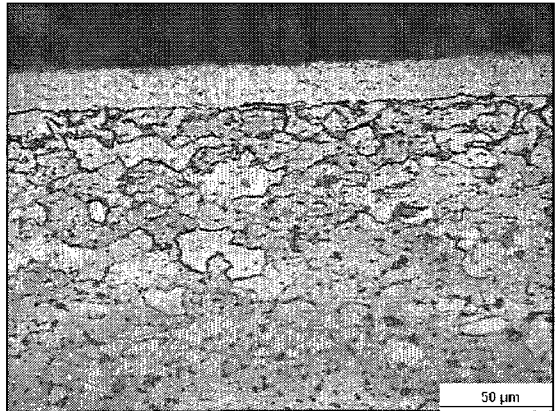
Figure 4.12 Microstructure of the gas ferritic nitrocarburized piston (process j, 580 °C / 2 hrs)

The micrographs of the piston samples show the varying thickness of the compound layer that resulted from the different nitrocarburizing and carbonitriding approaches. Measurements were taken at ten different locations in each piston sample to evaluate the average depth of the compound layer; the results are given in Table 4.1.

The thickness of the compound layer for the various nitrocarburizing processes ranges from 8 to 30 μm. Typically, the compound layer thickness is less than 25 μm [4]. The ion ferritic nitrocarburizing processes resulted in a very thin compound layer that is in the range of 8 to 9 μm. The data obtained from the gas ferritic nitrocarburizing processes a-d are compared in Figure 4.13, where the depths of the compound layer are plotted as a function of their respective nitrocarburizing temperatures. The thickness of the compound layer reached a maximum at about 535 °C. At temperatures above 535 °C, the thickness decreased due to the decreased nitrogen activity in steel in equilibrium with the gas atmosphere [104]. The decreased nitrocarburizing time is another factor associated with the decrease in layer thickness.

Table 4.1 Case depths of pistons for various ferritic nitrocarburizing (a-j) and carbonitriding process (k).

Process		Symbol	Average of Case Depth (μm)
Gas ferritic nitrocarburizing	510 °C / 15 hrs	a	18.73 ± 2.43
	540 °C / 10 hrs	b	20.02 ± 1.26
	565 °C / 5 hrs	c	12.28 ± 1.20
	595 °C / 4 hrs	d	14.22 ± 1.97
Ion ferritic nitrocarburizing	560 °C / 15 hrs	e	8.61 ± 2.22
	525 °C / 24 hrs	f	9.18 ± 1.14
Gas ferritic nitrocarburizing (controlled nitrogen potential)	525 °C / 52 hrs	g	8.42 ± 2.13
	570 °C / 4 hrs	h	29.92 ± 1.05
Vacuum ferritic nitrocarburizing	580 °C / 10 hrs	i	15.85 ± 1.62
Gas ferritic nitrocarburizing (water-base quenching)	580 °C / 2 hrs	j	18.81 ± 0.81
Gas carbonitriding	850 °C / 4 hrs	k	321.15 ± 10.23
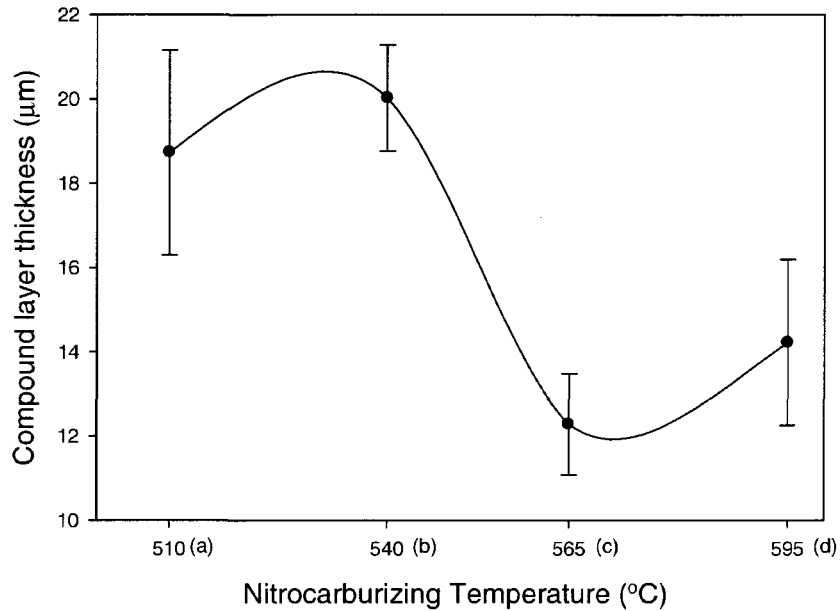
Figure 4.13 Compound layer thicknesses of pistons versus gas ferritic nitrocarburizing temperature.

A comparison of the compound layer thickness resulting from the gas, ion, and vacuum ferritic nitrocarburizing processes (a, b, e, f, and i) is shown in Figure 4.14. The compound layer thickness is plotted as a function of the nitrocarburizing temperature. It is apparent that similar compound layer thicknesses were obtained under the same nitrocarburizing conditions (gas or ion nitrocarburizing). The thickness of the compound layer produced by vacuum ferritic nitrocarburizing was closer to that for the gas nitrocarburizing treatment. Overall, linear regression reveals that the case depth decreased somewhat with increasing nitrocarburizing temperature. Case depth is influenced by multiple factors, not only associated with the time and temperature adopted, but also related to the nitrocarburizing approach applied.
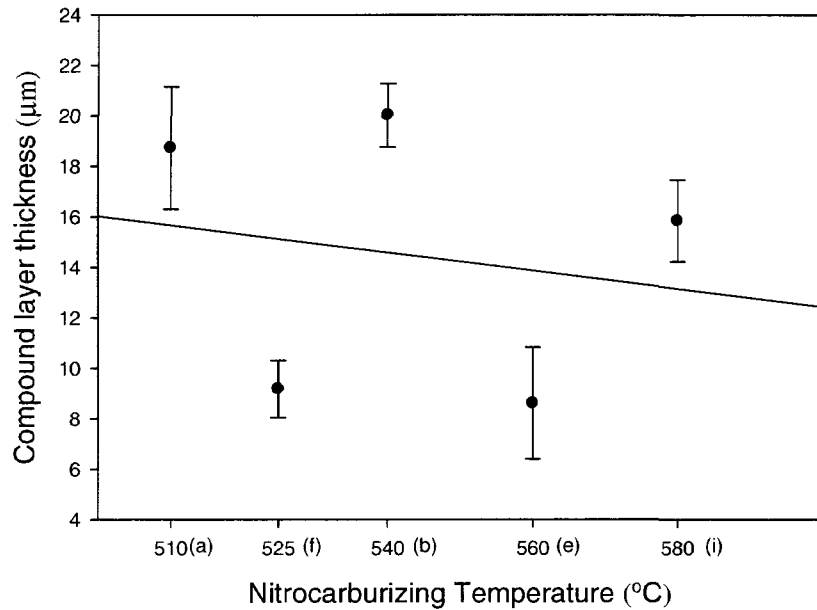
Figure 4.14 Variation of compound layer thickness with nitrocarburizing temperature (*a, b, e, f*, and *i*).

4.2.2.2 Compound Layer and Diffusion Zone of Navy C-rings

The micrographs of the four thickest C-rings for gas ferritic nitrocarburizing at 540 °C for 10 hrs are shown in Figure 4.15. For the thickest 1-NC C-ring series, Figure 4.15 (a), a very thin compound layer was formed at the surface of the steel. Beneath the compound layer, there were a small amount of pearlite as well as needle-like γ' phases in the ferrite matrix. In Figure 4.15 (b) and (c), the pearlite content increased as the C-ring thickness decreased from the 2-NC to 3-NC C-ring series. A thin compound layer, as well as an underlying diffusion zone containing gamma prime needles (Fe_4N), was also present in the steel. For the 5.05 mm-thick 4-NC C-ring series, a thicker compound layer was formed at the steel surface. In the diffusion zone, only gamma prime needles were visible in the ferrite matrix, Figure 4.15 (d).

(a)   (b)

(c)   (d)
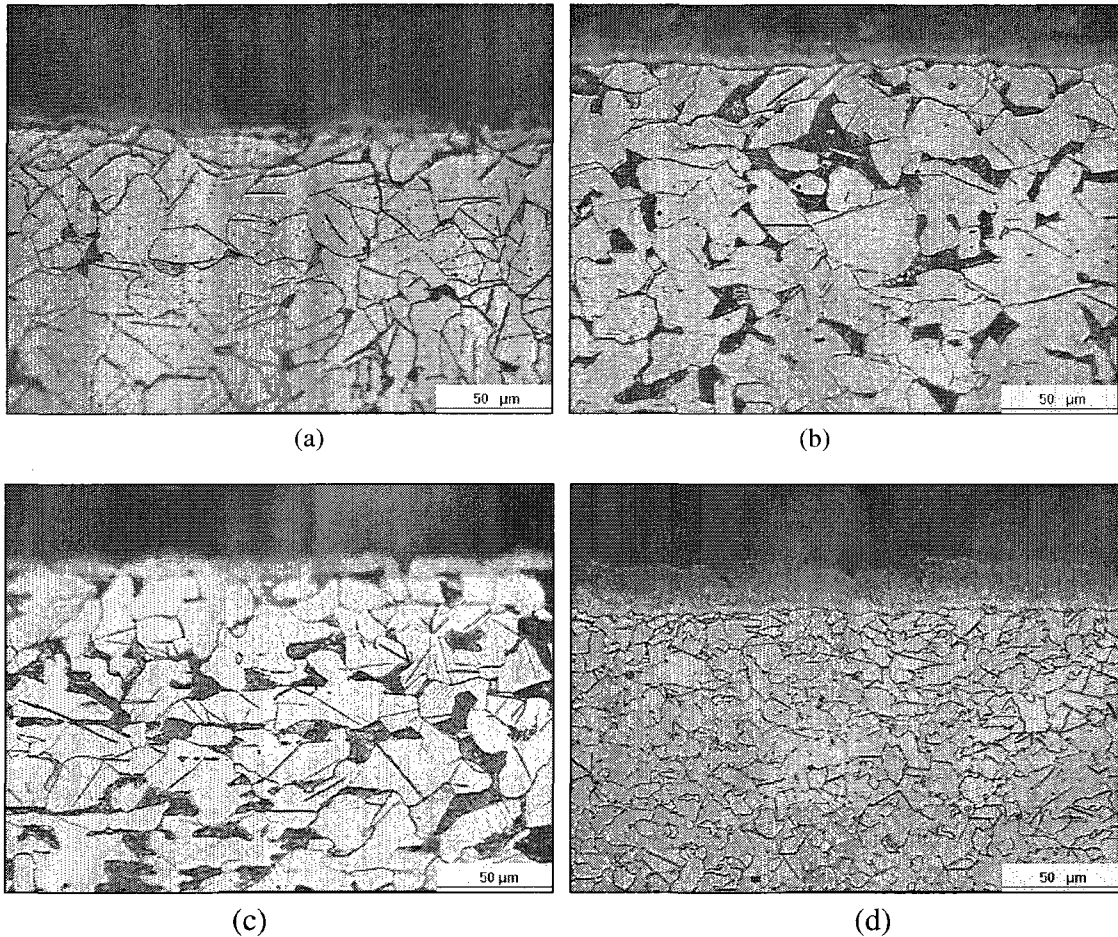
Figure 4.15 Optical micrographs of C-ring samples, gas ferritic nitrocarburizing at 540 °C for 10 hrs (process *b*). (a) 1-NC C-ring series; (b) 2-NC C-ring series; (c) 3-NC C-ring series; (d) 4-NC C-ring series.

The microstructures of the thinnest C-ring series, 5-NC, for the various ferritic nitrocarburizing processes were similar to the pistons subjected to the same heat treatment methods, as shown in Figures 4.16-4.25. A region of porosity was also visible at the surface of the compound layer. The difference is that the compound layer of the C-ring sample formed at 510 °C for 15 hrs by gas ferritic nitrocarburizing was thicker than that of the piston after the same processing, Figure 4.16. For the ion ferritic nitrocarburizing processes (*e* and *f*), the penetration of needle-like γ' phases into the diffusion zone was visible, which is different from the piston samples, Figures 4.20 and 4.21. Similar to the piston sample, a significant thickness difference between the gas ferritic nitrocarburizing with controlled nitrogen potential (*g* and *h*) was observed, as

shown in Figures 4.22 and 4.23. For gas ferritic nitrocarburizing with water base quenching (j), the presence of needle-like gamma prime phases into the diffusion zone was not evident, Figure 4.25.

A comparison between the 5-NC and 1-through 4-NC C-ring series for the gas ferritic nitrocarburizing at 540 °C for 10 hrs shows that a thicker compound layer was formed at the surface of 5-NC C-ring sample, with an underlying diffusion zone consisting gamma prime phases. No pearlite phase was observed in the diffusion zone.
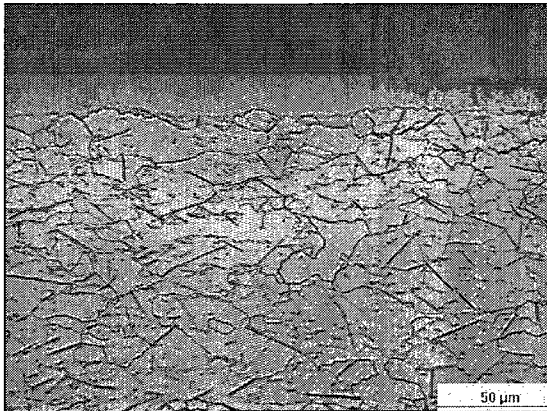
Figure 4.16 Microstructure of 5-NC C-ring (gas ferritic nitrocarburizing a, 510 °C / 15 hrs)
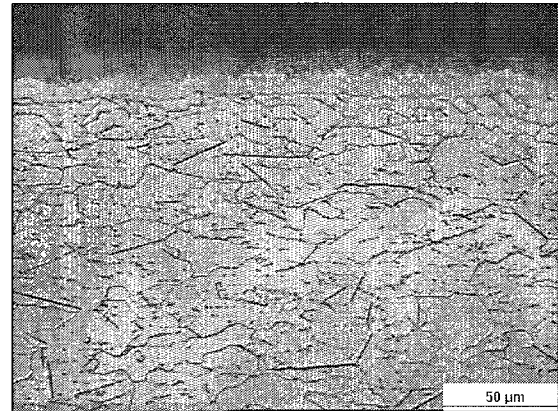
Figure 4.17 Microstructure of 5-NC C-ring (gas ferritic nitrocarburizing b, 540 °C / 10 hrs)
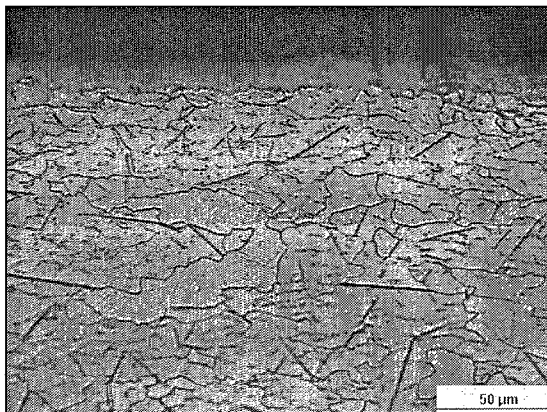
Figure 4.18 Microstructure of 5-NC C-ring (gas ferritic nitrocarburizing c, 565 °C / 5 hrs)
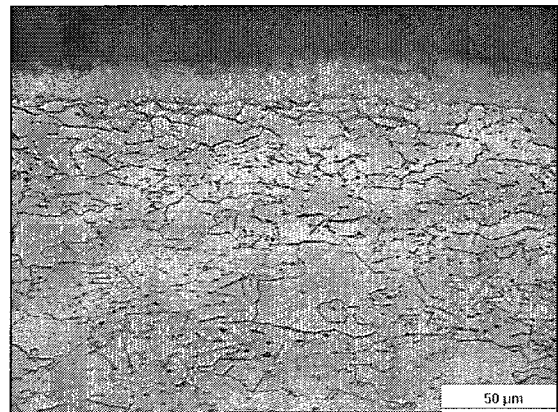
Figure 4.19 Microstructure of 5-NC C-ring (gas ferritic nitrocarburizing d, 595 °C / 4 hrs)
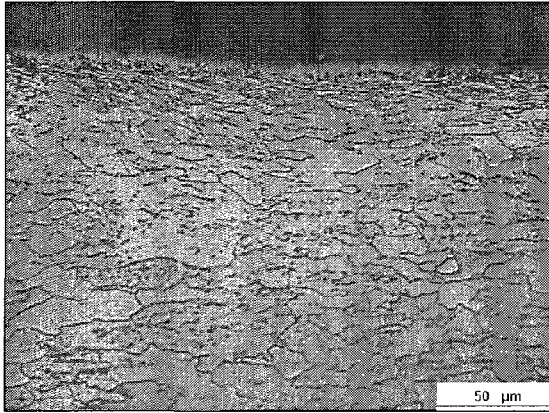
Figure 4.20 Microstructure of 5-NC C-ring (ion ferritic nitrocarburizing *e*, 560 °C / 15 hrs)
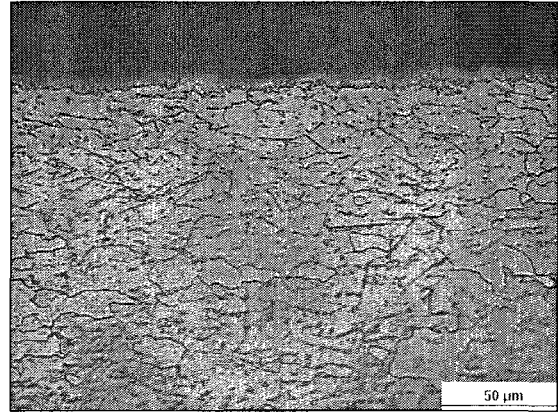
Figure 4.21 Microstructure of 5-NC C-ring (ion ferritic nitrocarburizing *f*, 525 °C / 24 hrs)
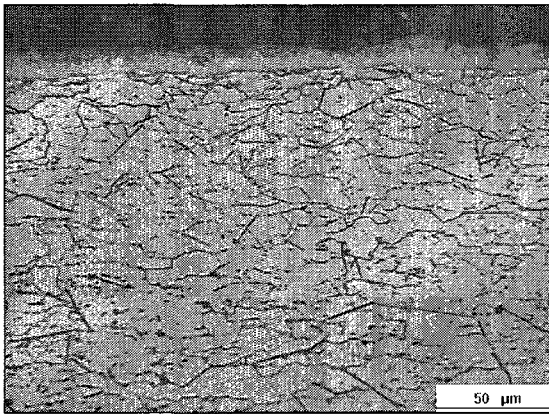
Figure 4.22 Microstructure of 5-NC C-ring (gas ferritic nitrocarburizing *g*, 525 °C / 52 hrs)
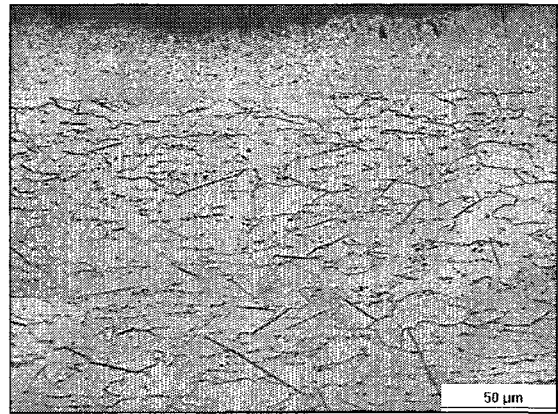
Figure 4.23 Microstructure of 5-NC C-ring (gas ferritic nitrocarburizing *h*, 570 °C / 4 hrs)
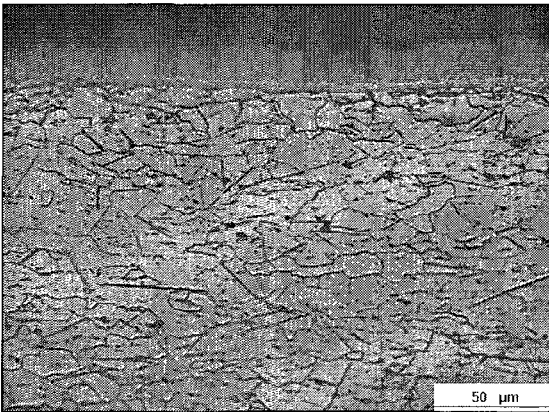
Figure 4.24 Microstructure of 5-NC C-ring (vacuum ferritic nitrocarburizing *i*, 580 °C / 10 hrs)
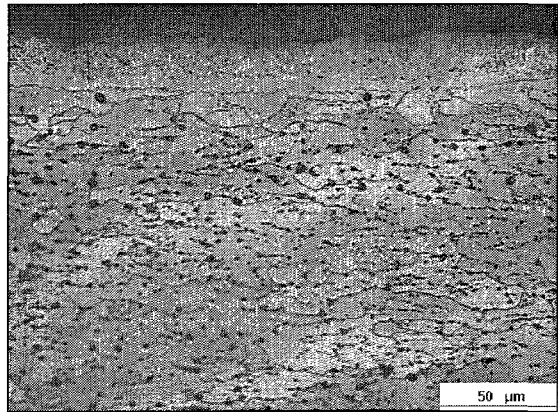
Figure 4.25 Microstructure of 5-NC C-ring (gas ferritic nitrocarburizing *j*, 580 °C / 2 hrs)

The average values of the compound layer thickness of the 5-NC C-ring specimens are given in Table 4.2.

Table 4.2 Case depths of 5-NC C-rings for the various ferritic nitrocarburizing (a-j) processes.

Process		Symbol	Average of Case Depth (μm)
Gas ferritic nitrocarburizing	510 °C / 15 hrs	*a*	29.85 ± 1.77
	540 °C / 10 hrs	*b*	19.16 ± 1.59
	565 °C / 5 hrs	*c*	13.73 ± 1.52
	595 °C / 4 hrs	*d*	19.12 ± 0.91
Ion ferritic nitrocarburizing	560 °C / 15 hrs	*e*	7.08 ± 1.24
	525 °C / 24 hrs	*f*	7.95 ± 1.30
Gas ferritic nitrocarburizing (controlled nitrogen potential)	525 °C / 52 hrs	*g*	12.31 ± 1.03
	570 °C / 4 hrs	*h*	34.07 ± 1.05
Vacuum ferritic nitrocarburizing	580 °C / 10 hrs	*i*	20.04 ± 1.11
Gas ferritic nitrocarburizing (water-base quenching)	580 °C / 2 hrs	*j*	22.80 ± 1.39

A comparison of the case depths for both the pistons and the 5-NC C-rings resulting from the different nitrocarburizing processes is shown in Figure 4.26. The thickness of the compound layer is in the range of 10-40 μm [10, 42]. The gaseous ferritic nitrocarburizing processes resulted in a thicker compound layer at the surface of C-ring specimens than the pistons, whereas the ion ferritic nitrocarburizing processes (*e* and *f*) produced thinner case on the C-ring samples.
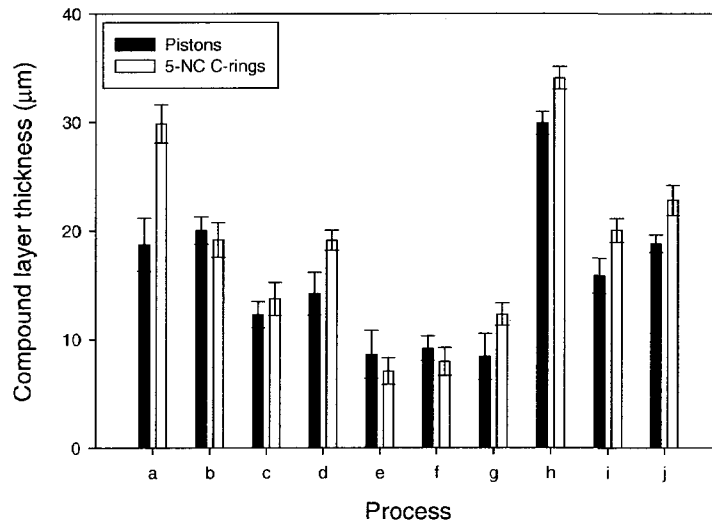
Figure 4.26 Compound layer thickness of both piston and 5-NC C-ring specimens for various ferritic nitrocarburizing processes (a-j).

65

4.3 SEM Analysis

Piston samples for gas and ion ferritic nitrocarburizing (a and e) were observed under the scanning electron microscope to further analyze the microstructure at a higher magnification. A SEM micrograph of the gas ferritic nitrocarburized piston is shown in Figure 4.27 (a). A well-formed compound layer with slight porosity was present at the surface of the nitrocarburized piston specimen. The underlying diffusion zone showed gamma prime (γ') needles (Fe_4N) in a ferrite matrix.

A different structure was observed for the ion nitrocarburized samples. In Figure 4.27 (b), a large amount of porosity was visible in a non-uniform compound layer at the surface of the piston sample. The compound-layer-like structures continue into the diffusion zone. However, few needle-like gamma prime phase particles were detected in the diffusion zone. As noted by Çelik et al [44], during ion nitrocarburizing, the diffusing carbon atoms inhibit the penetration of atomic nitrogen into the interstitial positions of the ε iron lattice. As a result, the nitrogen atoms accumulated in the low energy regions, such as grain boundaries, to form molecular nitrogen which led to the formation of more micropores [44].

| (a) | (b) |
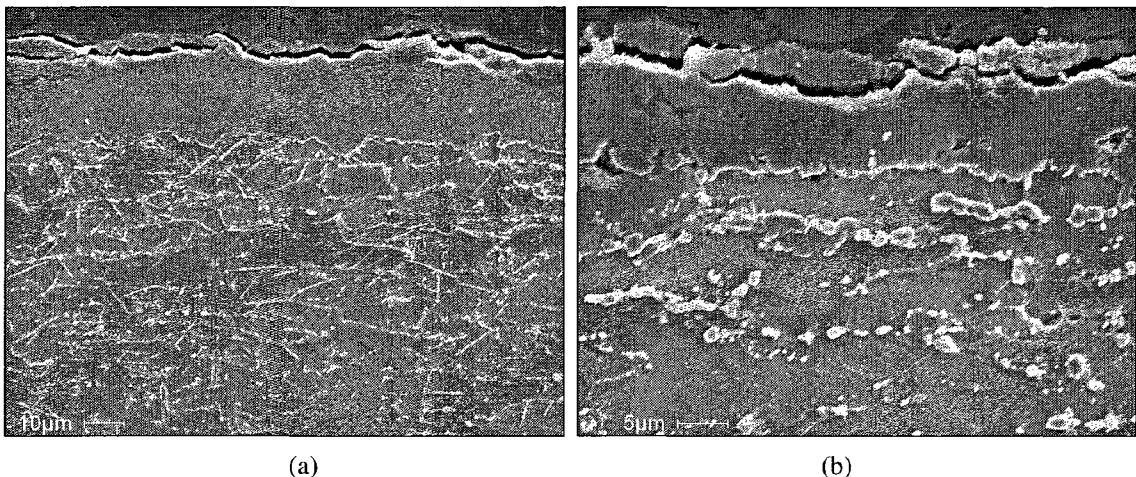
Figure 4.27 SEM micrographs of piston sample. (a) Gas ferritic nitrocarburized piston, process a (510 °C / 15 hrs); (b) Ion ferritic nitrocarburized piston, process e (560 °C / 15 hrs).

4.4 Microhardness Comparisons

Cross sections of the nitrocarburized specimens were subjected to Vickers microhardness testing to evaluate the hardness of the compound layer and the diffusion zone underneath. The hardness of the compound layer was measured at its midpoint using a Vickers indenter. The loads applied for the nitrocarburized samples were respectively 10 and 25 gf, while for the carbonitrided samples was 500 gf. The average values of the case hardness and standard deviation are summarized in Table 4.3. Both the ion ferritic nitrocarburizing (e and f) and gas ferritic nitrocarburizing with water-base quenching (j) resulted in a larger value of case hardness.

Table 4.3 Case hardness of pistons for various ferritic nitrocarburizing (a-j) and carbonitriding process (k).

Process		Symbol	Average of Case Hardness (HV)	Load (gf)
Gas ferritic nitrocarburizing	510 °C / 15 hrs	a	725 ± 119	10
	540 °C / 10 hrs	b	524 ± 125	10
	565 °C / 5 hrs	c	1053 ± 163	10
	595 °C / 4 hrs	d	1146 ± 165	10
Ion ferritic nitrocarburizing	560 °C / 15 hrs	e	1337 ± 189	10
	525 °C / 24 hrs	f	1544 ± 167	25
Gas ferritic nitrocarburizing (controlled nitrogen potential)	525 °C / 52 hrs	g	977 ± 188	10
	570 °C / 4 hrs	h	822 ± 111	10
Vacuum ferritic nitrocarburizing	580 °C / 10 hrs	i	1042 ± 145	10
Gas ferritic nitrocarburizing (water-base quenching)	580 °C / 2 hrs	j	1469 ± 133	25
Gas carbonitriding	850 °C / 4 hrs	k	995 ± 21	500

Hardness data for the gas, ion and vacuum nitrocarburizing processes (a, b, e, f, and i) are plotted as a function of the respective compound layer thickness in Figure 4.28. This shows that a thinner compound layer exhibited a higher case hardness. This relationship is due to the more compact nature of the thinner compound layer and/or a higher nitrogen content.

67
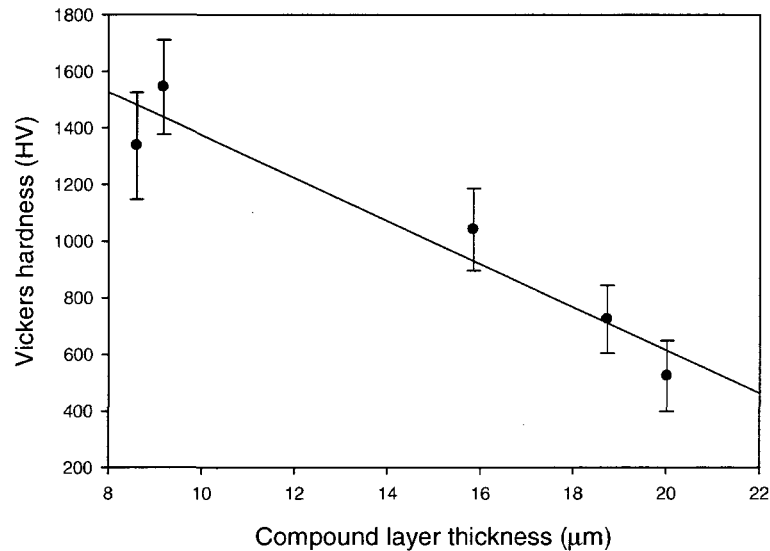
Figure 4.28 Effect of compound layer thickness on microhardness (a, b, e, f, and i).

The same piston samples subjected to gas, ion, and vacuum nitrocarburizing processes (a, b, e, f, and i) were then used to characterize the hardness profiles across the diffusion zone. Hardness traverses of the diffusion zone were made from the interface between the compound layer and the substrate to the same interface at the opposite face of the piston. The hardness profiles are shown in Figure 4.29. The highest hardness values were obtained in the nitrogen-rich region near to the interface due to the nitride precipitation phenomena in the matrix, and were in the range of 250 and 300 HV (100gf). The hardness of the samples decreased toward the mid-thickness of the sample, where the substrate hardness dropped to less than 150 HV. The hardness values increased again due to the penetration of nitrogen from the reverse side of the specimen. The hardness profiles for the ion ferritic nitrocarburizing processes were significantly higher than the other processes. Similar hardness levels were observed for the gas and vacuum nitrocarburizing processes.
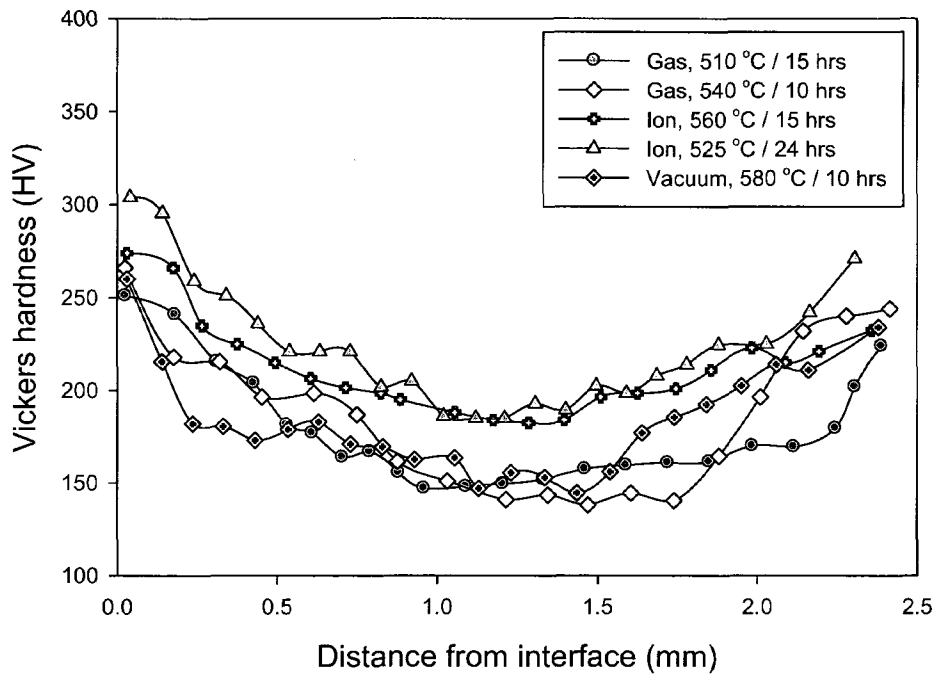
Figure 4.29 Hardness profiles of pistons after various ferritic nitrocarburizing processes (*a*, *b*, *e*, *f*, and *i*).

A typical hardness survey taken on the cross section of a gas carbonitrided piston sample is shown in Figure 4.30. This graph illustrates that the martensitic case has the highest hardness value. With increasing distance from the surface of the specimen, the hardness values decreased significantly. Upon reaching about 0.6mm below the surface, the hardness leveled off due to the uniform phase composition at the core of the sample.
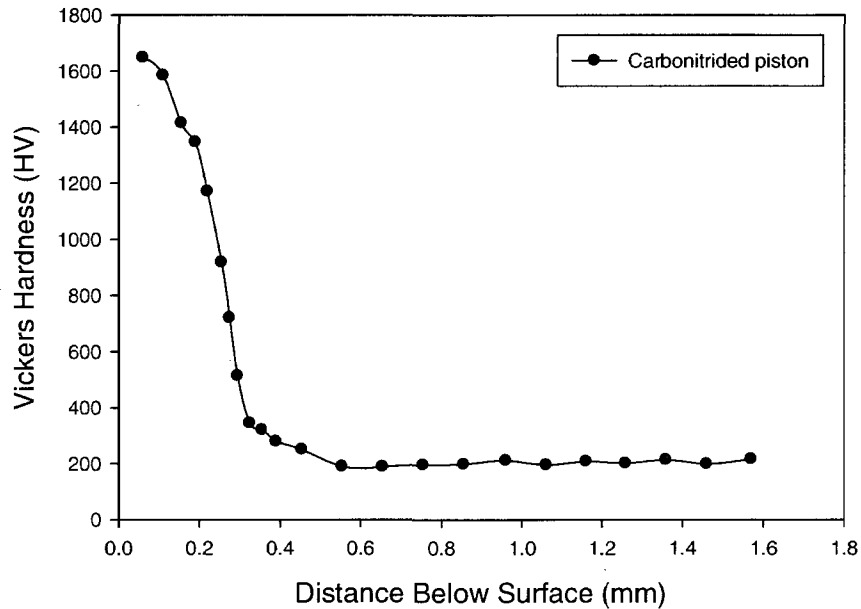
Figure 4.30 Variation of hardness with distance below the surface for a carbonitrided piston.

4.5 Phase Analyses for Nitrocarburized and Carbonitrided C-rings

Phase analysis was performed at the surface of the nitrocarburized and carbonitrided 1-NC C-ring series using the XRD method. The results of x-ray diffraction analysis for processes *a-k* are given in Table 4.4.

Table 4.4 Surface phase analysis of the nitrocarburized and carbonitrided 1-NC C-rings.

Process	Fe_3C	Fe_3N (ε)	Fe_4N (γ')
a	-	-	-
b	-	+	-
c	-	+	-
d	-	+	-
e	+	+	+
f	+	+	+
g	-	+	+
h	-	+	-
i	-	+	-
j	-	+	-
k	-	-	-

The XRD analysis demonstrates that the various ferritic nitrocarburizing processes resulted in a compound layer mainly consisting of ε and γ' phases, which is

consistent with the findings of Kolozsváry [92]. The gaseous ferritic nitrocarburized compound layer was composed predominantly of the ε iron-carbonitride phase [18], except for the sample from process a, in which no nitride phase was detected. The ion ferritic nitrocarburized sample contained both the ε and γ' phases, which is in agreement with the findings of Bell *et al.* [56]. The Fe_3C and Fe_4N phases were only detected in the ion ferritic nitrocarburized samples, with the exception of a gas ferritic nitrocarburized (g) sample containing Fe_4N phases. For the gas carbonitrided sample, none of the above phases were found.

4.6 Summary

Different microstructures were formed in the piston and C-ring samples after the nitrocarburizing or carbonitriding processes due to the various heat treatment methods and parameters applied, as well as the varying specimen thickness. A very thick and hard martensitic case was formed at the steel surface after gas carbonitriding and subsequent quenching. However, a typical compound layer at the surface and an underlying diffusion zone containing needle-like γ' phases are produced for the ferritic nitrocarburizing processes. Similar microstructures were obtained for the 5-NC C-ring series and pistons under the same nitrocarburizing condition, with the compound layer thicknesses ranging from 10-40 μm. For the C-ring series with different thicknesses, a thin compound layer was formed at the surface of the 1-NC to 3-NC C-ring samples; both pearlite and needle-like γ' phases were present in the ferrite matrix. The ion ferritic nitrocarburizing processes (e and f) resulted in a very thin but very hard compound layer at the surface of the specimen as well as a hard diffusion zone, compared to the gas and vacuum nitrocarburizing processes.

As expected, the hardness profiles for both the nitrocarburizing and carbonitriding show the highest values near the surface due to the case hardening. Beneath the surface of the material, the hardness decreased as the distance increased from the surface to the substrate. The XRD phase analysis shows that the ion ferritic nitrocarburized C-ring specimens contained both ε and γ' iron-carbonitrides in the compound layer, while the surface of the gas and vacuum nitrocarburized C-rings was mainly composed of the ε

71

phase alone. The texture of the SAE 1010 steel piston after stamping station shows a rolling direction of <111> and a rolling plane of (112).

V. EFFECTS OF HEAT TREATMENT ON DIMENSIONAL DISTORTION

This section discusses the distortion associated with the various ferritic nitrocarburizing and carbonitriding processes for both the Navy C-ring and piston specimens. The nitrocarburizing and carbonitriding processes were evaluated in terms of size and shape distortion. Four specified dimensions for each piston and C-ring sample both before and after nitrocarburizing or carbonitriding were measured using a Coordinate Measuring Machine (CMM). The average values obtained from the individual tests were then summarized to compare between nitrocarburizing and carbonitriding, or among the various ferritic nitrocarburizing processes. The size and shape distortion values associated with each test specimen are presented in Appendix A.

The average size (OD, ID, and gap) and shape (flatness) distortion values for the 1-through 5-NC C-ring samples are shown in Tables 5.1-5.4. The data are identified in a ranked order with the smallest dimensional change being ranked 1. For the OD changes, Table 5.1, both nitrocarburizing and carbonitriding led to a small expansion of the outside diameter in all the C-ring samples, except for the carbonitrided 5-NC sample. Processes *b*, *c* and *i* led to smaller OD changes, whereas processes *e*, *g* and *h* produced larger OD distortion. Gas carbonitriding (*k*) produced the largest OD distortion in the 1-NC series. However, it also produced the smallest OD changes in the 4-NC and 5-NC series.

Table 5.1 OD changes of C-ring specimens (unit: %)

| Rank | OD | | | | | | | | | |
| | 1-NC Series | | 2-NC Series | | 3-NC Series | | 4-NC Series | | 5-NC Series | |
	Process	Average values	Process	Average values	Process	Average values	Process	Average values	Process	Average values
1	*c*	0.0438	*b*	0.0374	*b*	0.0409	*k*	0.0295	*k*	-0.0195
2	*b*	0.0463	*c*	0.0383	*c*	0.0440	*i*	0.0308	*c*	0.0380
3	*i*	0.0464	*d*	0.0393	*i*	0.0448	*d*	0.0336	*i*	0.0420
4	*d*	0.0491	*i*	0.0400	*j*	0.0461	*c*	0.0340	*a*	0.0541
5	*g*	0.0503	*a*	0.0418	*d*	0.0463	*j*	0.0348	*d*	0.0548
6	*a*	0.0509	*f*	0.0435	*a*	0.0472	*b*	0.0360	*b*	0.0549
7	*j*	0.0511	*j*	0.0454	*f*	0.0541	*f*	0.0379	*j*	0.0576
8	*e*	0.0550	*g*	0.0475	*h*	0.0557	*a*	0.0472	*f*	0.0618
9	*f*	0.0566	*h*	0.0513	*g*	0.0569	*e*	0.0481	*e*	0.0751
10	*h*	0.0599	*e*	0.0516	*e*	0.0622	*h*	0.0516	*g*	0.0766
11	*k*	0.1146	*k*	--	*k*	--	*g*	0.0610	*h*	0.0771

For the ID measurements shown in Table 5.2, the ID changes in the 1-NC C-ring series are positive. While for the other C-ring series, the ID dimension experienced either a small expansion or small contraction depending on temperature-time combinations and specimen thickness. Processes c and i resulted in smaller ID changes, whereas process g led to larger ID distortion. The C-rings subjected to gas carbonitriding were noted to have experienced the largest ID changes when compared to those subjected to ferritic nitrocarburizing.

Table 5.2 ID changes of C-ring specimens (unit: %)

Rank	ID									
	1-NC Series		2-NC Series		3-NC Series		4-NC Series		5-NC Series	
	Process	Average values	Process	Average values	Process	Average values	Process	Average values	Process	Average values
1	h	0.0057	b	0.0008	b	0.0004	i	-0.0024	i	0.0047
2	i	0.0171	a	0.0009	a	0.0009	f	0.0057	c	-0.0079
3	c	0.0201	j	0.0017	c	0.0012	d	-0.0070	d	-0.0156
4	j	0.0202	i	0.0020	i	0.0013	b	-0.0087	e	0.0158
5	a	0.0203	c	0.0029	d	0.0018	c	-0.0108	a	0.0166
6	d	0.0213	d	-0.0038	j	-0.0022	j	-0.0139	j	-0.0184
7	e	0.0226	e	0.0097	h	-0.0075	e	0.0144	f	0.0187
8	g	0.0241	g	0.0133	g	0.0163	h	-0.0212	b	-0.0209
9	b	0.0248	f	0.0143	e	0.0282	a	-0.0216	g	0.0218
10	f	0.0466	h	-0.0155	f	0.0285	g	0.0240	h	-0.0364
11	k	0.1565	k	--	k	--	k	-0.0343	k	-0.1230

A summary of the gap distortion measurements in Table 5.3 shows that the gap width tended to contract after the various nitrocarburizing processes. Processes c and d led to smaller gap changes; processes g produced larger gap changes in the 1-through 4-NC series. The carbonitriding resulted in a larger gap distortion in the 1-NC and the 5-NC series samples than the nitrocarburizing processes. For shape distortion evaluation, the flatness changes are shown in Table 5.4. The flatness of the C-ring samples after carbonitriding was improved, which means that the difference between the maximum and minimum points of deviation from a reference surface was reduced compared to the sample before carbonitriding. On the other hand, for the nitrocarburized specimens, most flatness values are positive, which reveals the flatness of the C-rings was deteriorated.

Table 5.3 Gap changes of C-ring specimens (unit: %)

Rank	Gap									
	1-NC Series		2-NC Series		3-NC Series		4-NC Series		5-NC Series	
	Process	Average values	Process	Average values	Process	Average values	Process	Average values	Process	Average values
1	a	-0.0139	c	-0.0424	j	-0.2128	k	0.0833	g	-0.1370
2	c	0.0311	i	-0.1054	d	-0.2377	d	-0.2030	d	-0.1650
3	j	0.0441	b	-0.1066	e	-0.2453	i	-0.2168	b	-0.1820
4	i	-0.0727	d	-0.1173	c	-0.2484	b	-0.2367	c	-0.1893
5	b	0.0798	a	-0.1361	b	-0.2528	c	-0.2452	f	-0.2082
6	d	0.0936	j	-0.1609	f	-0.2604	e	-0.2556	e	-0.2173
7	h	-0.0955	g	-0.2945	a	-0.2644	j	-0.2710	j	-0.2683
8	f	0.0993	h	-0.2984	i	-0.2966	g	-0.2924	i	-0.3034
9	e	-0.3042	f	-0.3225	h	-0.3521	h	-0.3475	a	-0.3703
10	g	-0.3416	e	-0.4143	g	-0.4761	a	-0.3524	h	-0.4096
11	k	2.4424	k	--	k	--	f	-0.3772	k	-1.2482

Table 5.4 Flatness changes of C-ring specimens (unit: %)

Rank	Flatness									
	1-NC Series		2-NC Series		3-NC Series		4-NC Series		5-NC Series	
	Process	Average values	Process	Average values	Process	Average values	Process	Average values	Process	Average values
1	c	0.38	g	15.90	f	9.30	g	-1.47	a	0.60
2	d	0.41	d	20.83	i	14.51	f	5.32	g	-6.53
3	g	3.43	j	36.48	e	24.95	h	10.85	h	10.09
4	i	-4.30	i	41.30	c	35.78	e	14.00	d	13.52
5	h	5.46	h	41.96	j	40.63	a	16.79	e	16.36
6	a	-7.14	a	56.57	a	46.37	k	-18.38	c	18.67
7	e	-7.44	b	61.76	g	56.93	b	21.70	j	26.55
8	k	-8.05	f	66.51	d	87.71	i	33.23	i	31.98
9	b	-9.68	e	79.57	b	101.29	c	47.92	b	38.37
10	j	10.39	c	97.22	h	127.70	d	48.89	f	-41.62
11	f	11.46	k	--	k	--	j	93.32	k	-42.29

For the piston specimens, the ID dimensions (size distortion) were evaluated at -11 mm and -15 mm longitudinal height positions from the lockup surface. In Table 5.5, all the ID results associated with ferritic nitrocarburizing were positive, and those induced by gas carbonitriding were negative. As such, the ID dimension of the pistons expanded after ferritic nitrocarburizing process, but contracted after gas carbonitriding. Comparing the nitrocarburizing processes, a, b and c gave rise to smaller size distortions; processes e, f and g showed relatively larger size distortions. The values of total flatness

and flatness taper (shape distortion) indicated that the gas carbonitriding process resulted in a more severe shape distortion compared to the ferritic nitrocarburizing, with magnitudes more than five times larger than those for ferritic nitrocarburizing. Processes c, f and g caused smaller flatness distortions. Processes i and j induced larger flatness changes.

Table 5.5 Dimensional Changes of Pistons (unit: %)

Rank	ID@-11 mm		ID@-15 mm		Total Flatness		Flatness Taper	
	Process	Average values	Process	Average values	Process	Average values	Process	Average values
1	a	0.0183	k	-0.0055	g	5.11	g	21.94
2	b	0.0240	a	0.0381	c	15.64	f	23.69
3	c	0.0255	b	0.0479	f	16.27	c	24.00
4	h	0.0304	c	0.0538	a	16.43	d	31.96
5	d	0.0406	h	0.0554	e	21.37	b	32.03
6	j	0.0426	j	0.0664	d	21.52	a	32.36
7	i	0.0442	d	0.0683	h	25.02	e	35.98
8	k	-0.0615	i	0.0694	b	25.11	h	43.24
9	e	0.0657	e	0.0763	j	39.67	j	76.47
10	g	0.0705	f	0.0913	i	49.27	i	99.73
11	f	0.0745	g	0.0915	k	515.30	k	507.84

5.1 Comparisons between nitrocarburizing (a-d) and carbonitriding (k)

Comparisons of dimensional changes resulted from the gas ferritic nitrocarburizing (a-d) and carbonitriding (k) processes are presented for both the C-ring and piston samples.

5.1.1 1-NC Navy C-rings

The dimensional changes for the standard 1-NC C-ring series are plotted as a function of heat treatment temperature in Figures 5.1-5.4. Comparisons of the OD and ID changes in Figures 5.1 and 5.2 show that both the nitrocarburizing and carbonitriding processes led to OD and ID expansion. The carbonitriding process (k) was responsible for the largest OD and ID changes. For the different gas ferritic nitrocarburizing processes, process c gave smaller OD and ID distortion in comparison with the other processes.
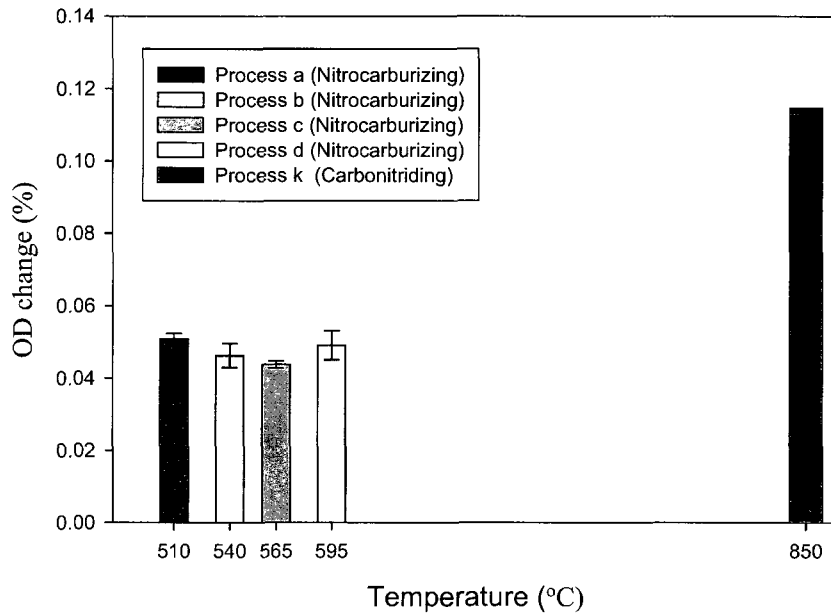
Figure 5.1 OD change of C-rings as a function of nitrocarburizing/carbonitriding temperature (*a-d*, and *k*).
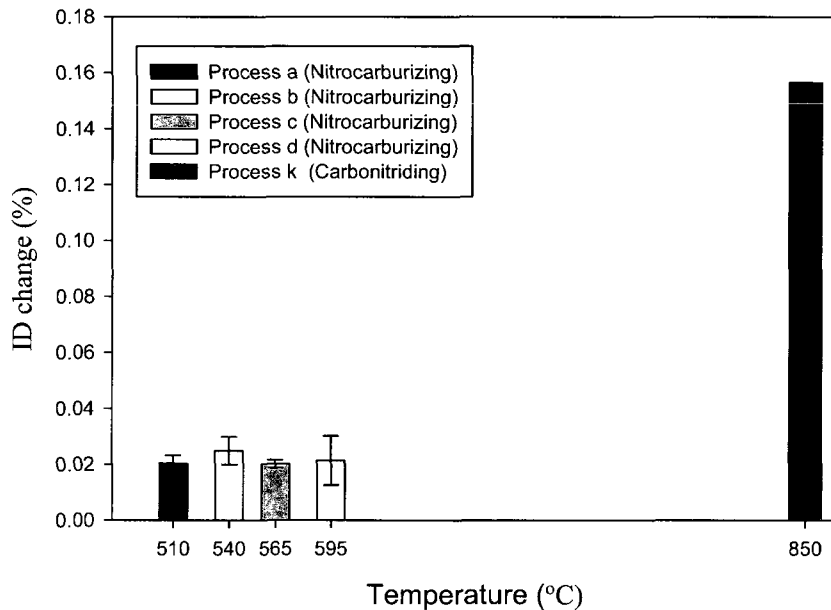
Figure 5.2 ID change of C-rings as a function of nitrocarburizing/carbonitriding temperature (*a-d*, and *k*).

For the gap changes in Figure 5.3, the gas ferritic nitrocarburizing processes (*a-d*) resulted in very small gap changes, whereas the gas carbonitriding (*k*) caused the largest

gap distortion. In Figure 5.4, the flatness of the C-ring samples was improved after nitrocarburizing processes *a*, *b*, as well as gas carbonitriding (*k*), which means the difference between the maximum and minimum points of deviation was reduced compared to the samples before treatment. On the other hand, process *c* and *d* produced a small deterioration in flatness.
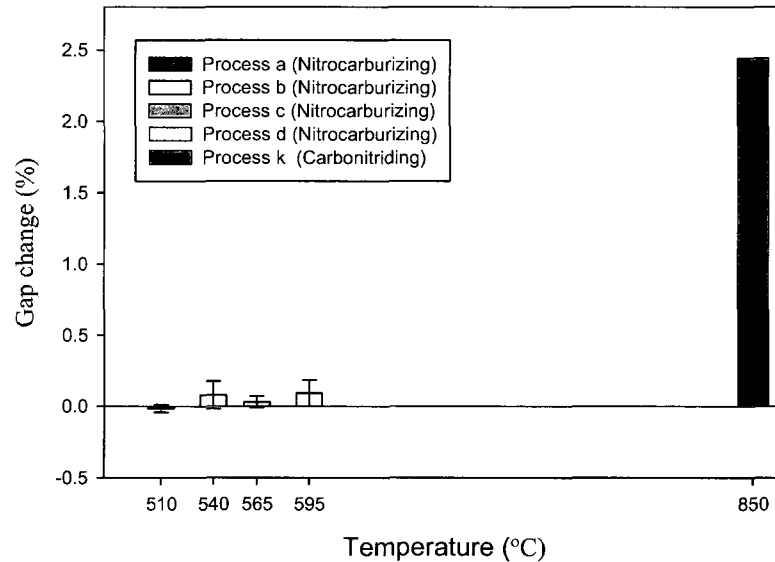
Figure 5.3 Gap change of C-rings as a function of nitrocarburizing/carbonitriding temperature (*a-d*, and *k*).
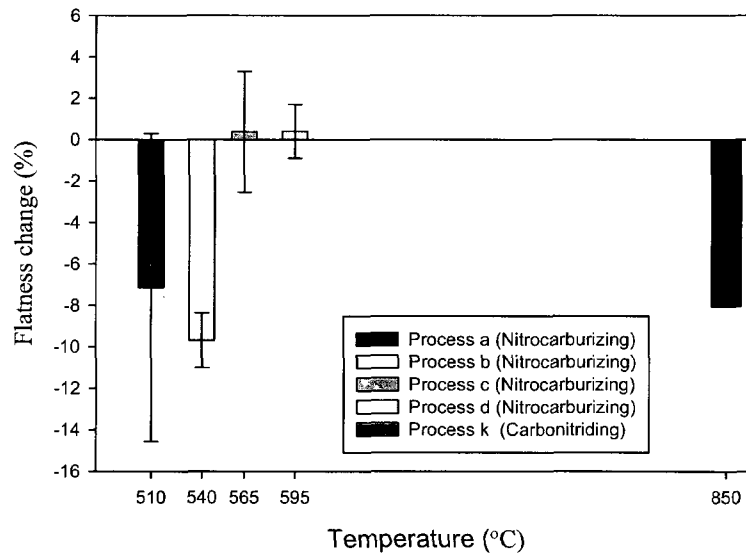
Figure 5.4 Flatness change of C-rings as a function of nitrocarburizing/carbonitriding temperature (*a-d*, and *k*).

78

5.1.2 Torque Converter Pistons

A comparison of the ID dimensional changes of pistons for gas ferritic nitrocarburizing and carbonitriding processes is shown in Figure 5.5. It can be seen that the ID dimension of pistons expanded after ferritic nitrocarburizing processes, but contracted after gas carbonitriding. For the ferritic nitrocarburizing processes, the ID values increased with increasing nitrocarburizing temperature. ID changes at the -15 mm longitudinal height positions were larger than those at the -11 mm height. In Figure 5.6, the ferritic nitrocarburizing processes led to small increases in total flatness and flatness taper values, whereas gas carbonitriding resulted in more severe shape distortion. Process c gave the smallest flatness and flatness taper changes than the other processes.
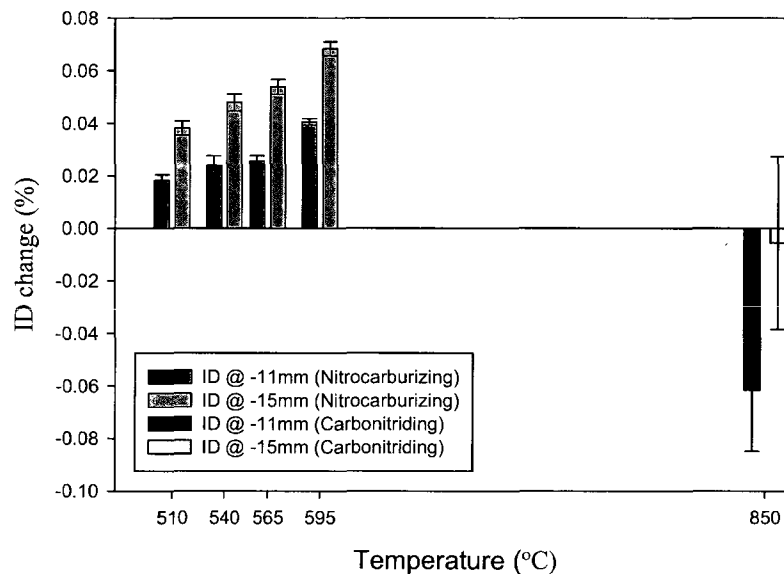
Figure 5.5 ID change of pistons as a function of nitrocarburizing/carbonitriding temperature (*a-d*, and *k*).

79
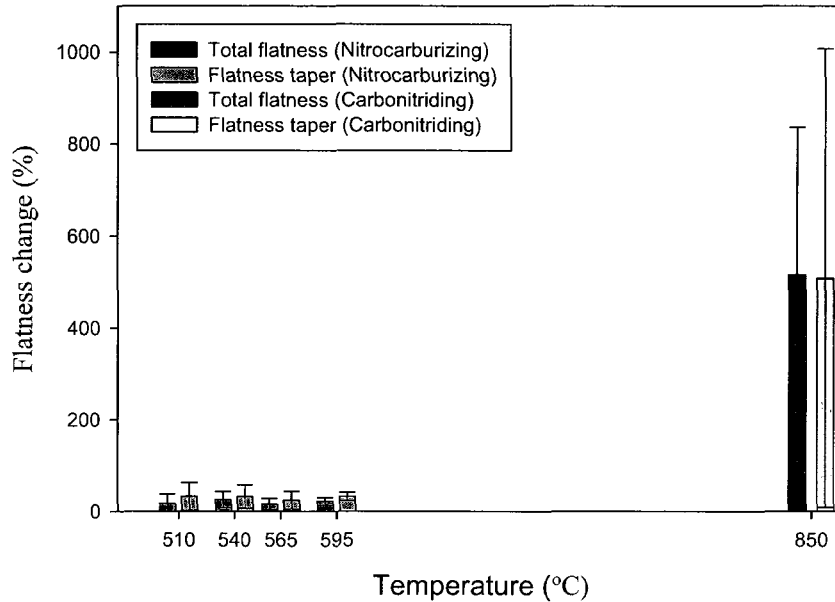
Figure 5.6 Flatness change of pistons as a function of nitrocarburizing/carbonitriding temperature (*a-d*, and *k*).

5.2 Comparisons between gas ferritic nitrocarburizing (a-d)

Emphasis was placed on comparing both the size and shape distortions for the C-ring samples subjected to the gas ferritic nitrocarburizing processes (*a-d*).

5.2.1 1—5-NC Navy C-rings

A comparison of the OD changes resulting from the different gas ferritic nitrocarburizing processes is shown in Figure 5.7. The OD changes were similar in the same series (thickness) of specimens for the different nitrocarburizing temperatures. A comparison of the different C-ring series reveals that the OD dimensions of 1-NC and 5-NC series varied over a wider range from sample to sample with temperature, particularly for the thinnest 5-NC series. A huge deviation of OD dimension was observed in the 5-NC series, which was processed at 510 °C for a longer heat treatment time of 15 hours. The 565 °C / 5 hrs process (*c*) resulted in the smallest OD change compared to the other temperature-time combinations.
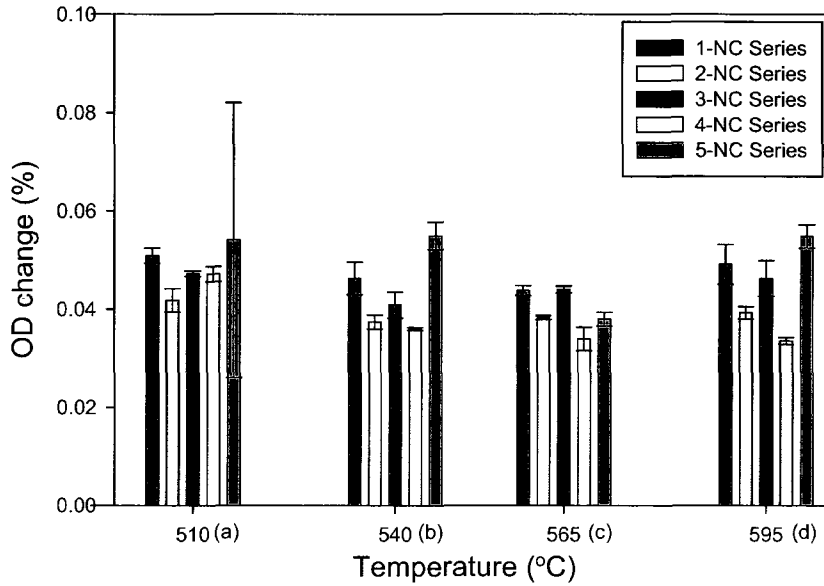
Figure 5.7 OD change of nitrocarburized C-rings as a function of nitrocarburizing temperature (a-d).

In Figure 5.8, the ID dimension after nitrocarburizing increased in the 1-NC series, whereas it decreased in the 4-NC series. The 2-NC and 3-NC series showed smaller ID changes than the other series. Similar to the OD results, the 1-NC and 5-NC series showed larger ID distortion than the other series. The ID dimension of the 5-NC series varied widely from sample to sample after the 15-hour heat treatment at 510 °C (a).
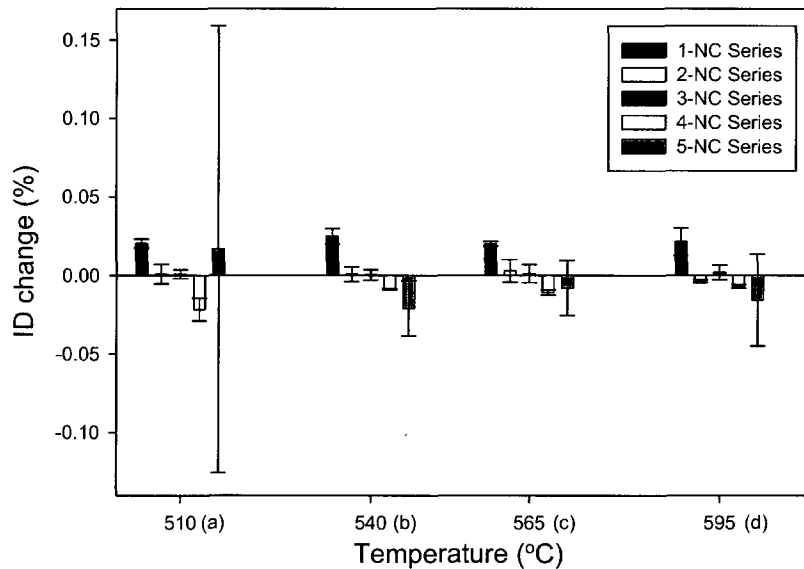
Figure 5.8 ID change of nitrocarburized C-rings as a function of nitrocarburizing temperature (a-d).

81

Figure 5.9 shows that the gap tended to close up as the C-ring thickness decreased from the 1-NC to the 5-NC series. Nitrocarburizing at 565 °C for 5 hours (c) led to smaller changes in gap width than other nitrocarburizing schedules. A comparison of the flatness changes resulting from the different ferritic nitrocarburizing processes is shown in Figure 5.10. The flatness values after nitrocarburizing were increased, except for the 1-NC series. Because the reported values of flatness are referred to the reference surface as a standard, positive values means the flatness was deteriorated. The 2-NC and 3-NC C-rings showed larger flatness distortion than the other series.
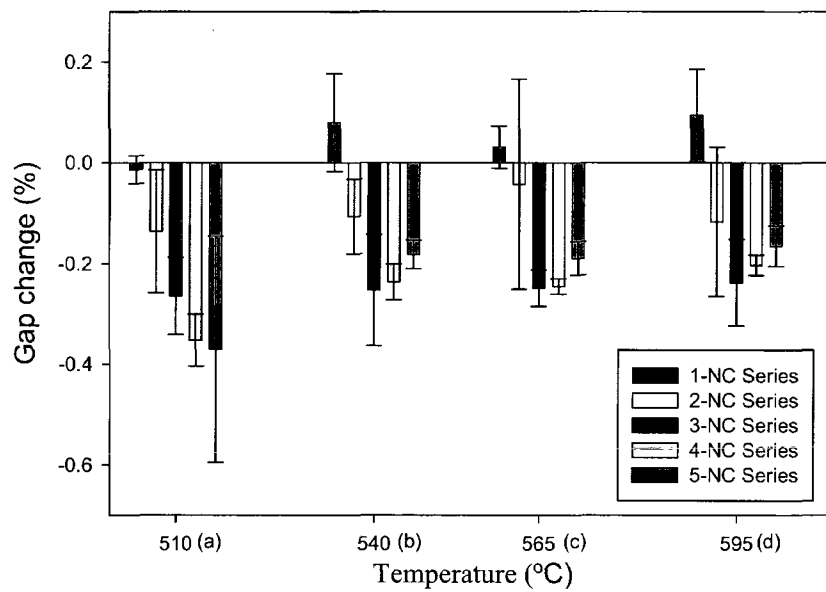
Figure 5.9 Gap change of nitrocarburized C-rings as a function of temperature (a-d).
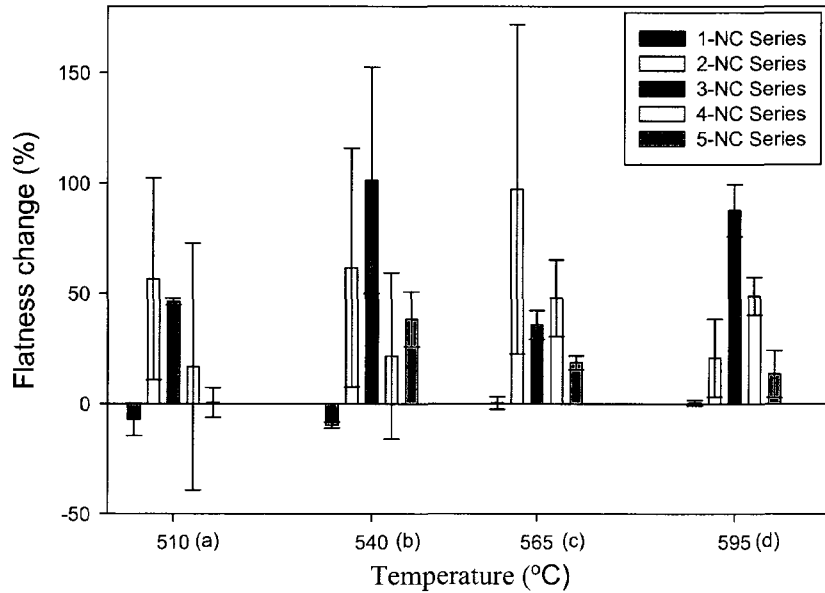
Figure 5.10 Flatness change of nitrocarburized C-rings as a function of nitrocarburizing temperature (a-d).

5.3 Comparisons between gas/ion/vacuum ferritic nitrocarburizing (f/g/i/j)

The dimensional changes resulting from the gas ferritic nitrocarburizing with nitrogen potential control or quenching, as well as from the ion and vacuum ferritic nitrocarburizing processes are compared and analyzed.

5.3.1 1-NC Navy C-rings

The dimensional changes for the 1-NC C-ring series after different ferritic nitrocarburizing processes (f, g, i and j) at different heat treatment temperatures are shown in Figures 5.11-5.14. As shown in Figures 5.11 and 5.12, ion nitrocarburizing (f) produced the largest OD and ID changes. Gas nitrocarburizing and quenching (j) resulted in larger OD and ID changes than vacuum nitrocarburizing (i) at the same nitrocarburizing temperature. The gap tended to close up after gas nitrocarburizing with nitrogen potential control (g) and vacuum nitrocarburizing (i) in Figure 5.13. The flatness deteriorated after nitrocarburizing, Figure 5.14, except for the vacuum nitrocarburizing process.
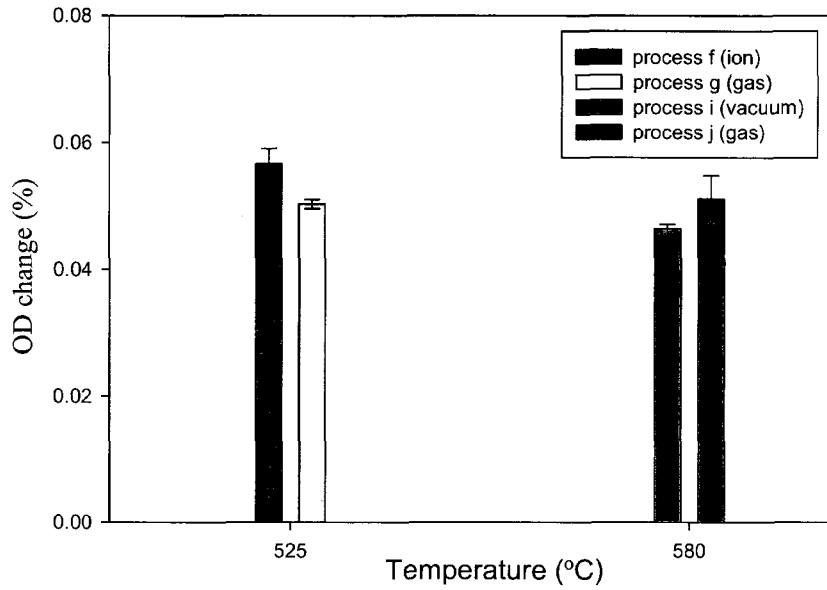
Figure 5.11 OD change of C-rings as a function of nitrocarburizing temperature (f, g, i and j).
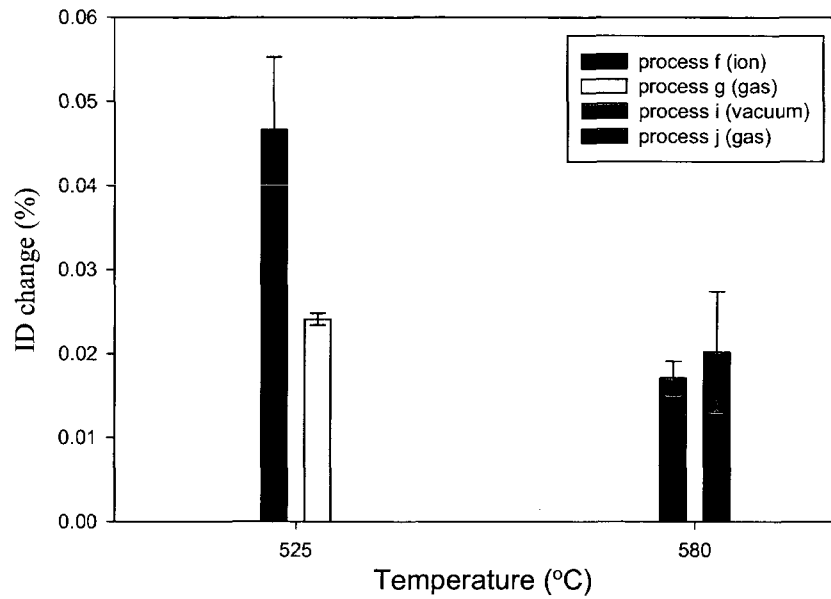
Figure 5.12 ID change of C-rings as a function of nitrocarburizing temperature (f, g, i and j).
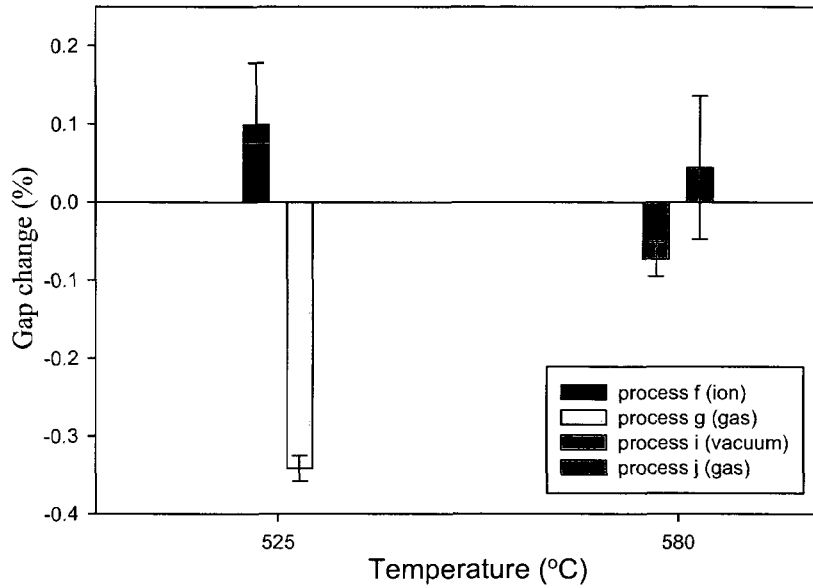
Figure 5.13 Gap change of C-rings as a function of nitrocarburizing temperature (f, g, i and j).
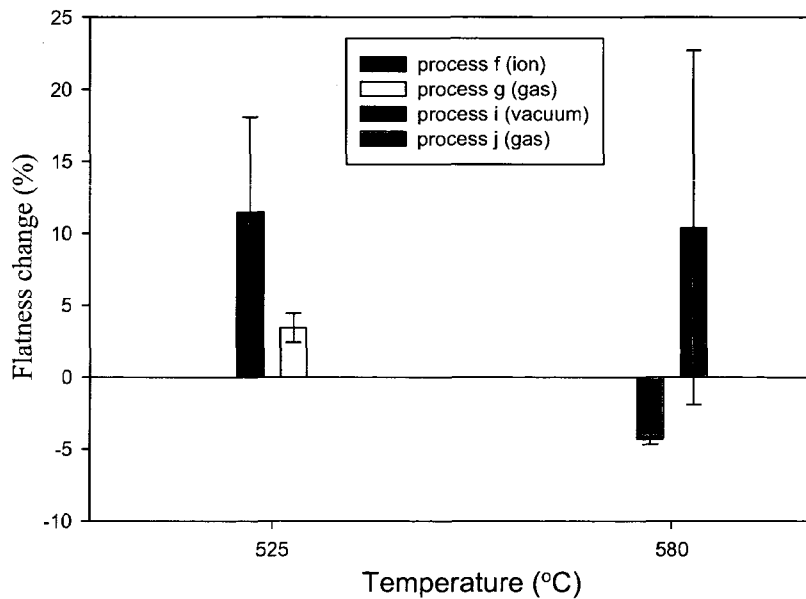
Figure 5.14 Flatness change of C-rings as a function of nitrocarburizing temperature (f, g, i and j).

5.3.2 Torque Converter Pistons

Comparisons of the dimensional changes in the pistons between the different ferritic nitrocarburizing processes (f, g, i and j) are shown in Figures 5.15-5.18. The ID changes resulting from the different nitrocarburizing processes were similar at the same

temperature and measuring position, as shown in Figures 5.15 and 5.16. Ion ferritic nitrocarburizing (f) and gas nitrocarburizing with nitrogen potential control (g) produced larger ID changes, but smaller flatness changes, than the other processes. For the same nitrocarburizing procedure, the ID changes at -15 mm longitudinal height were always larger than those at -11 mm. The values of total flatness and flatness taper varied with the different nitrocarburizing processes, as shown in Figures 5.17 and 5.18. Vacuum nitrocarburizing (i) led to the largest total flatness and flatness taper changes of the nitrocarburizing processes.
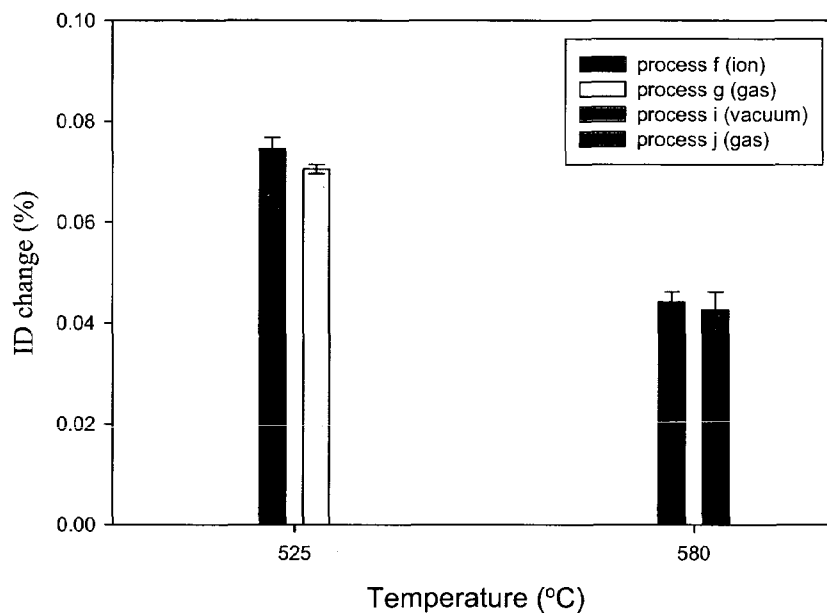
Figure 5.15 ID change (@-11 mm) of pistons as a function of nitrocarburizing temperature (f, g, i and j).
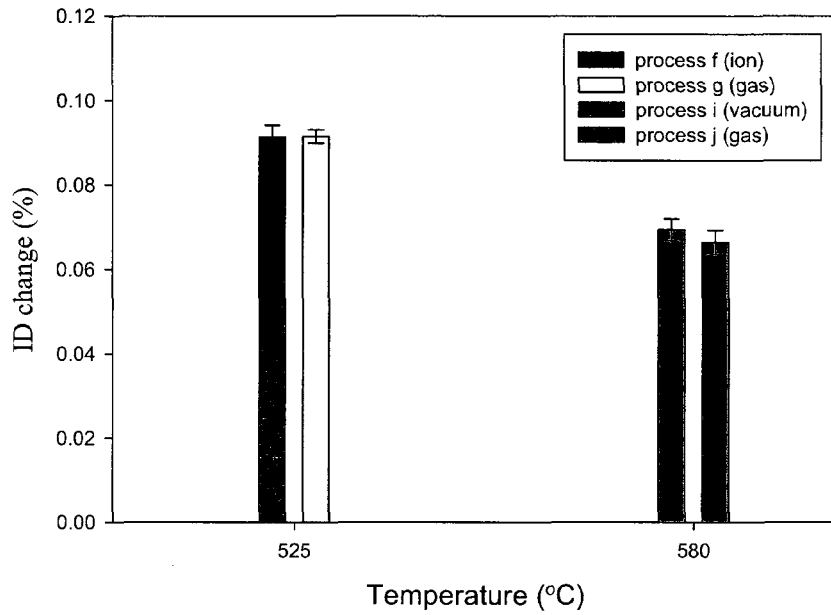
Figure 5.16 ID change (@-15 mm) of pistons as a function of nitrocarburizing temperature (f, g, i and j).
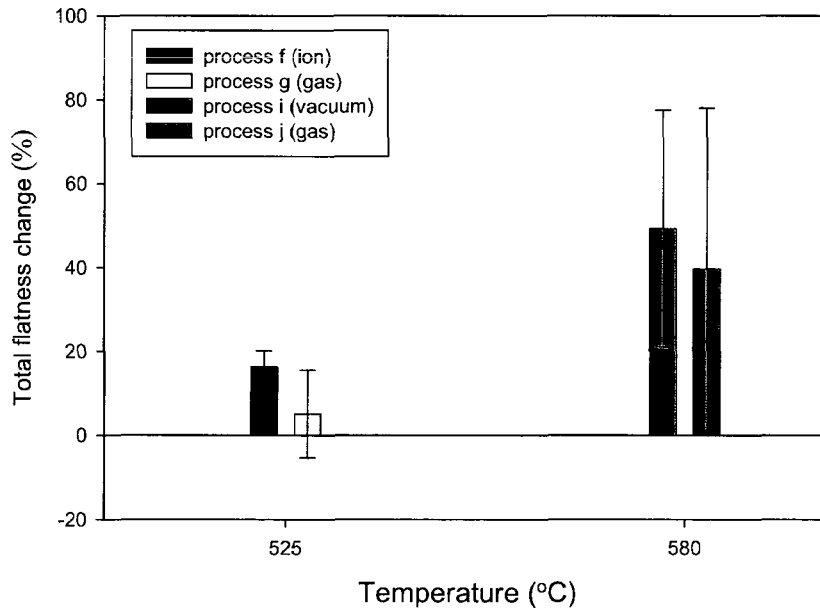
Figure 5.17 Total flatness change of pistons as a function of nitrocarburizing temperature (f, g, i and j).
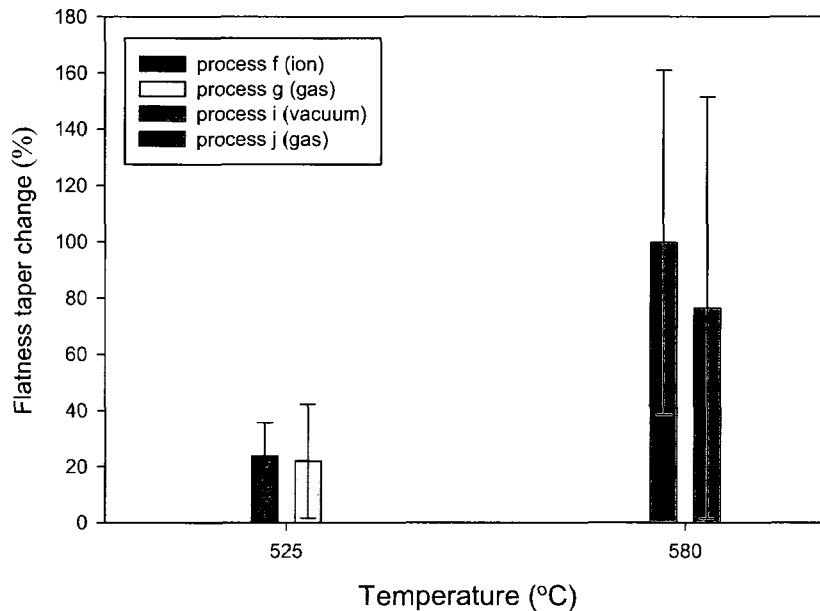
Figure 5.18 Flatness taper change of pistons as a function of nitrocarburizing temperature (*f*, *g*, *i* and *j*).

5.4 Comparisons between gas/ion/vacuum ferritic nitrocarburizing (e/h/i)

Comparisons between the ion, gas, and vacuum ferritic nitrocarburizing performed at different temperatures are presented for both the Navy C-rings and piston specimens.

5.4.1 1—5-NC Navy C-rings

Comparisons of dimensional changes in the C-ring samples between the ion, gas and vacuum ferritic nitrocarburizing processes (*e*, *h*, and *i*) are shown in Figures 5.19-5.22. The various nitrocarburizing processes produced a small OD expansion, as seen in Figure 5.19. Vacuum ferritic nitrocarburizing (*i*) produced the smallest OD changes. As shown in Figure 5.20, the ID tended to contract as the C-ring thickness decreased from the 1-NC to the 5-NC series after gas ferritic nitrocarburizing (*h*). Vacuum ferritic nitrocarburizing (*i*) produced smaller ID changes than the other processes. A comparison between the different C-ring series with varying thicknesses shows that, the 2-NC and 4-NC series experienced smaller OD and ID distortion than the other series. The OD and

ID dimensions of the 5-NC series, which is the thinnest, varied over a wider range from sample to sample and with temperature.
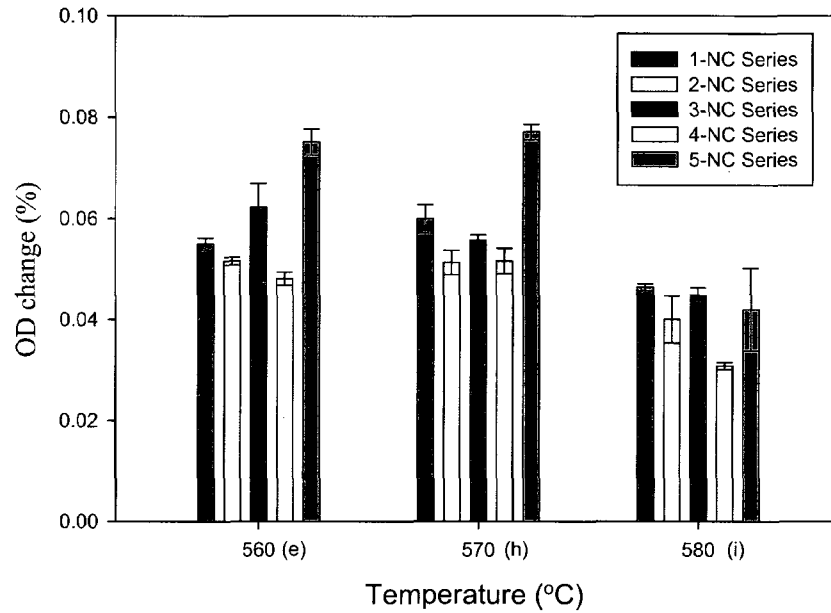
Figure 5.19 OD change of C-rings as a function of nitrocarburizing temperature (*e*, *h*, and *i*).
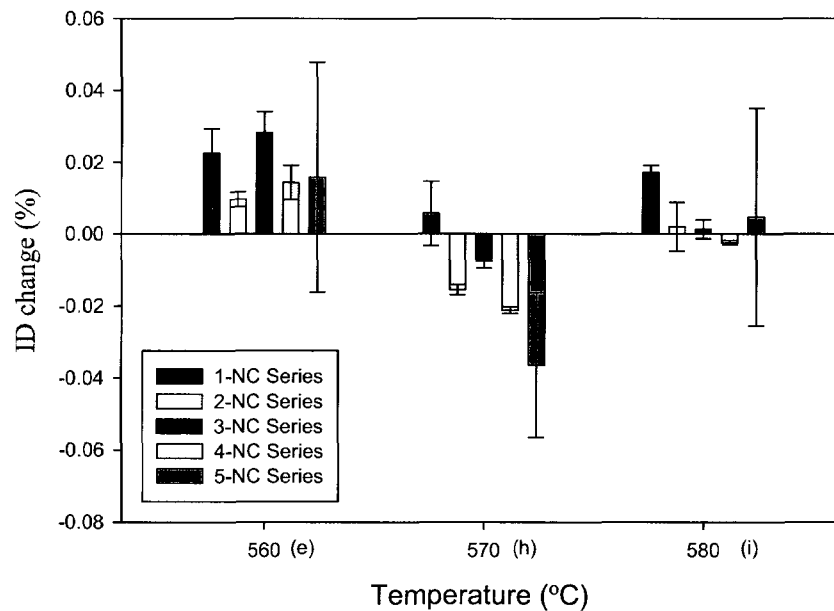
Figure 5.20 ID change of C-rings as a function of nitrocarburizing temperature (*e*, *h*, and *i*).

89
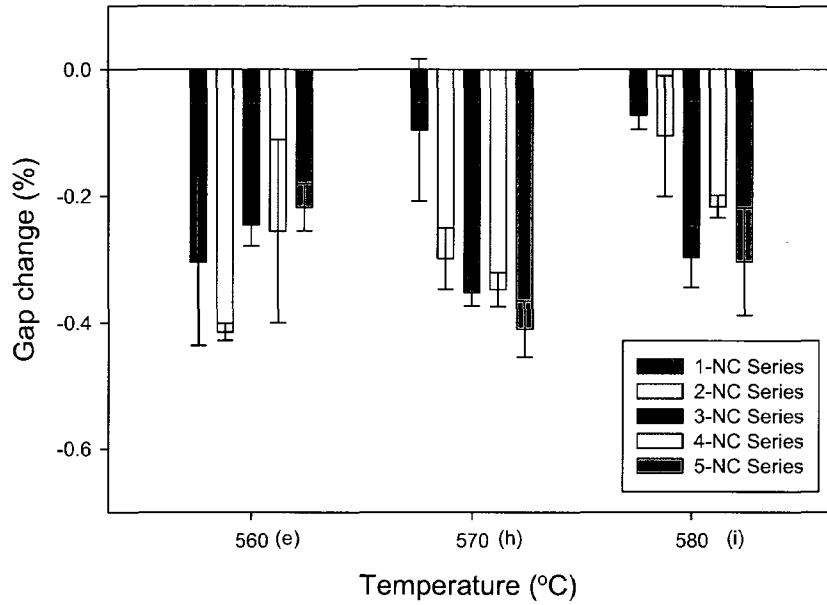
Figure 5.21 Gap change of C-rings as a function of nitrocarburizing temperature (*e*, *h*, and *i*).
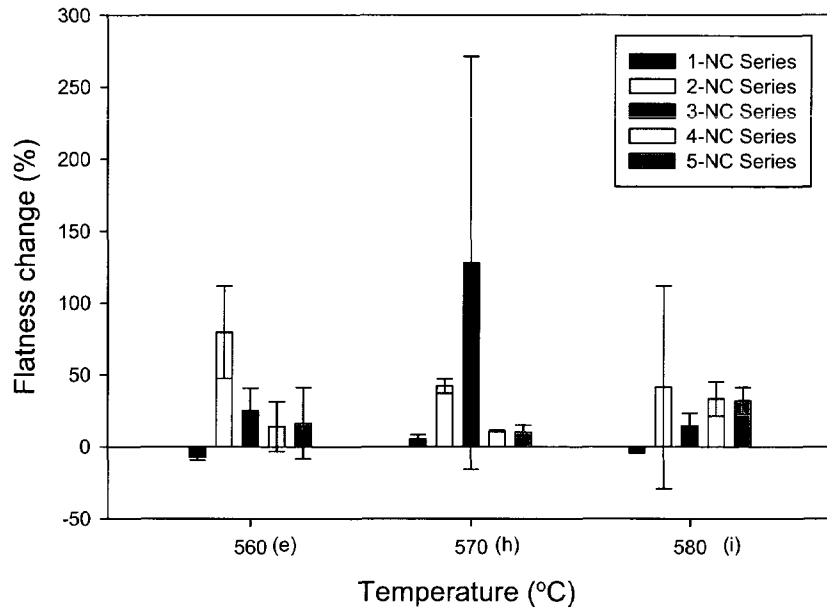
Figure 5.22 Flatness change of C-rings as a function of nitrocarburizing temperature (*e*, *h*, and *i*).

In Figure 5.21, it can be seen that all the nitrocarburizing processes resulted in a gap contraction. The gap width after gas ferritic nitrocarburizing (*h*) tended to decrease

as the C-ring thickness decreased from the 1-NC to the 5-NC series. Vacuum ferritic nitrocarburizing (i) produced smaller gap changes than the other processes. Figure 5.22 shows a small negative flatness change for the 1-NC series, and a small positive change for the 4-NC and 5-NC series. The 2-NC and 3-NC series showed larger flatness changes, especially the flatness change for the 3-NC series treated at 570 °C (h), which varied over a wide range from small negative values to large positive values. Vacuum ferritic nitrocarburizing (i) at 580 °C led to smaller flatness changes than the other processes.

5.4.2 Torque Converter Pistons

Comparisons of the dimensional changes of the piston samples for the ion, gas and vacuum ferritic nitrocarburizing processes (e, h, and i) are shown in Figures 5.23-5.25. All the ferritic nitrocarburizing processes led to an ID expansion and increase in total flatness and flatness taper values. For the same nitrocarburizing process in Figure 5.23, ID changes at -15 mm longitudinal height were always larger than those at -11 mm. The gas ferritic nitrocarburizing at 570 °C for 4 hours (h) led to the smallest ID changes at both of the height positions.
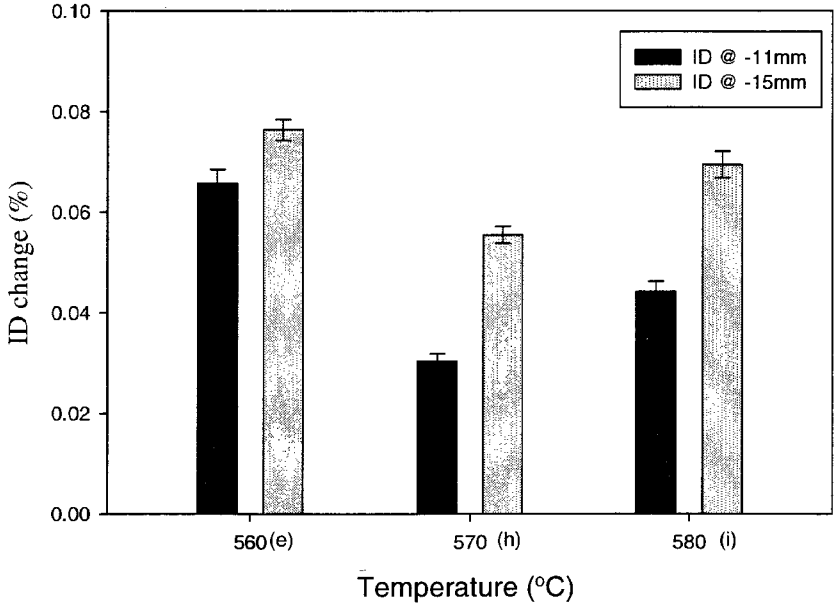
Figure 5.23 ID change of pistons as a function of nitrocarburizing temperature (e, h, and i).

91
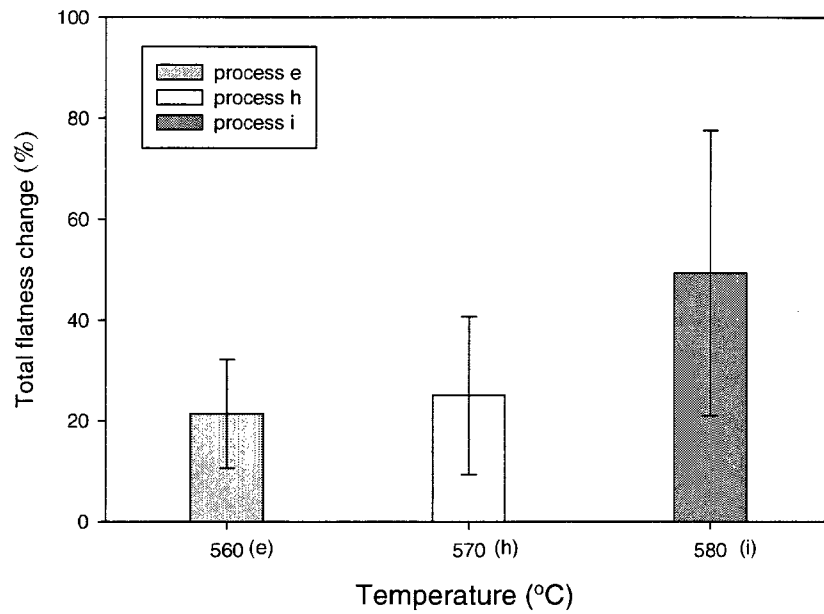
Figure 5.24 Total flatness change of pistons as a function of nitrocarburizing temperature (*e*, *h*, and *i*).
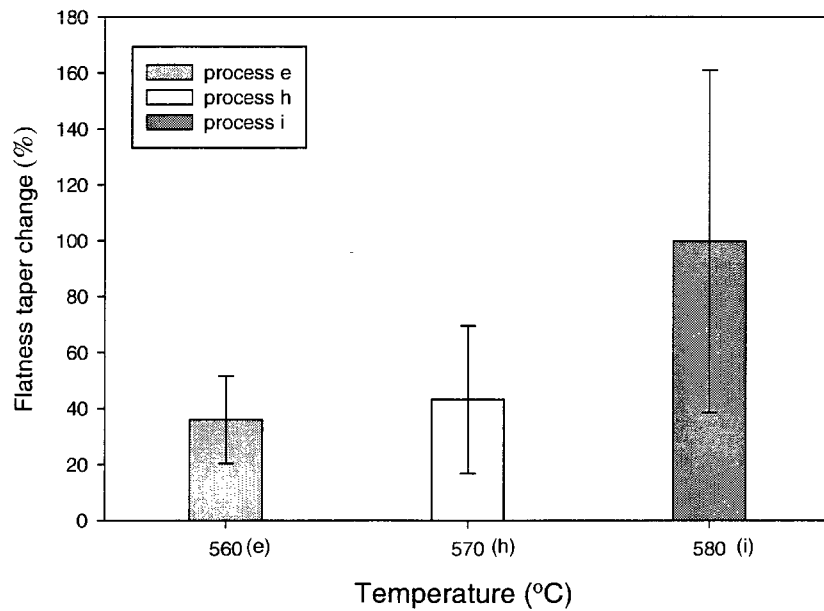
Figure 5.25 Flatness taper change of pistons as a function of nitrocarburizing temperature (*e*, *h*, and *i*).

As shown in Figures 5.24 and 5.25, the ion ferritic nitrocarburizing process (*e*) led to the smallest total flatness and flatness taper changes, whereas the vacuum ferritic nitrocarburizing (*i*) resulted in the largest total flatness and flatness taper changes. By comparing the different ferritic nitrocarburizing processes, *e*, *h* and *i*, it can be seen that the total flatness and flatness taper changes tended to increase with the increasing nitrocarburizing temperature.

5.5 Summary

A comparison between the carbonitriding and various ferritic nitrocarburizing processes (*a-k*) shows that:

(1) Both the carbonitriding and the different ferritic nitrocarburizing processes gave rise to size and shape distortions in the C-ring and piston samples. For the different ferritic nitrocarburizing processes, the gas ferritic nitrocarburizing at 565 °C for 5 hours (*c*) gave smaller OD, ID, gap and flatness distortion in comparison with the other processes.

(2) For the C-ring specimens, all processes led to a small OD expansion. The C-rings subjected to gas carbonitriding experienced larger ID, gap and flatness distortion than those subjected to ferritic nitrocarburizing. The gap width of C-rings tended to contract after the various nitrocarburizing processes.

(3) For the piston samples, the ID dimension of pistons expanded after ferritic nitrocarburizing process, but contracted after gas carbonitriding. The gas carbonitriding process resulted in a more severe shape distortion compared to the ferritic nitrocarburizing. Additionally, ID changes at -15 mm longitudinal height positions were larger than those at -11 mm after ferritic nitrocarburizing, due to the geometrical structure of pistons.

A comparison between the different thickness Navy C-rings for the various ferritic nitrocarburizing processes shows that:

(1) The thinnest C-ring series, 5-NC, showed larger OD, ID, and gap distortion than the other series due to its thinnest thickness.

(2) The 2-NC and 3-NC C-rings showed larger flatness distortion than the other series.

A comparison between the various ferritic nitrocarburizing processes (*e-j*) shows that vacuum ferritic nitrocarburizing (*i*) led to smaller OD, ID, gap, and flatness distortion in the C-ring samples and a smaller ID distortion in the piston specimens. However, it also resulted in the largest flatness changes in the pistons.

VI. EFFECTS OF HEAT TREATMENT ON RESIDUAL STRESSES

This section discusses the residual stress state at the surface of both the nitrocarburized and carbonitrided specimens. Eight Navy C-ring samples from the thickest and thinnest series, and eleven pistons were used for the surface residual stress determination. The measurements were taken on the ε-phase compound layer in the nitrocarburized samples and the martensite phase in the carbonitrided sample using an XRD method.

6. 1 Residual Stresses in Navy C-rings

The results of the residual stress measurements for the 1-NC and the 5-NC series are given in Table 6.1. The gas ferritic nitrocarburizing processes generated tensile residual stresses in the ε-nitride surface layer of both the specimen series. This result is in agreement with the findings of Kolozsváry [92] and Watkins et al. [105] that tensile residual stresses are present in the ε compound layer of nitrided steel. The gas ferritic nitrocarburizing at 510 °C for 15 hours (a) generated smaller tensile residual stresses in both the 1-NC and 5-NC C-ring series. It should be noted that the residual stresses are lower for the thinner 5-NC C-ring series, compared to the thicker 1-NC series under the same nitrocarburizing condition.

Table 6.1 Surface residual stress analysis of C-ring Samples for gas ferritic nitrocarburizing

Process		Symbol	Surface Residual Stress (MPa)	
			1-NC Series	5-NC Series
Gas ferritic nitrocarburizing	510 °C / 15 hrs	a	86.2 ± 17.2	48.3 ± 14.5
	540 °C / 10 hrs	b	101.4 ± 18.6	73.8 ± 10.3
	565 °C / 5 hrs	c	140.0 ± 19.3	112.4 ± 15.2
	595 °C / 4 hrs	d	103.4 ± 17.9	55.2 ± 9.7

The residual stresses together with the thickness of the compound layer for the 5-NC series are plotted as a function of nitrocarburizing temperature (a-d), in Figure 6.1.

As the compound layer thickness decreased, the residual stresses increased. The thinner layers exhibited higher residual stress values, which may be due predominantly to the more compact nature of the thinner compound layers, and a minor effect of the complex influence of the relaxation process during the long heat treating cycle [92]. The thickness of the compound layer is dependent on the temperature, atmosphere composition, steel grade and heat treatment time [17, 45]. Compared to the samples nitrocarburized at 510 °C and 540 °C (*a* and *b*), the thickness of the compound layer is smaller in the samples nitrocarburized at 565 °C and 595 °C (*c* and *d*). This is, in part, due to the shorter heat treatment times and the decreased nitrogen activity in steel [104].
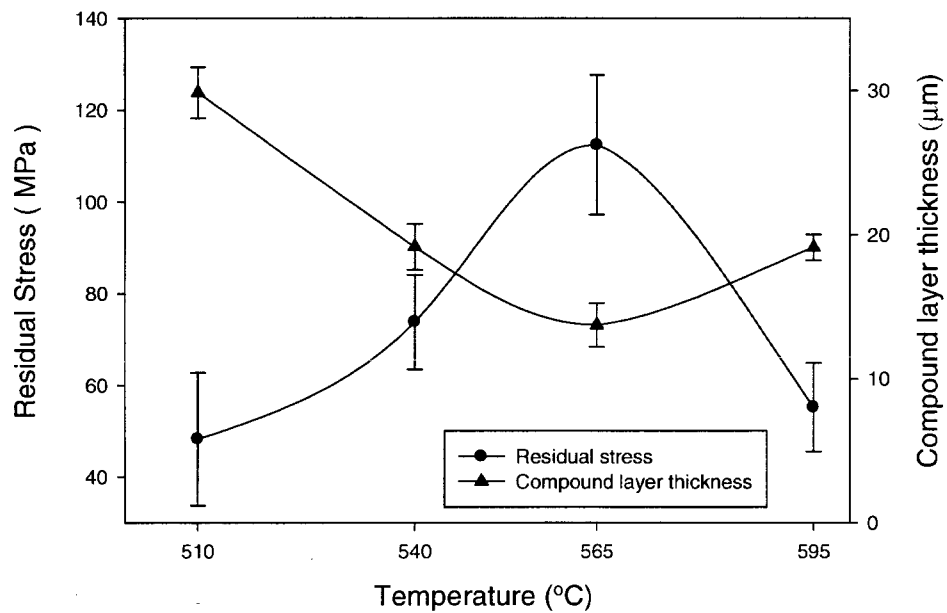
Figure 6.1 Comparison of the effects of nitrocarburizing temperature on the residual stresses and compound layer thicknesses for the 5-NC C-ring samples.

6.2 Residual Stresses in Torque Converter Pistons

The values of the residual stresses at the surface of the piston samples for both the nitrocarburizing and carbonitriding processes (*a-k*) are given in Table 6.2.

Table 6.2 Surface residual stress analysis of pistons for nitrocarburizing and carbonitriding

Process		Symbol	Surface Residual Stress (MPa)
Gas ferritic nitrocarburizing	510 °C / 15 hrs	a	122.0 ± 10.3
	540 °C / 10 hrs	b	146.9 ± 19.3
	565 °C / 5 hrs	c	268.2 ± 26.2
	595 °C / 4 hrs	d	76.5 ± 22.8
Ion ferritic nitrocarburizing	560 °C / 15 hrs	e	186.2 ± 21.4
	525 °C / 24 hrs	f	224.1 ± 18.6
Gas ferritic nitrocarburizing (controlled nitrogen potential)	525 °C / 52 hrs	g	172.4 ± 9.7
	570 °C / 4 hrs	h	241.3 ± 23.4
Vacuum ferritic nitrocarburizing	580 °C / 10 hrs	i	262.7 ± 20.0
Gas ferritic nitrocarburizing (water-base quenching)	580 °C / 2 hrs	j	252.3 ± 19.3
Gas carbonitriding	850 °C / 4 hrs	k	-188.9 ± 26.2

The residual stress analysis shows that tensile residual stresses were present in the ε-nitride surface layer of the piston specimens after various nitrocarburizing processes. However, the carbonitriding led to favorable compressive residual stresses. It is known that compressive residual stresses can improve the surface fatigue resistance of the specimen, while tensile residual stresses decrease it [84, 106]. Another point to be noted is that both the resulting stresses on the surface and the distribution of stresses across the section will affect the fatigue strength of a component [86]. The residual stresses developed during the various nitrocarburizing processes are in a range of 75-270 MPa. These results can be compared with the results obtained in the previous study by the research group at the University of Windsor [16], in which the residual stress measurement was carried out on piston specimens that were gas nitrocarburized at 510 °C for 14 hours. Similar tensile residual stresses were measured at the surface of the specimens with values ranging between 75 and 215 MPa.

Residual stresses are dependent on the interaction of heat treatment time, temperature, deformation and microstructure of the material [107]. According to Grosch [9], a specific distribution of residual stress is produced after carbonitriding. The residual

stresses in the case were identified as compressive residual stresses, which turned into tensile residual stresses when the case depth was reached. The residual stresses resulting from the nitrocarburizing processes are more complicated due to the presence of both the compound layer and the diffusion zone. The absence of phase transformation at the lower heat treatment temperature also plays a role. Additionally, the increased carbon content in the substrate, especially in the compound layer, helps to increase the residual stress levels [92].

Specimen Series
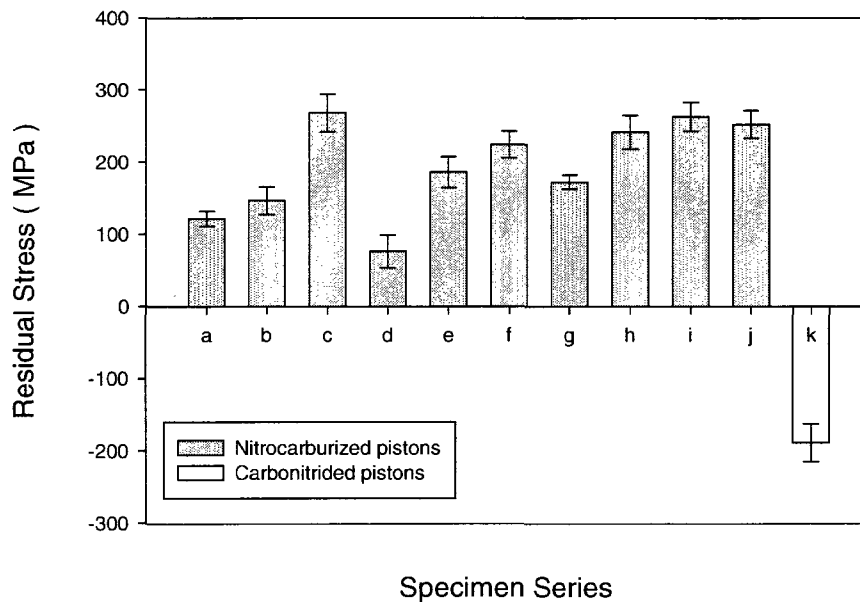
Figure 6.2 Residual stresses of piston samples for nitrocarburizing and carbonitriding.

Figure 6.2 shows the results of residual stresses in the pistons subjected to all the different heat treatment processes *a-k*. The residual stresses for the nitrocarburized pistons were tensile, whereas compressive stresses were associated with the carbonitrided pistons. Among the various ferritic nitrocarburizing processes, the gas ferritic nitrocarburizing at 595 °C for 4 hours (*d*) generated the smallest tensile residual stresses in the piston samples; whereas the largest residual stresses were generated in the gas ferritic nitrocarburized piston at 565 °C for 5 hours (*c*).

The residual stress values versus nitrocarburizing temperatures for the 1-NC and 5-NC C-ring series, as well as the piston samples for the gas ferritic nitrocarburizing

processes (*a-d*) are plotted in Figure 6.3. The magnitude of the residual stress tended to increase with increasing nitrocarburizing temperature, reaching a maximum value at about 565 °C. The main causes of the residual stresses in the compound layer are related to the volume changes during the formation of different phases and the internal stresses produced by molecular nitrogen formation within the porosity. The carbon level in the compound layer also has a significant effect on residual stress, with increased carbon contents being responsible for increased residual stress levels [92]. The residual stresses in the thinner C-ring specimens (5-NC series) are always lower than the thicker specimens (1-NC series) and the pistons.
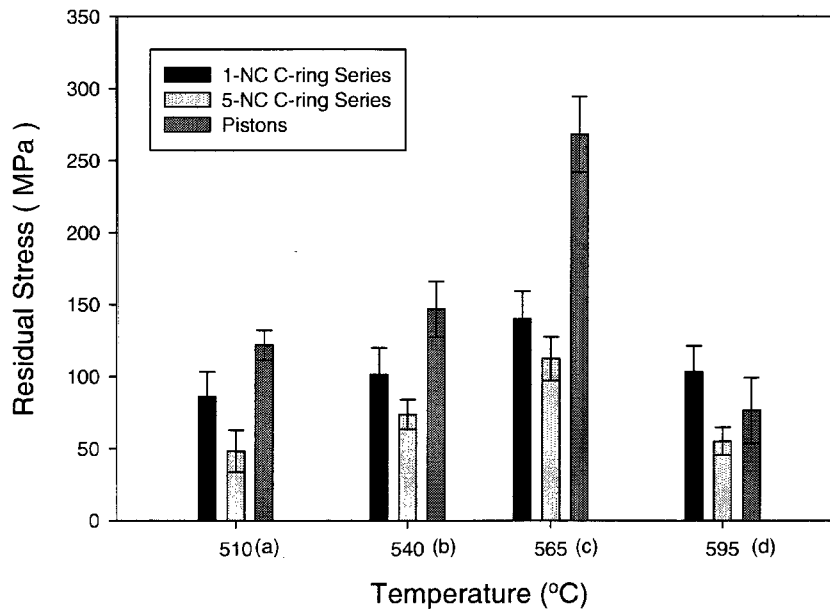
Figure 6.3 Variation of residual stress in the nitrocarburized C-ring and piston samples (*a-d*).

The residual stresses and the microhardness at the piston surface are plotted as a function of nitrocarburizing temperature (processes *a*, *b*, *e*, *f*, and *i*) in Figure 6.4. The changes in residual stress levels with nitrocarburizing temperature were similar to the changes in microhardness. A compound layer containing high residual stresses also showed high hardness values. As pointed out by Champoux *et al.* [108], a comparison between a steel and an aluminum alloy shows that, the stability of residual stresses depends on the hardness of the material; the harder the material is, the more stable the

residual stresses are. Comparing the various nitrocarburizing processes, the gas nitrocarburizing processes (*a* and *b*) led to smaller tensile residual stresses and surface hardness. On the other hand, the ion and vacuum nitrocarburizing (*e*, *f*, and *i*) resulted in larger residual stresses and microhardness values, which may be partially associated with the more compact nature of the compound layer.

The residual stress values of piston samples versus microhardness for all the different nitrocarburizing processes (*a-j*) are plotted in Figure 6.5. The trend line indicates that the increase in tensile residual stress is associated with an increase in microhardness.
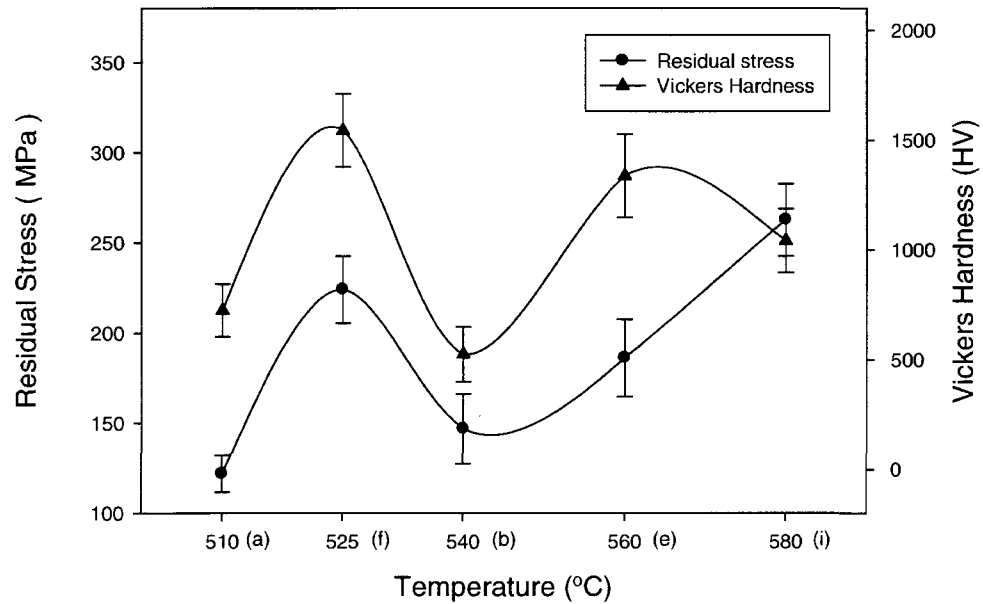
Figure 6.4 Variation of residual stresses and case hardness with nitrocarburizing temperature for pistons.
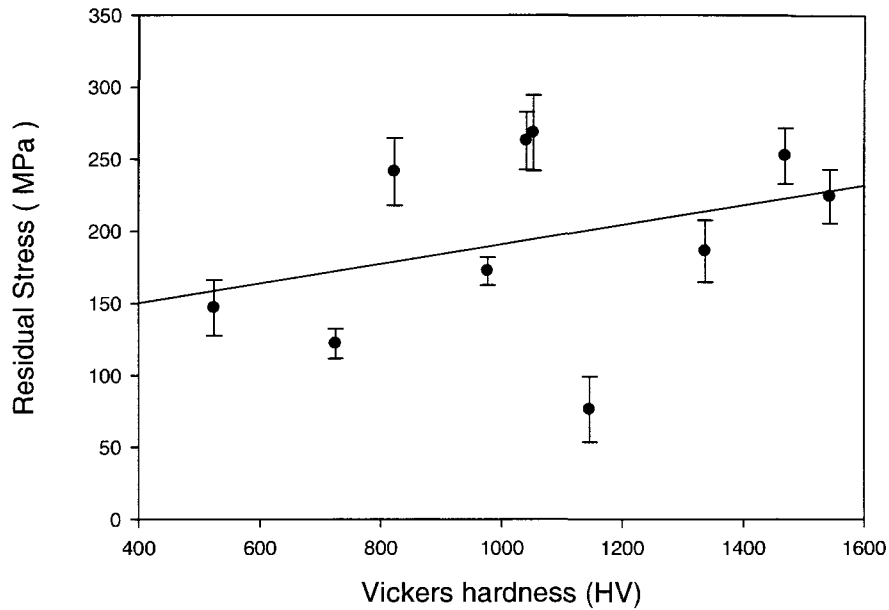
Figure 6.5 Variation of residual stresses versus microhardness for nitrocarburized pistons (*a-j*).

6.3 Summary

The various nitrocarburizing processes generated tensile residual stresses in the ε-nitride surface layer of both the piston and C-ring specimens. In comparison, compressive residual stresses were produced by the carbonitriding process. Gas ferritic nitrocarburizing at 510 °C for 15 hours and 595 °C for 4 hours (*a* and *d*) resulted in smaller tensile residual stresses in the 1-NC and 5-NC C-ring series, as well as the piston samples. On the other hand, the largest residual stresses were generated in the gas ferritic nitrocarburized piston at 565 °C for 5 hours (*c*). The residual stresses in the thinner 5-NC C-ring specimens are always lower than the thicker 1-NC series and the pistons. The values of residual stresses were associated with the compound layer thickness and the microhardness of the material. The thinner compound layer exhibited higher residual stress values; a compound layer containing higher hardness values also showed higher residual stresses.

VII. CONCLUSIONS AND RECOMMENDATIONS FOR FUTURE WORK

The main focus of this study was to investigate the potential of ferritic nitrocarburizing as an alternative to the current gas carbonitriding process to improve the surface characteristics of SAE 1010 plain carbon steel automotive components without producing unacceptable part distortion. To better understand the ferritic nitrocarburizing process, a variety of gas, ion, and vacuum ferritic nitrocarburizing processes with different heat treatment parameters were investigated. The carbonitriding and the various ferritic nitrocarburizing processes were compared quantitatively in terms of resultant microstructure and properties, size and shape distortions, as well as the residual stress state.

7.1 Conclusions

According to the experimental results obtained from the various ferritic nitrocarburizing and carbonitriding processes, the following conclusions were drawn.

1. Texture from Pole Figure

Crystallographic texture analysis shows a <111> rolling direction and (112) rolling plane of piston specimens after the stamping station.

2. Optical Microstructure

A variety of microstructures were formed in the piston and C-ring samples after different nitrocarburizing or carbonitriding processes. The variations in microstructure are influenced by the heat treatment methods and parameters applied, as well as the specimen thickness.

(a) The gas carbonitriding and a subsequent oil quenching process resulted in a very thick and hard martensitic case at the surface, which consists of tempered martensite and retained austenite, and a core containing ferrite, needle-like bainite, and pearlite.

(b) For the pistons and 5-NC C-ring samples with the same specimen thickness, the various ferritic nitrocarburizing processes generated a compound layer with thickness

ranging from 10-40 μm. The diffusion zone underneath showed the penetration of needle-like gamma prime (γ') phases into the ferrite matrix.

- The gas ferritic nitrocarburizing (*a-d*) and the vacuum ferritic nitrocarburizing (*i*) processes gave rise to a well-formed compound layer at the steel surface, with a diffusion zone containing needle-like γ' phases.

- The ion ferritic nitrocarburizing processes (*e* and *f*) generated a shallower but harder compound layer at the surface of both the piston and C-ring specimens.

- Gas ferritic nitrocarburizing with controlled nitrogen potential (*g* and *h*) resulted in a very thin compound layer at 525 °C for 52 hours, but a very thick layer at 570 °C for 4 hours, which is correlated with both the nitrocarburizing time and temperature.

- Gas ferritic nitrocarburizing with its subsequent water base quenching (*j*) led to a well-formed compound layer at the surface, whereas the penetration of gamma prime phases into the diffusion zone was not evident.

(c) For the C-rings with varying thickness, different microstructures were produced after the gas ferritic nitrocarburizing process (*b*). In the thicker 1-NC to 3-NC C-ring series, a thin compound layer was generated at the surface. In the underlying diffusion, both the needle-like gamma prime phases and the pearlite phases were present in the ferrite matrix. In comparison, the thinner 4-NC and 5-NC C-rings showed a thicker compound layer, together with the absence of pearlite phases in the diffusion zone.

3. SEM Analysis

High magnification SEM observations showed that gas ferritic nitrocarburizing at 510 °C for 15 hours (*a*) resulted in a well-formed compound layer with slight porosity at the surface, and an underlying diffusion zone containing gamma prime needles. Ion ferritic nitrocarburizing at 560 °C for 15 hours (*e*) led to a larger amount of porosity in a poor quality compound layer with little gamma prime phase detected in the diffusion zone; the diffusing carbon atoms inhibited the penetration of atomic nitrogen into the interstitial positions of the ε iron lattice. As a result, the nitrogen atoms accumulated in the low energy regions, such as grain boundaries, to form molecular nitrogen, which led to the formation of more micropores.

4. Hardness Results

As expected, both the carbonitriding and ferritic nitrocarburizing processes generated a surface case with high hardness. Hardness profiles across the section of the nitrocarburized and carbonitrided pistons show the hardness values gradually decreased in direction of the case depth. Maximum hardness values were obtained in the vicinity of the surface, and are associated with the penetration of hardening species, such as carbon and nitrogen. As the distance increased from the surface to the substrate, the hardness decreased due to the limited penetration of hardening species into the matrix. For the various nitrocarburizing processes, the nitrogen-rich region near the interface between the compound layer and the substrate exhibited higher hardness values than the other regions. The hardness profiles for the ion ferritic nitrocarburizing processes (e and f) were significantly higher than the other processes.

5. Phase Analysis

The XRD phase analysis of the thickest C-rings indicated the presence of predominantly ε-Fe_3N phase in the compound layer for the various gas and vacuum ferritic nitrocarburizing processes. Ion ferritic nitrocarburizing (e and f) resulted in both ε and γ' iron-carbonitrides at the surface of C-rings. The nitrides formed in the compound layer are beneficial to improve surface hardness. As a result, the ion ferritic nitrocarburizing processes generated higher hardness levels in the C-ring specimens.

6. Residual Stresses

The various ferritic nitrocarburizing processes imparted tensile residual stresses in the ε-nitride surface layer of both the C-ring and piston specimens, whereas compressive residual stresses were present at the surface of the carbonitrided piston samples. The values of residual stresses are associated with the compound layer thickness and the microhardness of the material.

(a) A thinner compound (ε-nitride) layer gave rise to higher residual stress values, which is believed to be predominantly due to the more compact nature of the thinner compound layers, and a minor effect of the complex influence of the relaxation process during the long heat treating cycle.

104

(b) A compound layer containing higher hardness values showed higher residual stresses. Concerning the evolution of residual stress during fatigue, it is generally believe that the stability of residual stresses depends on the hardness of the material.

(c) Comparing the various nitrocarburizing processes, gas ferritic nitrocarburizing at 510 °C for 15 hours and 595 °C for 4 hours (*a* and *d*) resulted in smaller tensile residual stresses in both the C-ring series and the piston samples. On the other hand, the largest residual stresses were generated in the gas ferritic nitrocarburized piston at 565 °C for 5 hours (*c*).

(d) The tensile residual stresses in the ε-nitride layer were lower in the thinnest C-ring specimens than in the thickest specimens and the pistons. This is partly due to the larger dimensional changes of OD, ID, and gap width in the thinnest C-rings help to relieve the existing residual stresses in the specimens.

7. Dimensional Distortion

(1) A comparison between the carbonitriding and various ferritic nitrocarburizing processes (*a-k*) shows that all of the processes gave rise to both size and shape distortions in the C-ring and piston samples. Carbonitriding was noted to produce larger overall distortion values in both the Navy C-rings and pistons. Distortion in the carbonitriding process is due to the phase changes on heating as well as the thermal and transformation stresses developed upon quenching. The smaller dimensional changes associated with the nitrocarburizing process are attributed to the low heat treatment temperatures; the treatment is carried out in the ferritic phase region, and no transformations to or from austenite occur.

(a) For the C-ring specimens, all processes led to a small expansion of the OD dimension. The C-ring samples subjected to the gas carbonitriding experienced larger ID, gap and flatness distortion than those processed using ferritic nitrocarburizing. The gap width of C-rings tended to contract after the different nitrocarburizing processes.

(b) For the piston samples, the gas carbonitriding process produced a contraction of the ID and a more severe shape distortion (at least 5 times greater) than ferritic nitrocarburizing. By comparison, the ferritic nitrocarburizing processes produced smaller

dimensional distortions. ID changes at -15 mm longitudinal height were larger than those at -11 mm due to the geometry of the pistons.

(2) A comparison between the Navy C-rings for the gas, ion, and vacuum ferritic nitrocarburizing processes (a-d, e, h, and i) shows that the dimensional changes of the C-ring samples varied according to the specific ferritic nitrocarburizing approach applied and their thicknesses.

(a) The 5-NC C-ring series showed larger OD, ID, and gap distortion than the other series because they had the smallest thickness.

(b) The thicker 2-NC and 3-NC C-rings showed larger flatness distortion than the other series.

(3) A comparison between the gas, ion, and vacuum ferritic nitrocarburizing processes (e-j) shows that vacuum ferritic nitrocarburizing (i) led to smaller OD, ID, gap, and flatness distortion in the C-ring samples and a smaller ID distortion in the piston specimens. However, it also generated the largest total flatness and flatness taper changes in the pistons.

(4) The size and shape distortions can be reduced by choosing appropriate nitrocarburizing methods and parameters.

(a) In comparison with the other ferritic nitrocarburizing processes, the gas ferritic nitrocarburizing process (c) performed at 565 °C for 5 hours led to smaller changes in OD, ID, gap, and flatness in both the C-ring and piston samples. However, it also led to the largest tensile residual stresses in the ε-nitride surface layers.

7.2 Summary of Conclusions

The conclusions of this research support the potential of ferritic nitrocarburizing as a replacement for the current carbonitriding process. The lower heat treatment temperature as well as the absence of phase transformations during ferritic nitrocarburizing helps to reduce the likelihood of both size and shape distortion. By choosing appropriate nitrocarburizing methods and parameters, as well as proper specimen thickness, minimal size and shape distortions and a higher surface hardness can be achieved. A remaining issue is that the nitrocarburizing process is associated with the

development of tensile stresses at the surface of material, which are generally believed to decrease the fatigue resistance. Additional testing is required to study the effect of tensile stresses on the fatigue properties of the torque converter pistons and to determine whether or not the nitrocarburized pistons meet the product performance specifications in the automotive production. Compressive stresses in the underlying diffusion zone may mitigate the surface tensile stress.

7.3 Recommendations for Future Work

Suggestions to improve the accuracy and validity of the experimental results, and for further testing to help determine the potential of ferritic nitrocarburizing to replace the current carbonitriding process are outlined below.

1. Further comparisons between the gas ferritic nitrocarburizing (c) and vacuum ferritic nitrocarburizing (i) processes are needed to develop an appropriate nitrocarburizing process that can contribute to lower dimensional distortion.

2. More piston samples for gas ferritic nitrocarburizing with a subsequent water base quenching (j) are required to determine the existence of gamma prime phases in the diffusion zone and its relationship with the microhardness values.

3. Further study is needed for the gas ferritic nitrocarburized C-rings, since the residual stresses was measured using the (302) reflection of the ε-phase (Fe_3N), while the phase analysis showed that none of these nitrides were detected in the C-ring specimens after gas ferritic nitrocarburizing (a).

4. A profile of residual stress distribution measured from the surface of steel to the core would be beneficial to understand the residual stress state in the nitrocarburized and carbonitrided specimens.

5. Wear tests need to be performed to simulate the movement of the lockup piston clutch against the torque converter shell, to compare the fatigue properties at the surface of the nitrocarburized and carbonitrided pistons in a light loading application.

6. For the ion and gas nitrocarburized pistons, which present very different hardness profiles and diffusion zone microstructures, analyses of the distribution of nitrogen and carbon in steel would be helpful, especially the nitrogen profiles.

7. Indentation methods could be used to determine elastic modulus values for the coatings obtained by the different methods. More accurate modulus values would provide better residual stress calculations.

APPENDIX A

Outside Diameter Changes of 1—5-NC Navy C-rings (Size Distortion)

Process	Specimen		Outside Diameter (mm)			
	Series	No.	Before Heat Treatment	After Heat Treatment	Average Change (%)	Standard Deviation
Gas Ferritic Nitrocarburizing (process a, 510 °C / 15 hrs)	1-NC	1	50.7844	50.8108	0.0509	0.0015
		2	50.7925	50.8178		
	2-NC	1	50.7888	50.8092	0.0418	0.0024
		2	50.7858	50.8079		
	3-NC	1	50.7989	50.8227	0.0472	0.0006
		2	50.7911	50.8153		
	4-NC	1	50.7846	50.8091	0.0472	0.0015
		2	50.7880	50.8114		
	5-NC	1	50.7762	50.7936	0.0541	0.0280
		2	50.7851	50.8226		
Gas Ferritic Nitrocarburizing (process b, 540 °C / 10 hrs)	1-NC	1	50.7932	50.8179	0.0463	0.0033
		2	50.7708	50.7931		
	2-NC	1	50.7950	50.8135	0.0374	0.0014
		2	50.7661	50.7856		
	3-NC	1	50.7612	50.7829	0.0409	0.0027
		2	50.7905	50.8103		
	4-NC	1	50.7864	50.8046	0.0360	0.0003
		2	50.7869	50.8053		
	5-NC	1	50.7857	50.8146	0.0549	0.0028
		2	50.7902	50.8171		
Gas Ferritic Nitrocarburizing (process c, 565 °C / 5 hrs)	1-NC	1	50.7751	50.7977	0.0438	0.0010
		2	50.7947	50.8166		
	2-NC	1	50.7934	50.8130	0.0383	0.0004
		2	50.7661	50.7854		
	3-NC	1	50.7720	50.7946	0.0440	0.0007
		2	50.7865	50.8086		
	4-NC	1	50.7855	50.8019	0.0340	0.0024
		2	50.7854	50.8035		
	5-NC	1	50.7910	50.8108	0.0380	0.0014
		2	50.7926	50.8114		
Gas Ferritic Nitrocarburizing (process d, 595 °C / 4 hrs)	1-NC	1	50.7850	50.8085	0.0491	0.0040
		2	50.8011	50.8275		
	2-NC	1	50.7842	50.8037	0.0393	0.0013
		2	50.7731	50.7935		
	3-NC	1	50.7812	50.8060	0.0463	0.0036
		2	50.7848	50.8070		

	4-NC	1	50.7804	50.7972	0.0336	0.0007
		2	50.7854	50.8027		
	5-NC	1	50.7864	50.8151	0.0548	0.0024
		2	50.7919	50.8189		
Ion Ferritic Nitrocarburizing (process _e_, 560 °C / 15 hrs)	**1-NC**	1	50.7975	50.8259	0.0550	0.0012
		2	50.7708	50.7983		
	2-NC	1	50.7707	50.7972	0.0516	0.0008
		2	50.7778	50.8037		
	3-NC	1	50.7815	50.8148	0.0622	0.0047
		2	50.7845	50.8144		
	4-NC	1	50.7888	50.8137	0.0481	0.0013
		2	50.7850	50.8090		
	5-NC	1	50.7823	50.8195	0.0751	0.0026
		2	50.7879	50.8270		
Ion Ferritic Nitrocarburizing (process _f_, 525 °C / 24 hrs)	**1-NC**	1	50.8028	50.8324	0.0566	0.0024
		2	50.8021	50.8300		
	2-NC	1	50.7675	50.7901	0.0435	0.0014
		2	50.7969	50.8185		
	3-NC	1	50.7817	50.8080	0.0541	0.0032
		2	50.7880	50.8166		
	4-NC	1	50.7860	50.8041	0.0379	0.0032
		2	50.7799	50.8003		
	5-NC	1	50.7838	50.8152	0.0328	0.0411
		2	50.7829	50.7848		
Gas Ferritic Nitrocarburizing (process _g_, 525 °C / 52 hrs)	**1-NC**	1	50.7727	50.7985	0.0503	0.0007
		2	50.7741	50.7994		
	2-NC	1	50.7762	50.8214	0.0795	0.0135
		2	50.7709	50.8064		
	3-NC	1	50.7883	50.8168	0.0569	0.0011
		2	50.7851	50.8144		
	4-NC	1	50.7761	50.8067	0.0610	0.0011
		2	50.7803	50.8117		
	5-NC	1	50.7691	50.8089	0.0766	0.0025
		2	50.7868	50.8248		
Gas Ferritic Nitrocarburizing (process _h_, 570 °C / 4 hrs)	**1-NC**	1	50.7743	50.8037	0.0599	0.0028
		2	50.8052	50.8366		
	2-NC	1	50.7962	50.8007	0.0193	0.0148
		2	50.7795	50.7946		
	3-NC	1	50.7868	50.8147	0.0557	0.0011
		2	50.7833	50.8120		
	4-NC	1	50.7880	50.8133	0.0516	0.0025
		2	50.7790	50.8061		
	5-NC	1	50.7874	50.8260	0.0771	0.0015
		2	50.7863	50.8260		

Vacuum Ferritic Nitrocarburizing (process *i*, 580 °C / 10 hrs)	1-NC	1	50.7866	50.8104	0.0464	0.0007
		2	50.7832	50.8065		
	2-NC	1	50.7941	50.8127	0.0400	0.0047
		2	50.7780	50.8000		
	3-NC	1	50.7794	50.8027	0.0448	0.0015
		2	50.7621	50.7843		
	4-NC	1	50.7892	50.8051	0.0308	0.0007
		2	50.7918	50.8072		
	5-NC	1	50.7930	50.8114	0.0420	0.0082
		2	50.7901	50.8144		
Gas Ferritic Nitrocarburizing (process *j*, 580 °C / 2 hrs)	1-NC	1	50.7946	50.8219	0.0511	0.0037
		2	50.7732	50.7978		
	2-NC	1	50.7617	50.7836	0.0454	0.0032
		2	50.8005	50.8247		
	3-NC	1	50.7780	50.8014	0.0461	0.0000
		2	50.7870	50.8104		
	4-NC	1	50.7917	50.8094	0.0348	0.0000
		2	50.7929	50.8106		
	5-NC	1	50.7839	50.8135	0.0576	0.0010
		2	50.7836	50.8125		
Gas Carbonitriding (process *k*, 850 °C / 4 hrs)	1-NC	1	50.7817	50.8399	0.1146	0.0000
	4-NC	1	50.7865	50.8015	0.0295	0.0000
	5-NC	1	50.7861	50.7762	-0.0195	0.0000

111

Inside Diameter Changes of 1—5-NC Navy C-rings (Size Distortion)

Process	Specimen		Inside Diameter (mm)				Average Change (%)	Standard Deviation
	Series	No.	Before Heat Treatment		After Heat Treatment			
			ID 1	ID 3	ID 1	ID 3		
Gas Ferritic Nitrocarburizing (process a, 510 °C / 15 hrs)	1-NC	1	31.8130	31.8061	31.8193	31.8114	0.0203	0.0029
		2	31.8058	31.8005	31.8133	31.8072		
	2-NC	1	31.7941	31.7958	31.7928	31.7946	0.0009	0.0061
		2	31.8069	31.8017	31.8097	31.8025		
	3-NC	1	31.7812	31.7819	31.7816	31.7817	0.0009	0.0028
		2	31.7693	31.7673	31.7708	31.7668		
	4-NC	1	31.7586	31.7564	31.7537	31.7515	-0.0216	0.0072
		2	31.7608	31.7593	31.7518	31.7506		
	5-NC	1	31.7667	31.8066	31.7468	31.8791	0.0166	0.1423
		2	31.7655	31.7396	31.7573	31.7164		
Gas Ferritic Nitrocarburizing (process b, 540 °C / 10 hrs)	1-NC	1	31.8048	31.8052	31.8137	31.8147	0.0248	0.0049
		2	31.7927	31.7891	31.7998	31.7952		
	2-NC	1	31.8076	31.8028	31.8059	31.8028	0.0008	0.0046
		2	31.7799	31.7818	31.7811	31.7833		
	3-NC	1	31.7805	31.7793	31.7815	31.7797	0.0004	0.0033
		2	31.7683	31.7677	31.7669	31.7682		
	4-NC	1	31.7577	31.7594	31.7549	31.7567	-0.0087	0.0004
		2	31.7601	31.7612	31.7575	31.7583		
	5-NC	1	31.7579	31.7311	31.7558	31.7218	-0.0209	0.0176
		2	31.7599	31.7523	31.7580	31.7391		
Gas Ferritic Nitrocarburizing (process c, 565 °C / 5 hrs)	1-NC	1	31.7955	31.7899	31.8020	31.7963	0.0201	0.0014
		2	31.7947	31.7917	31.8016	31.7975		
	2-NC	1	31.8017	31.7970	31.8058	31.7981	0.0029	0.0072
		2	31.7860	31.7829	31.7851	31.7823		
	3-NC	1	31.7713	31.7663	31.7711	31.7644	0.0012	0.0057
		2	31.7726	31.7708	31.7740	31.7730		
	4-NC	1	31.7667	31.7711	31.7638	31.7680	-0.0108	0.0016
		2	31.7686	31.7618	31.7646	31.7581		
	5-NC	1	31.7666	31.7668	31.7664	31.7560	-0.0079	0.0175
		2	31.7627	31.7506	31.7625	31.7518		
Gas Ferritic Nitrocarburizing (process d, 595 °C / 4 hrs)	1-NC	1	31.7863	31.7890	31.7913	31.7928	0.0213	0.0088
		2	31.8189	31.8197	31.8284	31.8285		
	2-NC	1	31.7967	31.7978	31.7957	31.7969	-0.0038	0.0009
		2	31.7885	31.7870	31.7870	31.7856		
	3-NC	1	31.7871	31.7892	31.7882	31.7915	0.0018	0.0048
		2	31.7672	31.7698	31.7659	31.7700		

	4-NC	1	31.7645	31.7672	31.7624	31.7645	-0.0070	0.0012
		2	31.7591	31.7592	31.7568	31.7574		
	5-NC	1	31.7601	31.7797	31.7627	31.7625	-0.0156	0.0292
		2	31.7646	31.7567	31.7665	31.7496		
Ion Ferritic Nitrocarburizing (process *e*, 560 °C / 15 hrs)	1-NC	1	31.8238	31.8259	31.8327	31.8346	0.0226	0.0068
		2	31.7961	31.7997	31.8031	31.8039		
	2-NC	1	31.7899	31.7809	31.7934	31.7847	0.0097	0.0021
		2	31.8063	31.7996	31.8088	31.8021		
	3-NC	1	31.7807	31.7863	31.7910	31.7969	0.0282	0.0059
		2	31.7710	31.7762	31.7776	31.7845		
	4-NC	1	31.7582	31.7589	31.7620	31.7617	0.0144	0.0048
		2	31.7703	31.7663	31.7761	31.7722		
	5-NC	1	31.7640	31.7625	31.7740	31.7523	0.0158	0.0320
		2	31.7576	31.7260	31.7679	31.7360		
Ion Ferritic Nitrocarburizing (process *f*, 525 °C / 24 hrs)	1-NC	1	31.8229	31.8252	31.8405	31.8414	0.0466	0.0087
		2	31.8224	31.8209	31.8367	31.8321		
	2-NC	1	31.7819	31.7799	31.7877	31.7849	0.0143	0.0033
		2	31.8052	31.8125	31.8090	31.8161		
	3-NC	1	31.7837	31.7866	31.7920	31.7953	0.0285	0.0031
		2	31.7759	31.7707	31.7864	31.7794		
	4-NC	1	31.7569	31.7564	31.7571	31.7585	0.0057	0.0042
		2	31.7610	31.7625	31.7626	31.7659		
	5-NC	1	31.7631	31.7152	31.7727	31.7175	-0.0175	0.0594
		2	31.7657	31.7835	31.7646	31.7504		
Gas Ferritic Nitrocarburizing (process *g*, 525 °C / 52 hrs)	1-NC	1	31.7942	31.7926	31.8020	31.8005	0.0241	0.0007
		2	31.7944	31.7944	31.8020	31.8018		
	2-NC	1	31.7809	31.7811	31.7857	31.7862	0.0133	0.0027
		2	31.7847	31.7856	31.7882	31.7891		
	3-NC	1	31.7811	31.7805	31.7855	31.7847	0.0163	0.0033
		2	31.7752	31.7754	31.7809	31.7818		
	4-NC	1	31.7544	31.7589	31.7617	31.7659	0.0240	0.0018
		2	31.7658	31.7616	31.7739	31.7697		
	5-NC	1	31.7687	31.7741	31.7802	31.7768	0.0218	0.0197
		2	31.7629	31.7577	31.7759	31.7582		
Gas Ferritic Nitrocarburizing (process *h*, 570 °C / 4 hrs)	1-NC	1	31.8014	31.7988	31.8008	31.7981	0.0057	0.0090
		2	31.8165	31.8131	31.8213	31.8168		
	2-NC	1	31.8053	31.8117	31.8001	31.8063	-0.0155	0.0014
		2	31.7848	31.7873	31.7804	31.7826		
	3-NC	1	31.7700	31.7737	31.7670	31.7709	-0.0075	0.0020
		2	31.7795	31.7784	31.7779	31.7763		
	4-NC	1	31.7605	31.7601	31.7534	31.7537	-0.0212	0.0009
		2	31.7536	31.7559	31.7469	31.7492		

	5-NC	1	31.7655	31.7699	31.7581	31.7494	-0.0364	0.0201
		2	31.7629	31.7448	31.7563	31.7331		
Vacuum Ferritic Nitrocarburizing (process *i*, 580 °C / 10 hrs)	1-NC	1	31.7969	31.7939	31.8029	31.7994	0.0171	0.0020
		2	31.7917	31.7881	31.7974	31.7926		
	2-NC	1	31.8043	31.8041	31.8030	31.8030	0.0020	0.0068
		2	31.7813	31.7830	31.7844	31.7848		
	3-NC	1	31.7655	31.7592	31.7660	31.7587	0.0013	0.0026
		2	31.7762	31.7757	31.7777	31.7759		
	4-NC	1	31.7595	31.7613	31.7590	31.7606	-0.0024	0.0006
		2	31.7600	31.7606	31.7591	31.7597		
	5-NC	1	31.7632	31.7644	31.7639	31.7786	0.0047	0.0303
		2	31.7687	31.7919	31.7690	31.7827		
Gas Ferritic Nitrocarburizing (process *j*, 580 °C / 2 hrs)	1-NC	1	31.8207	31.8172	31.8293	31.8254	0.0202	0.0072
		2	31.7933	31.7929	31.7980	31.7971		
	2-NC	1	31.7752	31.7756	31.7752	31.7750	0.0017	0.0039
		2	31.7985	31.7981	31.7989	31.8004		
	3-NC	1	31.7909	31.7893	31.7907	31.7881	-0.0022	0.0014
		2	31.7672	31.7698	31.7663	31.7693		
	4-NC	1	31.7624	31.7642	31.7580	31.7594	-0.0139	0.0014
		2	31.7603	31.7606	31.7557	31.7568		
	5-NC	1	31.7634	31.7540	31.7595	31.7529	-0.0184	0.0278
		2	31.7584	31.7518	31.7588	31.7330		
Gas Carbonitriding (process *k*, 850 °C / 4 hrs)	1-NC	1	31.8002	31.7958	31.8421	31.8534	0.1565	0.0349
	4-NC	1	31.7581	31.7590	31.7455	31.7498	-0.0343	0.0076
	5-NC	1	31.7737	31.7961	31.7418	31.7498	-0.1230	0.0320

Gap Width Changes of 1—5-NC Navy C-rings (Size Distortion)

Process	Specimen		Gap Width				Average Change (%)	Standard Deviation
	Series	No.	Before Heat Treatment		After Heat Treatment			
			Top	Bottom	Top	Bottom		
Gas Ferritic Nitrocarburizing (process a, 510 °C / 15 hrs)	1-NC	1	6.4639	6.4450	6.4617	6.4425	-0.0139	0.0277
		2	6.4550	6.4438	6.4563	6.4436		
	2-NC	1	6.4287	6.4285	6.4154	6.4116	-0.1361	0.1220
		2	6.4414	6.4255	6.4419	6.4202		
	3-NC	1	6.4101	6.4031	6.3915	6.3815	-0.2644	0.0766
		2	6.3678	6.3735	6.3578	6.3561		
	4-NC	1	6.3657	6.3618	6.3469	6.3387	-0.3524	0.0518
		2	6.3638	6.3638	6.3426	6.3372		
	5-NC	1	6.3669	6.3654	6.3222	6.3506	-0.3703	0.2243
		2	6.3670	6.3648	6.3471	6.3499		
Gas Ferritic Nitrocarburizing (process b, 540 °C / 10 hrs)	1-NC	1	6.4509	6.4513	6.4589	6.4638	0.0798	0.0969
		2	6.4208	6.4204	6.4221	6.4192		
	2-NC	1	6.4403	6.4438	6.4280	6.4346	-0.1066	0.0741
		2	6.3784	6.3779	6.3742	6.3762		
	3-NC	1	6.3842	6.3825	6.3616	6.3660	-0.2528	0.1107
		2	6.3592	6.3738	6.3530	6.3546		
	4-NC	1	6.3650	6.3666	6.3517	6.3525	-0.2367	0.0356
		2	6.3686	6.3702	6.3502	6.3557		
	5-NC	1	6.3580	6.3592	6.3468	6.3470	-0.1820	0.0284
		2	6.3585	6.3601	6.3492	6.3465		
Gas Ferritic Nitrocarburizing (process c, 565 °C / 5 hrs)	1-NC	1	6.4318	6.4242	6.4357	6.4247	0.0311	0.0417
		2	6.4467	6.4434	6.4513	6.4424		
	2-NC	1	6.4413	6.4275	6.4365	6.4178	-0.0424	0.2082
		2	6.3553	6.3797	6.3718	6.3667		
	3-NC	1	6.3697	6.3593	6.3539	6.3407	-0.2484	0.0363
		2	6.3863	6.3742	6.3733	6.3583		
	4-NC	1	6.3733	6.3769	6.3588	6.3602	-0.2452	0.0152
		2	6.3755	6.3668	6.3603	6.3507		
	5-NC	1	6.3704	6.3677	6.3569	6.3535	-0.1893	0.0330
		2	6.3644	6.3629	6.3544	6.3524		
Gas Ferritic Nitrocarburizing (process d, 595 °C / 4 hrs)	1-NC	1	6.4193	6.4258	6.4206	6.4264	0.0936	0.0918
		2	6.4930	6.5009	6.5051	6.5112		
	2-NC	1	6.4103	6.4217	6.4169	6.4077	-0.1173	0.1481
		2	6.3792	6.3884	6.3682	6.3768		
	3-NC	1	6.3992	6.4021	6.3886	6.3917	-0.2377	0.0858
		2	6.3745	6.3740	6.3555	6.3533		

115

	4-NC	1	6.3681	6.3713	6.3539	6.3576	-0.2030	0.0203
		2	6.3632	6.3629	6.3507	6.3516		
	5-NC	1	6.3569	6.3596	6.3492	6.3460	-0.1650	0.0403
		2	6.3645	6.3709	6.3552	6.3595		
Ion Ferritic Nitrocarburizing (process *e*, 560 °C / 15 hrs)	1-NC	1	6.4967	6.4995	6.4842	6.4679	-0.3042	0.1315
		2	6.4242	6.4335	6.4097	6.4134		
	2-NC	1	6.3971	6.3874	6.3707	6.3621	-0.4143	0.0133
		2	6.4273	6.4223	6.4000	6.3951		
	3-NC	1	6.3908	6.3949	6.3768	6.3811	-0.2453	0.0334
		2	6.3691	6.3698	6.3510	6.3531		
	4-NC	1	6.3670	6.3652	6.3423	6.3416	-0.2556	0.1445
		2	6.3719	6.3647	6.3651	6.3547		
	5-NC	1	6.3631	6.3650	6.3516	6.3496	-0.2173	0.0374
		2	6.3593	6.3606	6.3430	6.3485		
Ion Ferritic Nitrocarburizing (process *f*, 525 °C / 24 hrs)	1-NC	1	6.4972	6.5017	6.5078	6.5126	0.0993	0.0788
		2	6.4862	6.4861	6.4868	6.4898		
	2-NC	1	6.3686	6.3773	6.3533	6.3555	-0.3225	0.0590
		2	6.4528	6.4585	6.4283	6.4373		
	3-NC	1	6.3969	6.4012	6.3783	6.3856	-0.2604	0.0596
		2	6.3709	6.3679	6.3591	6.3474		
	4-NC	1	6.3620	6.3581	6.3361	6.3343	-0.3772	0.0239
		2	6.3666	6.3652	6.3425	6.3430		
	5-NC	1	6.3641	6.3662	6.3458	6.3580	-0.1233	0.1179
		2	6.3633	6.3618	6.3616	6.3586		
Gas Ferritic Nitrocarburizing (process *g*, 525 °C / 52 hrs)	1-NC	1	6.4246	6.4290	6.4037	6.4073	-0.3416	0.0163
		2	6.4248	6.4266	6.4014	6.4048		
	2-NC	1	6.3739	6.3666	6.3606	6.3462	-0.2945	0.1073
		2	6.3824	6.3758	6.3546	6.3622		
	3-NC	1	6.3931	6.3879	6.3575	6.3580	-0.4761	0.0557
		2	6.3908	6.3902	6.3631	6.3617		
	4-NC	1	6.3485	6.3527	6.3285	6.3333	-0.2924	0.0245
		2	6.3739	6.3680	6.3554	6.3515		
	5-NC	1	6.3779	6.3784	6.3716	6.3694	-0.1370	0.0281
		2	6.3635	6.3657	6.3545	6.3551		
Gas Ferritic Nitrocarburizing (process *h*, 570 °C / 4 hrs)	1-NC	1	6.4384	6.4355	6.4271	6.4221	-0.0955	0.1123
		2	6.4802	6.4783	6.4809	6.4777		
	2-NC	1	6.4408	6.4524	6.4232	6.4364	-0.2984	0.0486
		2	6.3868	6.3770	6.3668	6.3541		
	3-NC	1	6.3807	6.3737	6.3571	6.3504	-0.3521	0.0211
		2	6.3772	6.3722	6.3549	6.3516		
	4-NC	1	6.3708	6.3670	6.3475	6.3459	-0.3475	0.0270
		2	6.3514	6.3495	6.3276	6.3293		

116

Process	Sample	#					Value 1	Value 2
	5-NC	1	6.3629	6.3649	6.3373	6.3407	-0.4096	0.0443
		2	6.3664	6.3672	6.3362	6.3429		
Vacuum Ferritic Nitrocarburizing (process *i*, 580 °C / 10 hrs)	1-NC	1	6.4290	6.4273	6.4257	6.4215	-0.0727	0.0222
		2	6.4351	6.4220	6.4315	6.4160		
	2-NC	1	6.4301	6.4447	6.4255	6.4298	-0.1054	0.0952
		2	6.3809	6.3940	6.3806	6.3867		
	3-NC	1	6.3637	6.3616	6.3411	6.3438	-0.2966	0.0481
		2	6.3844	6.3825	6.3646	6.3671		
	4-NC	1	6.3651	6.3629	6.3524	6.3497	-0.2168	0.0178
		2	6.3651	6.3662	6.3498	6.3522		
	5-NC	1	6.3576	6.3603	6.3427	6.3458	-0.3034	0.0847
		2	6.3770	6.3762	6.3519	6.3534		
Gas Ferritic Nitrocarburizing (process *j*, 580 °C / 2 hrs)	1-NC	1	6.4926	6.4896	6.5001	6.4981	0.0441	0.0918
		2	6.4272	6.4308	6.4255	6.4280		
	2-NC	1	6.3796	6.3703	6.3680	6.3582	-0.1609	0.0526
		2	6.4326	6.4497	6.4204	6.4444		
	3-NC	1	6.4098	6.3809	6.3912	6.3841	-0.2128	0.1759
		2	6.3657	6.3650	6.3472	6.3446		
	4-NC	1	6.3668	6.3670	6.3483	6.3493	-0.2710	0.0271
		2	6.3645	6.3634	6.3464	6.3487		
	5-NC	1	6.3625	6.3637	6.3456	6.3480	-0.2683	0.0163
		2	6.3643	6.3636	6.3467	6.3455		
Gas Carbonitriding (process *k*, 850 °C / 4 hrs)	1-NC	1	6.4457	6.4430	6.6047	6.5988	2.4424	0.0344
	4-NC	1	6.3626	6.3662	6.3658	6.3736	0.0833	0.0466
	5-NC	1	6.3755	6.3712	6.2967	6.2909	-1.2482	0.0172

Flatness Changes of 1—5-NC Navy C-rings (Shape Distortion)

Process	Specimen		Flatness			
	Series	No.	Before Heat Treatment	After Heat Treatment	Average Change (%)	Standard Deviation
Gas Ferritic Nitrocarburizing (process *a*, 510 °C / 15 hrs)	1-NC	1	0.0654	0.0573	-7.1361	7.4236
		2	0.0424	0.0416		
	2-NC	1	0.0033	0.0041	56.5657	45.7120
		2	0.0045	0.0085		
	3-NC	1	0.0177	0.0261	46.3703	1.5377
		2	0.0053	0.0077		
	4-NC	1	0.0117	0.0183	16.7921	56.0286
		2	0.0184	0.0142		
	5-NC	1	0.0206	0.0217	0.5974	6.7068
		2	0.0193	0.0185		
Gas Ferritic Nitrocarburizing (process *b*, 540 °C / 10 hrs)	1-NC	1	0.0160	0.0146	-9.6847	1.3219
		2	0.0113	0.0101		
	2-NC	1	0.0034	0.0042	61.7647	54.0729
		2	0.0034	0.0068		
	3-NC	1	0.0032	0.0076	101.2897	51.2091
		2	0.0063	0.0104		
	4-NC	1	0.0121	0.0115	21.6965	37.6961
		2	0.0091	0.0135		
	5-NC	1	0.0169	0.0219	38.3724	12.4262
		2	0.0176	0.0259		
Gas Ferritic Nitrocarburizing (process *c*, 565 °C / 5 hrs)	1-NC	1	0.0123	0.0126	0.3792	2.9131
		2	0.0119	0.0117		
	2-NC	1	0.0022	0.0055	97.2222	74.6390
		2	0.0027	0.0039		
	3-NC	1	0.0052	0.0073	35.7767	6.5165
		2	0.0077	0.0101		
	4-NC	1	0.0160	0.0217	47.9200	17.3878
		2	0.0186	0.0298		
	5-NC	1	0.0206	0.0249	18.6722	3.1135
		2	0.0255	0.0297		
Gas Ferritic Nitrocarburizing (process *d*, 595 °C / 4 hrs)	1-NC	1	0.0151	0.0153	0.4058	1.2992
		2	0.0390	0.0388		
	2-NC	1	0.0027	0.0036	20.8333	17.6777
		2	0.0024	0.0026		

Process	Sample					
	3-NC	1	0.0034	0.0061	87.7059	11.7297
		2	0.0050	0.0098		
	4-NC	1	0.0122	0.0189	48.8876	8.5283
		2	0.0077	0.0110		
	5-NC	1	0.0184	0.0195	13.5154	10.6592
		2	0.0285	0.0345		
Ion Ferritic Nitrocarburizing (process *e*, 560 °C / 15 hrs)	1-NC	1	0.0200	0.0188	-7.4379	2.0335
		2	0.0507	0.0462		
	2-NC	1	0.0037	0.0058	79.5689	32.2612
		2	0.0042	0.0085		
	3-NC	1	0.0065	0.0074	24.9463	15.6980
		2	0.0086	0.0117		
	4-NC	1	0.0168	0.0212	13.9961	17.2454
		2	0.0111	0.0113		
	5-NC	1	0.0227	0.0304	16.3555	24.8409
		2	0.0248	0.0245		
Ion Ferritic Nitrocarburizing (process *f*, 525 °C / 24 hrs)	1-NC	1	0.0162	0.0173	11.4596	6.6036
		2	0.0186	0.0216		
	2-NC	1	0.0033	0.0053	66.5099	8.3493
		2	0.0029	0.0050		
	3-NC	1	0.0056	0.0073	9.2962	29.7846
		2	0.0119	0.0105		
	4-NC	1	0.0073	0.0084	5.3219	13.7838
		2	0.0113	0.0108		
	5-NC	1	0.0173	0.0101	16.5241	82.2260
		2	0.0225	0.0393		
Gas Ferritic Nitrocarburizing (process *g*, 525 °C / 52 hrs)	1-NC	1	0.0147	0.0151	3.4295	1.0019
		2	0.0145	0.0151		
	2-NC	1	0.0041	0.0043	15.9006	15.5882
		2	0.0026	0.0033		
	3-NC	1	0.0156	0.0224	56.9300	18.8660
		2	0.0074	0.0126		
	4-NC	1	0.0156	0.0166	-1.4678	11.1412
		2	0.0321	0.0291		
	5-NC	1	0.0151	0.0119	-6.5263	20.7406
		2	0.0172	0.0186		
Gas Ferritic Nitrocarburizing (process *h*, 570 °C / 4 hrs)	1-NC	1	0.0174	0.0180	5.4555	2.8386
		2	0.0268	0.0288		
	2-NC	1	0.0022	0.0032	41.9580	4.9448
		2	0.0026	0.0036		

	3-NC	1	0.0042	0.0053	127.7020	143.5589
		2	0.0089	0.0293		
	4-NC	1	0.0188	0.0209	10.8483	0.4553
		2	0.0152	0.0168		
	5-NC	1	0.0136	0.0145	10.0885	4.9085
		2	0.0236	0.0268		
Vacuum Ferritic Nitrocarburizing (process i, 580 °C / 10 hrs)	1-NC	1	0.0351	0.0335	-4.2994	0.3663
		2	0.0297	0.0285		
	2-NC	1	0.0035	0.0032	41.3025	70.5324
		2	0.0034	0.0065		
	3-NC	1	0.0058	0.0070	14.5115	8.7372
		2	0.0072	0.0078		
	4-NC	1	0.0120	0.0170	33.2300	11.9312
		2	0.0121	0.0151		
	5-NC	1	0.0114	0.0143	31.9816	9.2532
		2	0.0122	0.0169		
Gas Ferritic Nitrocarburizing (process j, 580 °C / 2 hrs)	1-NC	1	0.0220	0.0262	10.3882	12.3076
		2	0.0178	0.0181		
	2-NC	1	0.0027	0.0044	36.4815	37.4505
		2	0.0040	0.0044		
	3-NC	1	0.0064	0.0058	40.6250	70.7107
		2	0.0032	0.0061		
	4-NC	1	0.0057	0.0083	93.3198	67.4662
		2	0.0078	0.0188		
	5-NC	1	0.0193	0.0199	26.5544	33.1571
		2	0.0152	0.0228		
Gas Carbonitriding (process k, 850 °C / 4 hrs)	1-NC	1	0.0472	0.0434	-8.0508	0.0000
	4-NC	1	0.0185	0.0151	-18.3784	0.0000
	5-NC	1	0.0201	0.0116	-42.2886	0.0000

120

Outside Diameter Changes of Torque Converter Pistons (Size Distortion)

(Measured at -7.5 and -21.5 mm longitudinal height positions from the lockup surface of pistons)

Process	No.	Outside Diameter (mm)							
		Before Heat Treatment		After Heat Treatment		Average Change (%)		Standard Deviation	
		At -21.5	At -7.5	At -21.5	At -7.5	At -21.5	At -7.5	At -21.5	At -7.5
Gas Ferritic Nitrocarburizing (process *a*, 510 °C / 15 hrs)	1	261.18	260.66	261.22	260.76	0.0116	0.0366	0.0039	0.0025
	2	261.20	260.68	261.23	260.77				
	3	261.21	260.67	261.23	260.76				
	4	261.18	260.66	261.23	260.77				
	5	261.19	260.68	261.23	260.77				
	6	261.18	260.67	261.22	260.76				
	7	261.21	260.66	261.23	260.76				
	8	261.19	260.67	261.22	260.76				
	9	261.21	260.66	261.23	260.75				
	10	261.17	260.65	261.20	260.74				
Gas Ferritic Nitrocarburizing (process *b*, 540 °C / 10 hrs)	1	261.19	260.67	261.21	260.75	0.0096	0.0313	0.0045	0.0017
	2	261.18	260.66	261.20	260.74				
	3	261.18	260.66	261.20	260.74				
	4	261.18	260.67	261.20	260.74				
	5	261.19	260.67	261.21	260.75				
	6	261.19	260.67	261.20	260.75				
	7	261.18	260.67	261.24	260.76				
	8	261.19	260.67	261.22	260.76				
	9	261.18	260.66	261.21	260.74				
	10	261.19	260.66	261.20	260.74				
Gas Ferritic Nitrocarburizing (process *c*, 565 °C / 5 hrs)	1	261.19	260.67	261.17	260.71	-0.0077	0.0158	0.0031	0.0012
	2	261.18	260.66	261.15	260.70				
	3	261.18	260.66	261.15	260.70				
	4	261.21	260.67	261.18	260.71				
	5	261.20	260.67	261.17	260.71				
	6	261.18	260.66	261.15	260.70				
	7	261.18	260.66	261.16	260.70				
	8	261.18	260.67	261.17	260.71				
	9	261.17	260.66	261.17	260.70				
	10	261.18	260.65	261.17	260.70				
Gas Ferritic Nitrocarburizing (process *d*, 595 °C / 4 hrs)	1	261.18	260.66	261.22	260.77	0.0115	0.0378	0.0026	0.0014
	2	261.18	260.66	261.21	260.76				
	3	261.19	260.66	261.22	260.76				
	4	261.19	260.68	261.21	260.77				
	5	261.18	260.65	261.21	260.76				
	6	261.19	260.67	261.23	260.77				

	7	261.18	260.66	261.21	260.76				
	8	261.18	260.67	261.22	260.77				
	9	261.18	260.66	261.20	260.76				
	10	261.18	260.66	261.20	260.75				
Ion Ferritic Nitrocarburizing (process *e*, 560 °C / 15 hrs)	1	261.18	260.66	261.29	260.82	0.0378	0.0599	0.0048	0.0028
	2	261.18	260.65	261.28	260.81				
	3	261.18	260.67	261.28	260.83				
	4	261.19	260.66	261.29	260.83				
	5	261.18	260.66	261.27	260.81				
	6	261.21	260.66	261.28	260.81				
	7	261.18	260.66	261.28	260.81				
	8	261.18	260.65	261.29	260.82				
	9	261.21	260.67	261.32	260.83				
	10	261.19	260.67	261.30	260.83				
Ion Ferritic Nitrocarburizing (process *f*, 525 °C / 24 hrs)	1	261.19	260.68	261.35	260.89	0.0611	0.0796	0.0049	0.0045
	2	261.19	260.68	261.37	260.90				
	3	261.18	260.67	261.32	260.86				
	4	261.19	260.68	261.34	260.88				
	5	261.18	260.67	261.34	260.87				
	6	261.19	260.68	261.36	260.90				
	7	261.20	260.67	261.35	260.87				
	8	261.21	260.68	261.37	260.89				
	9	261.19	260.68	261.35	260.88				
	10	261.19	260.66	261.35	260.87				
Gas Ferritic Nitrocarburizing (process *g*, 525 °C / 52 hrs)	1	261.18	260.66	261.31	260.83	0.0506	0.0656	0.0010	0.0006
	2	261.18	260.67	261.31	260.84				
	3	261.18	260.66	261.30	260.83				
	4	261.18	260.66	261.32	260.83				
	5	261.19	260.68	261.32	260.85				
	6	261.18	260.66	261.31	260.84				
	7	261.19	260.67	261.33	260.84				
	8	261.18	260.66	261.31	260.83				
	9	261.19	260.67	261.32	260.83				
	10	261.18	260.66	261.31	260.83				
Gas Ferritic Nitrocarburizing (process *h*, 570 °C / 4 hrs)	1	261.21	260.68	261.29	260.81	0.0333	0.0508	0.0041	0.0013
	2	261.18	260.67	261.28	260.80				
	3	261.20	260.67	261.28	260.80				
	4	261.18	260.67	261.29	260.80				
	5	261.18	260.66	261.27	260.79				
	6	261.18	260.66	261.27	260.79				
	7	261.18	260.66	261.28	260.80				
	8	261.18	260.66	261.27	260.80				
	9	261.18	260.66	261.27	260.79				
	10	261.21	260.66	261.28	260.79				

Vacuum Ferritic Nitrocarburizing (process *i*, 580 °C / 10 hrs)	1	261.18	260.67	261.23	260.78	0.0188	0.0413	0.0032	0.0012
	2	261.18	260.66	261.24	260.77				
	3	261.18	260.67	261.24	260.78				
	4	261.18	260.66	261.23	260.77				
	5	261.18	260.67	261.23	260.77				
	6	261.18	260.66	261.22	260.76				
	7	261.19	260.68	261.24	260.78				
	8	261.18	260.66	261.23	260.77				
	9	261.18	260.66	261.23	260.77				
	10	261.22	260.67	261.25	260.78				
Gas Ferritic Nitrocarburizing (process *j*, 580 °C / 2 hrs)	1	261.18	260.66	261.24	260.75	0.0198	0.036	0.0031	0.0027
	2	261.18	260.65	261.23	260.75				
	3	261.18	260.67	261.24	260.77				
	4	261.19	260.67	261.24	260.76				
	5	261.19	260.67	261.24	260.75				
	6	261.18	260.67	261.22	260.75				
	7	261.20	260.68	261.24	260.77				
	8	261.18	260.67	261.24	260.77				
	9	261.18	260.66	261.24	260.76				
	10	261.18	260.67	261.25	260.77				
Gas Carbonitriding (process *k*, 850 °C / 4 hrs)	1	261.17	260.65	261.28	260.64	0.0031	-0.0144	0.0392	0.0124
	2	261.18	260.66	261.08	260.57				
	3	261.17	260.66	261.08	260.61				
	4	261.17	260.64	261.19	260.61				
	5	261.18	260.66	261.29	260.65				

Inside Diameter Changes of Torque Converter Pistons (Size Distortion)
(Measured at -11 and -15 mm longitudinal height positions from the lockup surface of pistons)

Process	No.	Inside Diameter (mm)							
		Before Heat Treatment		After Heat Treatment		Average Change (%)		Standard Deviation	
		At -11	At -15	At -11	At -15	At -11	At -15	At -11	At -15
Gas Ferritic Nitrocarburizing (process *a*, 510 °C / 15 hrs)	1	62.0668	62.1052	62.0774	62.1275	0.0183	0.0381	0.0022	0.0027
	2	62.0642	62.0992	62.0755	62.1234				
	3	62.0667	62.1043	62.0772	62.1270				
	4	62.0672	62.1048	62.0757	62.1250				
	5	62.0640	62.1011	62.0763	62.1256				
	6	62.0655	62.1023	62.0774	62.1261				
	7	62.0688	62.1088	62.0795	62.1326				
	8	62.0655	62.1018	62.0789	62.1283				
	9	62.0680	62.1071	62.0805	62.1313				
	10	62.0677	62.1074	62.0796	62.1320				
Gas Ferritic Nitrocarburizing (process *b*, 540 °C / 10 hrs)	1	62.0712	62.1085	62.0802	62.1343	0.024	0.0479	0.0036	0.0033
	2	62.0677	62.1060	62.0823	62.1351				
	3	62.0651	62.1036	62.0807	62.1359				
	4	62.0666	62.1033	62.0823	62.1338				
	5	62.0654	62.1029	62.0819	62.1328				
	6	62.0665	62.1049	62.0817	62.1348				
	7	62.0651	62.1038	62.0788	62.1307				
	8	62.0643	62.1017	62.0807	62.1319				
	9	62.0661	62.1044	62.0823	62.1360				
	10	62.0667	62.1039	62.0827	62.1350				
Gas Ferritic Nitrocarburizing (process *c*, 565 °C / 5 hrs)	1	62.0693	62.1060	62.0834	62.1378	0.0255	0.0538	0.0021	0.0028
	2	62.0680	62.1057	62.0827	62.1374				
	3	62.0675	62.1049	62.0823	62.1390				
	4	62.0672	62.1045	62.0820	62.1346				
	5	62.0667	62.1040	62.0848	62.1375				
	6	62.0660	62.1032	62.0814	62.1377				
	7	62.0651	62.1024	62.0821	62.1360				
	8	62.0645	62.1013	62.0810	62.1373				
	9	62.0662	62.1043	62.0835	62.1392				
	10	62.0678	62.1067	62.0836	62.1408				
Gas Ferritic	1	62.0647	62.1017	62.0894	62.1444	0.0406	0.0683	0.0013	0.0027

Nitrocarburizing (process *d*, 595 °C / 4 hrs)	2	62.0651	62.1029	62.0902	62.1446				
	3	62.0643	62.1016	62.0886	62.1421				
	4	62.0647	62.1013	62.0892	62.1425				
	5	62.0671	62.1067	62.0933	62.1505				
	6	62.0648	62.1018	62.0889	62.1421				
	7	62.0668	62.1044	62.0932	62.1497				
	8	62.0656	62.1028	62.0909	62.1442				
	9	62.0661	62.1046	62.0920	62.1479				
	10	62.0663	62.1043	62.0915	62.1483				
Ion Ferritic Nitrocarburizing (process *e*, 560 °C / 15 hrs)	1	62.0654	62.1028	62.1046	62.1486				
	2	62.0676	62.1064	62.1072	62.1524				
	3	62.0656	62.1033	62.1061	62.1504				
	4	62.0668	62.1031	62.1086	62.1506				
	5	62.0669	62.1048	62.1055	62.1511	0.0657	0.0763	0.0027	0.0021
	6	62.0688	62.1068	62.1085	62.1540				
	7	62.0676	62.1054	62.1084	62.1530				
	8	62.0674	62.1056	62.1111	62.1554				
	9	62.0667	62.1049	62.1097	62.1543				
	10	62.0651	62.1015	62.1059	62.1485				
Ion Ferritic Nitrocarburizing (process *f*, 525 °C / 24 hrs)	1	62.0647	62.1007	62.1103	62.1578				
	2	62.0647	62.1014	62.1106	62.1552				
	3	62.0673	62.1051	62.1119	62.1608				
	4	62.0654	62.1016	62.1124	62.1595				
	5	62.0674	62.1026	62.1136	62.1593	0.0745	0.0913	0.0023	0.0028
	6	62.0652	62.1018	62.1144	62.1618				
	7	62.0681	62.1054	62.1151	62.1632				
	8	62.0672	62.1049	62.1145	62.1624				
	9	62.0661	62.1029	62.1108	62.1587				
	10	62.0659	62.1036	62.1108	62.1585				
Gas Ferritic Nitrocarburizing (process *g*, 525 °C / 52 hrs)	1	62.0682	62.1060	62.1129	62.1645				
	2	62.0663	62.1049	62.1107	62.1633				
	3	62.0670	62.1067	62.1109	62.1633				
	4	62.0663	62.1050	62.1099	62.1620				
	5	62.0632	62.1000	62.1064	62.1559	0.0705	0.0915	0.0009	0.0016
	6	62.0650	62.1008	62.1078	62.1564				
	7	62.0650	62.1027	62.1086	62.1584				
	8	62.0661	62.1037	62.1099	62.1601				
	9	62.0664	62.1040	62.1101	62.1610				

	10	62.0670	62.1045	62.1111	62.1615				
Gas Ferritic Nitrocarburizing (process h, 570 °C / 4 hrs)	1	62.0654	62.1012	62.0838	62.1345	0.0304	0.0554	0.0014	0.0017
	2	62.0655	62.1033	62.0833	62.1363				
	3	62.0672	62.1051	62.0857	62.1393				
	4	62.0663	62.1046	62.0851	62.1382				
	5	62.0681	62.1058	62.0858	62.1392				
	6	62.0663	62.1048	62.0866	62.1401				
	7	62.0663	62.1039	62.0855	62.1387				
	8	62.0668	62.1039	62.0867	62.1395				
	9	62.0676	62.1055	62.0871	62.1414				
	10	62.0679	62.1047	62.0866	62.1395				
Vacuum Ferritic Nitrocarburizing (process i, 580 °C / 10 hrs)	1	62.0634	62.1006	62.0907	62.1435	0.0442	0.0694	0.002	0.0026
	2	62.0644	62.1026	62.0921	62.1459				
	3	62.0635	62.1000	62.0904	62.1426				
	4	62.0654	62.1032	62.0932	62.1466				
	5	62.0674	62.1057	62.0935	62.1466				
	6	62.0654	62.1022	62.0925	62.1458				
	7	62.0654	62.1026	62.0907	62.1435				
	8	62.0647	62.1018	62.0938	62.1483				
	9	62.0666	62.1053	62.0940	62.1482				
	10	62.0640	62.1022	62.0935	62.1465				
Gas Ferritic Nitrocarburizing (process j, 580 °C / 2 hrs)	1	62.0676	62.1056	62.0931	62.1476	0.0426	0.0664	0.0036	0.0029
	2	62.0664	62.1045	62.0934	62.1447				
	3	62.0639	62.1001	62.0919	62.1426				
	4	62.0652	62.1023	62.0926	62.1450				
	5	62.0646	62.1023	62.0939	62.1465				
	6	62.0666	62.1032	62.0943	62.1445				
	7	62.0647	62.1000	62.0927	62.1416				
	8	62.0630	62.1002	62.0853	62.1383				
	9	62.0648	62.1017	62.0904	62.1426				
	10	62.0646	62.1015	62.0879	62.1406				
Gas Carbonitriding (process k, 850 °C / 4 hrs)	1	62.0876	62.1148	62.0666	62.1374	-0.0615	-0.0055	0.0233	0.0329
	2	62.0851	62.1175	62.0321	62.0950				
	3	62.0867	62.1156	62.0393	62.0932				
	4	62.0895	62.1177	62.0443	62.1104				
	5	62.0854	62.1154	62.0610	62.1279				

Total Flatness Changes of Torque Converter Pistons (Shape Distortion)

Process	No.	Total Flatness(mm)			
		Before Heat Treatment	After Heat Treatment	Average Change (%)	Standard Deviation
Gas Ferritic Nitrocarburizing (process *a*, 510 °C / 15 hrs)	1	0.1529	0.1668	16.4332	21.0652
	2	0.2506	0.2721		
	3	0.1701	0.199		
	4	0.1245	0.2113		
	5	0.1672	0.2114		
	6	0.1297	0.1558		
	7	0.2015	0.2325		
	8	0.1799	0.1874		
	9	0.1679	0.1668		
	10	0.1617	0.1528		
Gas Ferritic Nitrocarburizing (process *b*, 540 °C / 10 hrs)	1	0.2078	0.2009	25.1092	17.477
	2	0.1612	0.1801		
	3	0.1255	0.1617		
	4	0.1873	0.2355		
	5	0.1729	0.1987		
	6	0.1614	0.1945		
	7	0.1702	0.2713		
	8	0.1939	0.2276		
	9	0.1435	0.1903		
	10	0.1869	0.2678		
Gas Ferritic Nitrocarburizing (process *c*, 565 °C / 5 hrs)	1	0.2098	0.2556	15.6402	12.2311
	2	0.1317	0.1576		
	3	0.2002	0.2381		
	4	0.2303	0.277		
	5	0.1668	0.1857		
	6	0.1834	0.2237		
	7	0.2037	0.2362		
	8	0.2191	0.2304		
	9	0.1677	0.2238		
	10	0.1873	0.1645		
Gas Ferritic Nitrocarburizing (process *d*, 595 °C / 4 hrs)	1	0.1649	0.1712	21.5156	8.16
	2	0.1644	0.1922		
	3	0.1903	0.2271		
	4	0.1647	0.1966		
	5	0.1913	0.2348		
	6	0.1787	0.2345		
	7	0.1502	0.1986		
	8	0.1698	0.2026		

	9	0.141	0.1802		
	10	0.1575	0.1928		
Ion Ferritic Nitrocarburizing (process _e_, 560 °C / 15 hrs)	1	0.1685	0.2141	21.3685	10.7728
	2	0.1591	0.1907		
	3	0.1987	0.2123		
	4	0.1563	0.1831		
	5	0.1965	0.246		
	6	0.1277	0.1614		
	7	0.1603	0.1786		
	8	0.1432	0.2087		
	9	0.3044	0.3631		
	10	0.1851	0.2124		
Ion Ferritic Nitrocarburizing (process _f_, 525 °C / 24 hrs)	1	0.2139	0.2373	16.2678	3.9066
	2	0.1425	0.1752		
	3	0.1799	0.2156		
	4	0.1575	0.1828		
	5	0.1946	0.218		
	6	0.1872	0.2265		
	7	0.2409	0.2798		
	8	0.2329	0.2661		
	9	0.1877	0.2174		
	10	0.2031	0.2308		
Gas Ferritic Nitrocarburizing (process _g_, 525 °C / 52 hrs)	1	0.1445	0.1466	5.1099	10.4323
	2	0.1202	0.1494		
	3	0.1247	0.1546		
	4	0.1917	0.1866		
	5	0.2015	0.2073		
	6	0.1718	0.1647		
	7	0.1801	0.1898		
	8	0.1931	0.1877		
	9	0.2104	0.2143		
	10	0.1535	0.1548		
Gas Ferritic Nitrocarburizing (process _h_, 570 °C / 4 hrs)	1	0.1683	0.2157	25.0152	15.6517
	2	0.1995	0.2672		
	3	0.226	0.2339		
	4	0.1616	0.2389		
	5	0.1535	0.1596		
	6	0.1391	0.1772		
	7	0.1644	0.1831		
	8	0.1541	0.2035		
	9	0.1826	0.2642		
	10	0.163	0.1911		
Vacuum Ferritic Nitrocarburizing (process _i_, 580 °C / 10 hrs)	1	0.1795	0.2946	49.2671	28.2447
	2	0.1923	0.261		
	3	0.1766	0.2113		

	4	0.1634	0.3257		
	5	0.1393	0.1654		
	6	0.1896	0.3631		
	7	0.1875	0.254		
	8	0.1904	0.2972		
	9	0.1787	0.2312		
	10	0.2079	0.2966		
Gas Ferritic Nitrocarburizing (process _j_, 580 °C / 2 hrs)	1	0.1597	0.1899	39.6723	38.4223
	2	0.1606	0.2548		
	3	0.1541	0.3226		
	4	0.2037	0.2564		
	5	0.1876	0.1563		
	6	0.1938	0.2307		
	7	0.2035	0.3932		
	8	0.1966	0.2265		
	9	0.1875	0.2308		
	10	0.1526	0.229		
Gas Carbonitriding (process _k_, 850 °C / 4 hrs)	1	0.2272	1.4799	515.2959	320.4697
	2	0.2003	0.397		
	3	0.2272	1.1948		
	4	0.1383	1.5106		
	5	0.1779	1.083		

Flatness Taper Changes of Torque Converter Pistons (Shape Distortion)

Process	No.	Flatness Taper (mm)			
		Before Heat Treatment	After Heat Treatment	Average Change (%)	Standard Deviation
Gas Ferritic Nitrocarburizing (process *a*, 510 °C / 15 hrs)	1	0.1061	0.1339	32.3624	30.3612
	2	0.1201	0.1268		
	3	0.1553	0.1496		
	4	0.0885	0.1748		
	5	0.1228	0.1731		
	6	0.0926	0.1294		
	7	0.0892	0.1141		
	8	0.0931	0.1401		
	9	0.1565	0.1488		
	10	0.0801	0.1152		
Gas Ferritic Nitrocarburizing (process *b*, 540 °C / 10 hrs)	1	0.1497	0.1252	32.0278	25.5347
	2	0.085	0.0984		
	3	0.0872	0.1125		
	4	0.1465	0.2035		
	5	0.0962	0.1306		
	6	0.149	0.1756		
	7	0.0904	0.1185		
	8	0.0877	0.1343		
	9	0.0897	0.119		
	10	0.0918	0.1675		
Gas Ferritic Nitrocarburizing (process *c*, 565 °C / 5 hrs)	1	0.1639	0.2264	24.0043	19.8652
	2	0.0854	0.1123		
	3	0.1832	0.1816		
	4	0.1258	0.1744		
	5	0.1432	0.1642		
	6	0.1246	0.1745		
	7	0.1218	0.1704		
	8	0.1729	0.1551		
	9	0.0887	0.1266		
	10	0.1035	0.1093		
Gas Ferritic Nitrocarburizing (process *d*, 595 °C / 4 hrs)	1	0.0924	0.1229	31.9598	9.3202
	2	0.0897	0.1278		
	3	0.1385	0.1898		
	4	0.0933	0.1257		

130

	5	0.1006	0.1264		
	6	0.1583	0.1821		
	7	0.1274	0.1542		
	8	0.0893	0.1167		
	9	0.0833	0.112		
	10	0.0921	0.134		
Ion Ferritic Nitrocarburizing (process *e*, 560 °C / 15 hrs)	1	0.0901	0.1245	35.9781	15.5851
	2	0.0927	0.1143		
	3	0.0935	0.1212		
	4	0.0906	0.1553		
	5	0.096	0.1226		
	6	0.0921	0.1241		
	7	0.0963	0.1304		
	8	0.0913	0.136		
	9	0.1879	0.2141		
	10	0.0896	0.1223		
Ion Ferritic Nitrocarburizing (process *f*, 525 °C / 24 hrs)	1	0.1675	0.1738	23.6931	12.0344
	2	0.0931	0.1239		
	3	0.0895	0.1204		
	4	0.0917	0.123		
	5	0.148	0.1666		
	6	0.1357	0.1719		
	7	0.2077	0.2395		
	8	0.1383	0.1711		
	9	0.1007	0.1412		
	10	0.1422	0.1606		
Gas Ferritic Nitrocarburizing (process *g*, 525 °C / 52 hrs)	1	0.0872	0.1161	21.9394	20.343
	2	0.0871	0.1224		
	3	0.0831	0.1143		
	4	0.1584	0.1496		
	5	0.101	0.1582		
	6	0.1454	0.1385		
	7	0.1525	0.1711		
	8	0.1098	0.1252		
	9	0.1362	0.1488		
	10	0.0929	0.1174		
Gas Ferritic Nitrocarburizing (process *h*, 570 °C / 4 hrs)	1	0.1139	0.1291	43.2378	26.3894
	2	0.1434	0.2095		
	3	0.119	0.1266		
	4	0.0866	0.128		

131

	5	0.088	0.1248		
	6	0.0889	0.1525		
	7	0.0869	0.1321		
	8	0.0898	0.1535		
	9	0.0897	0.1573		
	10	0.1159	0.1241		
Vacuum Ferritic Nitrocarburizing (process *i*, 580 °C / 10 hrs)	1	0.0852	0.2637	99.7329	61.2447
	2	0.0947	0.1566		
	3	0.1556	0.1809		
	4	0.0937	0.1838		
	5	0.0937	0.1169		
	6	0.1053	0.241		
	7	0.1247	0.2346		
	8	0.1127	0.2555		
	9	0.1077	0.1822		
	10	0.1018	0.2773		
Gas Ferritic Nitrocarburizing (process *j*, 580 °C / 2 hrs)	1	0.0901	0.1582	76.4736	75.0887
	2	0.0898	0.2018		
	3	0.09	0.305		
	4	0.1324	0.2383		
	5	0.1293	0.125		
	6	0.153	0.1695		
	7	0.158	0.3719		
	8	0.1435	0.143		
	9	0.1629	0.2158		
	10	0.1027	0.1752		
Gas Carbonitriding (process *k*, 850 °C / 4 hrs)	1	0.2153	1.1973	507.8373	499.4089
	2	0.1827	0.3281		
	3	0.223	0.942		
	4	0.0935	1.3723		
	5	0.1189	0.4915		

REFERENCES

1. C.M. Cotell and J. A. Sprague, Preface, ASM Handbook, Vol. 5, Surface Engineering, S.R. Lampman *et al.* (Editors), ASM International, Materials Park, OH, U.S.A., 1994, pp. 8-10.

2. Surface Engineering Division of the Institute of Materials, Minerals and Mining, Hub of Information, Materials World, Vol. 16, No. 9, 2008, pp. 35-37.

3. D. Rickerby, On the Surface, Materials World, Vol. 16, No. 9, 2008, pp. 33-34.

4. J.R. Davis (Editor), Surface Engineering for Corrosion and Wear Resistance, ASM International, Materials Park, OH, U.S.A., 2001, pp. 1-5, 115-116.

5. S. Lampman, "Introduction to Surface Hardening of Steels", ASM Handbook, Vol. 4, Heat Treating, S.R. Lampman *et al.* (Editors), ASM International, Materials Park, OH, U.S.A., 1991, pp. 259-267.

6. J. Dosset, "Carbonitriding", ASM Handbook, Vol. 4, Heat Treating, S.R. Lampman *et al.* (Editors), ASM International, Materials Park, OH, U.S.A., 1991, pp. 376-384.

7. ASM Committee on Gas Carburizing, Carburizing and Carbonitriding, American Society for Metals, Metals Park, OH, U.S.A., 1977, pp. 1-4, 125-147.

8. J.R. Davis (Editor), Surface Hardening of Steels: Understanding the Basics, ASM International, Materials Park, OH, U.S.A., 2002, pp. 1-5, 127-139, 195-212.

9. J. Grosch, "Heat Treatment with Gaseous Atmospheres", Steel Heat Treatment Handbook: Metallurgy and Technologies, G.E. Totten (Editor), Second Edition, CRC Press, Boca Raton, FL, U.S.A., 2007, pp. 422, 431-440, 446-463.

10. G. Krauss, Steels: Processing, Structure, and Performance, ASM International, Materials Park, OH, U.S.A., 2006, pp. 417-424, 456-460.

11. P. Schobesberger, T. Streng, and S. Abbas, Low-Distortion Heat Treatment of Thin Parts, Industrial Heating, Vol. 69, No. 2, 2002, pp. 30-34.

12. Kevin Sullivan's Autoshop 101, "Torque Converter", Toyota Series-Automatic Transmissions, Retrieved July 10 2009, from http://www.autoshop101.com/forms/AT02.pdf, pp. 6-19.

13. M. Narazaki and G.E. Totten, "Distortion of Heat-Treated Components", Steel Heat Treatment Handbook: Metallurgy and Technologies, G.E. Totten (Editor), Second Edition, CRC Press, Boca Raton, FL, U.S.A., 2007, pp. 608-637.

14. V. Campagna, R.J. Bowers, D.O. Northwood, X. Sun, and P. Bauerle, The Nitrocarburizing of Plain Carbon Steel Automotive Components, Proceedings of the 24th ASM Heat Treating Society Conference, September 17-19, Detroit, MI, U.S.A., ASM International, Materials Park, OH, U.S.A., 2007, pp. 239-244.

15. V. Campagna, R.J. Bowers, D.O. Northwood, X. Sun, and P. Bauerle, Distortion and Residual Stresses in Nitrocarburized and Carbonitrided SAE 1010 Plain Carbon Steel, SP-2192: Experiments in Automotive Engineering, Paper No. 2008-01-1421, SAE International, Warrendale, PA, U.S.A., 2008, pp. 69-75.

16. V. Campagna, D.O. Northwood, R.J. Bowers, X. Sun, and P. Bauerle, The Analysis and Control of Distortion in Carbonitrided and Nitrocarburized Thin-Shelled Plain Carbon Steel Automotive Powertrain Components, Journal of ASTM International, Vol. 6, No. 3, 2009, DOI: 10.1520/JAI101868, pp. 1-17.

17. D. Pye, Practical Nitriding and Ferritic Nitrocarburizing, ASM International, Materials Park, OH, U.S.A., 2003, pp. 1-22, 119-120, 167-183, 193-194, 201-202, 219-229.

18. T. Bell, "Gaseous and Plasma Nitrocarburizing," ASM Handbook, Vol. 4, Heat Treating, S.R. Lampman et al. (Editors), ASM International, Materials Park, OH, U.S.A., 1991, pp. 425-436.

19. D. Pye, "Nitriding Techniques, Ferritic Nitrocarburizing, and Austenitic Nitrocarburizing Techniques and Methods," Steel Heat Treatment: Metallurgy and Technologies, G.E. Totten (Editor), Second Edition, CRC Press, Boca Raton FL, U.S.A., 2007, pp. 528-536.

20. B. Hernández-Morales, O. Barba-Méndez, A. Ingalls-Cruz, and J.A. Barrera-Godínez, Mathematical Modelling of Temperature and Stress Evolution During Cooling of a Stainless Steel Navy C-ring Probe, International Journal of Materials and Product Technology, Vol. 24, Nos. 1-4, 2005, pp. 306-318.

21. G. Krauss, Steels: Heat Treatment and Processing Principles, ASM International, Materials Park, OH, U.S.A., 1990, pp. 47-53, 281-287, 310-315.

22. J.L. Dossett and H.E. Boyer, Practical Heat Treating, Second Edition, ASM International, Materials Park, OH, U.S.A., 2006, PP.141-145.

23. H.E. Boyer (Editor), Case Hardening of Steel, ASM International, Materials Park, OH, U.S.A., 1987, PP. 1-8, 54-69, 77-80, 319.

24. C.A. Stickels, "Gas Carburizing", ASM Handbook, Vol. 4, Heat Treating, S.R. Lampman *et al.* (Editors), ASM International, Materials Park, OH, U.S.A., 1991, pp. 312-324.

25. F.C. Campbell, Elements of Metallurgy and Engineering Alloys, ASM International, Materials Park, OH, U.S.A., 2008, pp. 397-405.

26. L. E. Gesser, S. R. Sagitova, and L. S. Liberman, Influence of Carbonitriding on the Life of Cutting Tools, Metal Science and Heat Treatment, Vol. 24, No. 6, 1982, pp. 399-402.

27. J.R. Davis (Editor), Gear Materials, Properties, and Manufacture, ASM International, Materials Park, OH, U.S.A., 2005, pp. 245-248.

28. V.M. Zinchenko, B.V. Georgievskaya, and V.A. Olovyanishnikov, Hardenability and phase composition of carbonitrided steels, Metal Science and Heat Treatment, Vol. 19, No. 4, 1977, pp. 257-261.

29. E.L. Gyulikhandanov, L.M. Semenova, and V.I. Shapochkin, Influence of High-Temperature Carbonitriding on the Structure, Phase Composition, and Properties of Low-Alloy Steels, Metal Science and Heat Treatment, Vol. 26, No. 4, 1984, 262-267.

30. C.R. Brooks, Heat Treatment of Ferrous Alloys, Hemisphere Publishing Corporation, 1979, pp. 4-6, 20-30, 43-46, 115-119.

31. H. Chandler, Heat Treater's Guide: Practices and Procedures for Irons and Steels, ASM International, Materials Park, OH, U.S.A., 1995, pp. 96-101, 883.

32. V. Rudnev, Handbook of Induction Heating, CRC Press, Boca Raton, FL, U.S.A., 2003, pp. 73-74.

33. J. Grosch, "Heat Treatment with Gaseous Atmospheres", Steel Heat Treatment Handbook, G.E. Totten and M.A.H. Howes (Editors), Marcel Dekker, Inc., NY, U.S.A., 1997, pp. 679-685.

34. C.H. Knerr, T.C. Rose, and J.H. Filkowski, "Gas Nitriding", ASM Handbook, Vol. 4, Heat Treating, S.R. Lampman *et al.* (Editors), ASM International, Materials Park, OH, U.S.A., 1991, pp. 387-395.

35. H. Gastrow and P. Unger, Gastrow Injection Molds: 130 Proven Designs, P. Unger (Editor), Fourth Edition, Hanser Verlag, 2006, pp. 29-30.

36. D. Pye, "Nitriding Techniques and Methods", Steel Heat Treatment Handbook, G.E. Totten and M.A.H. Howes (Editors), Marcel Dekker, Inc., NY, U.S.A., 1997, PP. 721-732, 759-761.

37. D. Lipiński and J. Ratajski, "Modeling of Microhardness Profile in Nitriding Process Using Artificial Neural Network", Advanced Intelligent Computing Theories and Applications: Third International Conference on Intelligent Computing, D. Huang, L. Heutte, and M. Loog (Editors), Springer, 2007, pp. 245-252.

38. S. Li, R.R. Manory, and J.H. Hensler, Compound Layer Growth and Compound Layer Porosity of Austenite Plasma Nitrocarburised Non-Alloyed Steel, Surface and Coatings Technology, Vol. 71, No. 2, 1995, pp. 112-120.

39. A.M. Maliska, A.M. de Oliveira, A.N. Klein, and J.L.R. Muzart, Surface Porosity Sealing Effect of Plasma Nitrocarburizing on Sintered Unalloyed Iron, Surface and Coatings Technology, Vol. 141, No. 2-3, 2001, pp. 128-134.

40. T. Bell, "Ferritic Nitrocarburizing", Source Book on Nitriding, ASM International, Metals Park, OH, U.S.A., 1977, pp. 266-278.

41. T. Bell, "Ferritic Thermochemical Heat Treatment Processes", Survey of the Heat Treatment of Engineering Components, Iron and Steel Institute, 1973, pp.49-53.

42. C. Dawes, Nitrocarburising and its Influence on Design in the Automotive Sector, Heat Treatment of Metals, Vol. 18, No.1, 1991, pp. 19-30.

43. A. Wells, Metallographic Analysis of Compound Layers on Ferritic Nitrocarburized Plain Low Carbon Steel, Journal of Materials Science, Vol. 20, No. 7, 1985, pp. 2439-2445.

44. A. Çelik, M. Karakan, A. Alsaran, and I. Efeoglu, The Investigation of Structural, Mechanical and Tribological Properties of Plasma Nitrocarburized AISI 1020 Steel, Surface and Coatings Technology, Vol. 200, No. 5-6, 2005, pp. 1926-1932.

45. L. Sproge and S.J. Midea, Analysis and Control of Nitriding and Nitrocarburizing Atmospheres, Second International Conference on Carburizing and Nitriding with Atmospheres, Cleveland, OH, ASM International, Metals Park, OH, U.S.A., 1995, pp. 303-307.

46. D.H. Herring, "Comparing Carbonitriding and Nitrocarburizing", Heat Treating Progress, 2002, pp. 17-19.

47. J. Pan, "Factors Affecting Final Part Shaping", G.E. Totten, M. Howes, and T. Inoue (Editors), Handbook of Residual Stress and Deformation of Steel, ASM International, Materials Park, OH, U.S.A., 2002, pp. 169-174.

48. V. Campagna, R.J. Bowers, D.O. Northwood, X. Sun, and P. Bauerle, Distortion and Residual Stresses in Nitrocarburized and Carbonitrided SAE 1010 Plain Carbon Steel, SAE International Journal of Materials & Manufacturing, Vol. 1, No. 1, 2009, pp. 690-696.

49. I. V. Etchells, A Approach to Salt Bath Nitrocarburizing, Heat Treatment of Metals, Vol. 4, No. 8, 1981, pp. 85-88.

50. M. Mirjani, F. Ashrafizadeh, and A. Shafyei, Plasma and Gaseous Nitrocarburizing of C60W Steel for Tribological Applications, Transactions of Materials and Heat Treatment Proceedings of the 14th IFHTSE Congress, Vol.25, No. 5, 2004, pp. 338-342.

51. S.V. Matveev, V.V. Malakhov, K.Sh. Yagudin, A.Ya. Arzhankin, and G.V. Osipova, Short-Term Gas Nitrocarburizing of Tools for Cutting and Die Forging, Metal Science and Heat Treatment, Vo. 47, No. 9-10, 2005, pp. 484-486.

52. B. Edenhofer and J.W. Bouwman, "Vacuum Heat Treatment", Steel Heat Treatment Handbook, G.E. Totten and M.A.H. Howes (Editors), Marcel Dekker, Inc., NY, U.S.A., 1997, pp. 483-525.

53. B. Edenhofer, J.W. Bouwman, and D.H. Herring, "Vacuum Heat Processing", Steel Heat Treatment: Equipment and Process Design, G.E. Totten (Editor), Second Edition, CRC Press, Boca Raton, FL, U.S.A., 2007, pp. 239-242.

54. M. Bauccio and American Society for Metals, ASM Metals Reference Book, Third Edition, ASM International, Materials Park, OH, U.S.A., 1993, pp. 67, 94, 205-206.

55. D. Jordan, H. Antes, V. Osterman, and T. Jones, Low Torr-range Vacuum Nitriding of 4140 Steel, Journal of Heat Treating Progress, Vol.8, No. 2, 2008, pp. 33-38.

56. T. Bell, Y. Sun, and A. Suhadi, Environmental and Technical Aspects of Plasma Nitrocarburising Vacuum, Vol. 59, No. 1, 2000, pp. 14-23.

57. L. Shi and R.R. Manory, Surface Morphology and Compound Layer Prores of Plasma Nitrocarburized Low Carbon Steel, Metallurgical and Materials Transactions A, Vol. 27 (a), 1996, pp. 135-143.

58. B. Jeong and M. Kim, Effects of the Process Parameters on the Layer Formation Behavior of Plasma Nitrided Steels, Surface and Coatings Technology, Vol. 141, No. 2-3, 2001, pp. 182-186.

59. M. Karakan, A. Alsaran, and A. Çelik, Effect of Process Time on Structural and Tribological Properties of Ferritic Plasma Nitrocarburized AISI 4140 Steel, Materials and Design, Vol. 25, No. 4, 2004, pp. 349-353.

60. A.M. Staines and T. Bell, Technological Importance of Plasma-Induced Nitrided and Carburized Layers on Steel, Thin Solid Films, Vol. 86, No. 2-3, 1981, p.201.

61. T. Mueller, A. Gebeshuber, R. Kullmer, C. Lugmair, S. Perlot, and M. Stoiber, Minimizing Wear Through Combined Thermochemical and Plasma Activated Diffusion and Coating Processes, Materiali in Tehnologije, Vol. 38, No. 6, 2004, pp. 353-357.

62. C. Jaoul, T. Belmonte, T. Czerwiec, and N. David, Nitrocarburizing Treatments Using Flowing Afterglow Processes, Applied Surface Science, Vol. 252, No. 23, 2006, pp. 8360-8366.

63. W. Rembges and W. Oppel, Process Control of Plasma Nitriding and Plasma Nitrocarburizing in Industry, Surface & Coatings Technology, Vol.59, No. 1, 1993, pp. 129-134.

64. Y.T. Sun and T. Bell, A Numerical Model of Plasma Nitriding of Low Alloy Steels, Materials Science and Engineering A, Vol. 224, No. 1/2, 1997, pp. 33-47.

65. H.W. Walton, "Deflection Methods to Estimate Residual Stress," Handbook of Residual Stress and Deformation of Steel, G.E. Totten, M. Howes, and T. Inoue (Editors), ASM International, Materials Park, OH, U.S.A., 2002, pp. 89-98.

66. H.J. French, The Quenching of Steels, American Society for Steel Treating, Cleveland, OH, U.S.A., 1930, pp. 132-136.

67. C.E. Bates, G.E. Totten, and R.L. Brennan, "Quenching of Steel," ASM Handbook, Vol. 4, Heat Treating, S.R. Lampman et al. (Editors), ASM International, Materials Park, OH, U.S.A., 1991, pp. 76-80, 99-100.

68. M.A.H. Howes, "Factors Affecting Distortion in Hardened Steel Components: I", Industrial Heating, Vol.60, No. 10, 1993, pp. 65-70.

69. M.J. Nunney, Light and Heavy Vehicle Technology, Fourth Edition, Butterworth-Heinemann, 2007, pp. 319-322.

70. J.Y. Wong, Theory of Ground Vehicles, Third Edition, Wiley-IEEE, 2001, pp. 240-243.

71. J. Erjavec, Automotive Technology: A Systems Approach, Fourth Edition, Cengage Learning, 2004, pp. 999-1011.

72. T.C. Tszeng, W.T. Wu and J.P. Tang, Prediction of Distortion During Heat Treating and Machining Processes, Heat Treating, Proceedings of the 16th Conference, J.L. Dossett and R.E. Luetje (Editors), Cincinnati Convention Center. Cincinnati, Ohio, 1996, ASM International, Materials Park, OH, U.S.A., 1996, pp. 9-15.

73. M. Solari and P. Bilmes, "Component Design", Failure Analysis of Heat Treated Steel Components, L. Canale, R. Mesquita and G.E.Totten (Editors), ASM International, Materials Park, OH, U.S.A., 2008, pp. 31-34.

74. Y. Altschuler, T. Kaatz, and B. Cina, "Relief of Residual Stresses in a High-Strength Aluminum Alloy by Cold Working", Mechanical Relaxation of Residual Stresses, L. Mordfin (Editor), ASTM International, 1988, pp, 19-28.

75. G.E. Totten and M.A.H. Howes, "Distortion of Heat-Treated Components", Steel Heat Treatment Handbook, G.E. Totten and M.A.H. Howes (Editors), Marcel Dekker, Inc., NY, U.S.A., 1997, pp. 251-256.

76. D.S. Mackenzie, "The Heat Treatment and Quenching of Gears", Heat Treating: Proceedings of the 23rd Heat Treating Society Conference, D. Herring and R. Hill (Editors), ASM International, Materials Park, OH, U.S.A., 2006, pp. 304-307.

77. A.K. Sinha, "Defects and Distortion in Heat-Treated Parts," ASM Handbook, Vol. 4, Heat Treating, S.R. Lampman et al. (Editors), ASM International, Materials Park, OH, U.S.A., 1991, pp. 601-619.

78. B.A. Becherer, T. Vasco, and L. Ryan, "Control of Distortion in Tool Steels," ASM Handbook, Vol. 4, Heat Treating, S.R. Lampman et al. (Editors), ASM International, Materials Park, OH, U.S.A. 1991, pp. 761-766.

79. R.T. von Bergen, "The Effects of Quenchant Media Selection and Control on the Distortion of Engineered Steel Parts," Quenching and Distortion Control Conference Proceedings, Chicago, IL U.S.A., 22-25 Sept. 1992, G.E. Totten (Editor), ASM International, Materials Park, OH, U.S.A., 1992, pp. 275-282.

80. J. Grum, Overview of Residual Stress After Quenching Part II: Factors Affecting Quench Residual Stresses, International Journal of Materials and Product Technology, Vol. 24, Nos. 1-4, 2005, pp. 53-58.

81. S. Malkin, Grinding Technology: Theory and Applications of Machining with Abrasives, SME, 1996, pp. 9-11, 45-47.

82. G. Parrish, The Influence of Microstructure on the Properties of Case-Carburized Components, American Society for Metals, 1980, pp. 195-208.

83. M.A.H. Howes, "Factors Affecting Distortion in Hardened Steel Components: II", Industrial Heating, Vol.60, No. 12, 1993, pp. 30-32.

84. T. Réti, "Residual Stresses in Carburized, Carbonitrided, and Case-Hardened Components," Handbook of Residual Stress and Deformation of Steel, G.E. Totten, M. Howes, and T. Inoue (Editors), ASM International, Materials Park, OH, U.S.A., 2002, pp. 189-199.

85. J. Grum, "Induction Heating," Handbook of Residual Stress and Deformation of Steel, G.E. Totten, M. Howes, and T. Inoue (Editors), ASM International, Materials Park, OH, U.S.A., 2002, pp. 220-221.

86. B. Liščić, "Steel Heat Treatment", Steel Heat Treatment: Metallurgy and Technologies, G.E. Totten (Editor), Second Edition, CRC Press, Boca Raton, FL, U.S.A., 2007, pp. 312-321.

87. C. Ruud, "Measurement of Residual Stresses", Handbook of Residual Stress and Deformation of Steel, G.E. Totten, M. Howes, and T. Inoue (Editors), ASM International, Materials Park, OH, U.S.A., 2002, pp. 99-115.

88. H.C. Child, Residual Stress in Heat-treated Components, Heat Treatment of Metals, Vol. 8, No. 4, 1981, pp. 89-94.

89. C.O. Ruud, "Residual Stresses and Their Measurement," Proceedings of the First Conference on Quenching & Control of Distortion, 22-25 September 1992, Chicago, IL, U.S.A., ASM International, Materials Park, OH U.S.A., 1992, pp. 193-198.

90. B. Liščić, "Steel Heat Treatment", Steel Heat Treatment Handbook, G.E. Totten, and M.A.H. Howes (Editors), Marcel Dekker, Inc., NY, U.S.A., 1997, pp. 569-579.

91. E. Macherauch and O. Vöhringer, "Residual Stresses After Quenching", Theory and Technology of Quenching, B. Liscic, H.M. Tensi, and W. Luty (Editors), Springer-Verlag, 1992, pp. 117-181.

92. Z. Kolozváry, "Residual Stresses in Nitriding," Handbook of Residual Stress and Deformation of Steel, G.E. Totten, M. Howes, and T. Inoue (Editors), ASM International, Materials Park, OH, U.S.A., 2002, pp. 209-219.

93. J.A. Pineault, M. Belassel, and M.E. Brauss, "X-Ray Diffraction Residual Stress Measurement in Failure Analysis," ASM Handbook, Vol. 11, Failure Analysis and Prevention, W.T. Becker and R.J. Shipley (Editors), ASM International, Materials Park, OH, U.S.A., 2002, pp. 484-497.

94. M. Belassel, J. Pineault, and M.E. Brauss, Review of Residual Stress Determination and Exploitation Techniques Using X-ray Diffraction Method, Materials Science Forum, Vols. 524-525, 2006, pp. 229-234.

95. J. Pineault, M. Belassel, M. Brauss, and J. Ladouceur, Mapping Residual Stress Garadients Via X-Ray Diffraction, SP-2094: Experiments in Automotive Engineering, Paper No. 2007-01-0802, SAE International, Warrendale, PA, U.S.A., 2007, pp. 23-26.

96. U. F. Kocks, C. N. Tomé, H.-R. Wenk, A. J. Beaudoin, and H. Mecking, Texture and Anisotropy: Preferred Orientations in Polycrystals and Their Effect on Materials Properties, Cambridge University Press, 2000, pp. 127-143.

97. J. Goldstein, D.E. Newbury, P. Echlin, D.C. Joy, C.E. Lyman, E. Lifshin, and L. Sawyer, Scanning Electron Microscopy and X-Ray Microanalysis, Third Edition, J. Goldstein (Editor), Springer, 2003, pp.1-20, 537-543.

98. J.A. Bosch, Coordinate Measuring Machines and Systems, CRC Press, 1995, pp. 39-42.

99. D.V. Rosato, N.R. Schott, and M.G. Rosato, Plastics Engineering, Manufacturing & Data Handbook, Springer, 2001, p. 1851.

100. J.D. Meadows, Geometric Dimensioning and Tolerancing: Applications and Techniques for Use in Design, Manufacturing, and Inspection, CRC Press, 1995, pp. 57, 222-228.

101. ASTM International, Standard Test Method for Verifying the Alignment of X-Ray Diffraction Instrumentation for Residual Stress Measurement, ASTM Standard E915-96, ASTM International, West Conshohocken, PA, 2002.

102. H. Hu, Texture of Metals. Texture, Vol.1, No. 4, 1974, pp. 233-258.

103. D. P. Field, Textured Structures, ASM Handbook: Metallography and Microstructures, ASM International, 2004, pp. 215-226.

104. R. Leppänen, H. Jonsson, Properties of Nitrided Components-A Result of the Material and the Nitriding Process, Technical report 1/1999, ISSN 0284-3366, Ovako Steel, 1999, pp. 3-13.

105. T.R. Watkins, R.D. England, C. Klepser, and N. Jayaraman, Measurement and Analysis of Residual Stress in ε-Phase Iron Nitride Layers as a Function of Depth, Advances in X-ray Analysis, Vol. 43 CD ROM, T.C. Huang et al. (Editors), ICDD, Newtown Square, PA U.S.A., 2000, pp. 31-38.

106.   C. Kanchanomai, W. Limtrakarn, Effect of Residual Stress on Fatigue Failure of Carbonitrided Low-Carbon Steel, Journal of Materials Engineering and Performance, Vol.17, No. 6, 2008, pp. 879-887.

107.   H.K.D.H. Bhadeshia, "Material Factors", Handbook of Residual Stress and Deformation of Steel, G.E. Totten, M. Howes, and T. Inoue (Editors), ASM International, Materials Park, OH, U.S.A., 2002, pp. 1-9.

108.   R.L. Champoux, J.H. Underwood, and J.A. Kapp, Analytical and Experimental Methods for Residual Stress Effects in Fatigue, ASTM International, 1988, pp. 26-27.

PUBLICATIONS AND PRESENTATIONS

Publications

1. C. Nan, D.O. Northwood, R.J. Bowers, X. Sun and P. Bauerle, Residual Stresses and Dimensional Changes in Ferritic Nitrocarburized Navy C-rings and Prototype Stamped Parts Made from SAE 1010 Steel, Proceedings of the SAE World Congress & Exhibition, April 2009, Detroit, MI, U.S.A., Paper No. 2009-01-0425, SAE International, Warrendale, PA, U.S.A.. Also accepted for publication in the SAE International Journal of Materials & Manufacturing.

2. C. Nan, D.O. Northwood, R.J. Bowers and X. Sun, Distortion in Ferritic Nitrocarburized SAE 1010 Plain Carbon Steel, Proceedings of the 2009 SEM Annual Conference and Exposition on Experimental and Applied Mechanics, 1-3 June 2009, Albuquerque, New Mexico, U.S.A.

3. C. Nan, D.O. Northwood, R.J. Bowers, X. Sun and P. Bauerle, The use of Navy C-ring specimens to study distortion in ferritic nitrocarburized 1010 steel, Proceedings of the Surface Effects and Contact Mechanics IX, Computational Methods and Experiments, WIT Transactions on Engineering Sciences, WIT Press 2009, Vol. 62, pp. 13-25.

4. C. Nan, D.O. Northwood, R.J. Bowers and X. Sun, Study on the Dimensional Changes and Residual Stresses in Carbonitrided and Ferritic Nitrocarburized SAE 1010 Plain Carbon Steel. Accepted for publication in the Proceedings of the Thermec' 2009 International Conference, 25-29 August 2009, Technical University-Berlin, Germany.

5. C. Nan, D.O. Northwood, R.J. Bowers and X. Sun, Nitrocarburizing of a SAE 1010 Steel Automotive Component. Submitted on 25 April 2009 for publication in Materials Forum.

Presentations

1. C. Nan, D.O. Northwood, R.J. Bowers and X. Sun, Residual Stresses and Dimensional Changes in Ferritic Nitrocarburized Navy C-rings and Prototype Stamped Parts Made from SAE 1010 Steel, SAE World Congress & Exhibition, April 2009, Detroit, MI, U.S.A.

2. C. Nan, D.O. Northwood, R.J. Bowers and X. Sun, Distortion in Ferritic Nitrocarburized SAE 1010 Plain Carbon Steel, 2009 SEM Annual Conference and Exposition on Experimental and Applied Mechanics, 1-3 June 2009, Albuquerque, New Mexico, U.S.A.

3. C. Nan, D.O. Northwood, R.J. Bowers, X. Sun and P. Bauerle, The use of Navy C-ring specimens to study distortion in ferritic nitrocarburized 1010 steel, Contact Mechanics and Surface Treatment 2009, 9 – 11 June 2009, Algarve, Portugal.

4. C. Nan, D.O. Northwood, R.J. Bowers and X. Sun, Nitrocarburizing of a SAE 1010 Steel Automotive Component, Materials and Austceram 2009, 1-3 July 2009, Gold Coast, Australia.

VITA AUCTORIS

Chunyan Nan was born in 1982 in Jilin, P. R. China. She obtained her Bachelor's Degree of Engineering in Metal Materials Engineering at the University of Jilin in 2005. She is currently a candidate for the Master's degree in Engineering Materials at the University of Windsor and hopes to graduate in Fall 2009.